Multi-source Parameter Estimation and Tracking using Antenna Arrays

by

Zhuqing Tang

A Thesis submitted in fulfilment of requirements for
the degree of Doctor of Philosophy (PhD)
and
the Diploma of Imperial College London (DIC)

July 2022

Supervisor: Prof. A. Manikas

Imperial College London

Department of Electrical and Electronic Engineering

Imperial College London

Department of Electrical and Electronic Engineering

Abstract

This thesis is concerned with multi-source parameter estimation and tracking using antenna arrays in wireless communications. Various multi-source parameter estimation and tracking algorithms are presented and evaluated.

Firstly, a novel multiple-input multiple-output (MIMO) communication system is proposed for multi-parameter channel estimation. A manifold extender is presented for increasing the degrees of freedom (DoF). The proposed approach utilises the extended manifold vectors together with superresolution subspace type algorithms, to achieve the estimation of delay, direction of departure (DOD) and direction of arrival (DOA) of all the paths of the desired user in the presence of multiple access interference (MAI).

Secondly, the MIMO system is extended to a virtual-spatiotemporal system by incorporating the temporal domain of the system towards the objective of further increasing the degrees of freedom. In this system, a multi-parameter estimation of delay, Doppler frequency, DOD and DOA of the desired user, and a beamformer that suppresses the MAI are presented, by utilising the proposed virtual-spatiotemporal manifold extender and the superresolution subspace type algorithms.

Finally, for multi-source tracking, two tracking approaches are proposed based on an arrayed Extended Kalman Filter (arrayed-EKF) and an arrayed Unscented Kalman Filter (arrayed-UKF) using two type of antenna arrays: rigid array and flexible array. If the array is rigid, the proposed approaches employ a spatiotemporal state-space model and a manifold extender to track the source parameters, while if it is flexible the array locations are also tracked simultaneously.

Throughout the thesis, computer simulation studies are presented to investigate and evaluate the performance of all the proposed algorithms.

Declaration of Originality

I hereby declare that this thesis is my own work. Where other sources of information have been used, they have been acknowledged.

Copyright Declaration

Acknowledgments

Firstly, I would like to express my deepest gratitude to my research supervisor Professor Athanassios Manikas for his invaluable guidance and the time and effort he has invested in me throughout my Ph.D research. He has given me extensive guidance in academia with his wide knowledge and taught me to be creative and to think deeply. His way of thinking has a significant impact on my research. I sincerely appreciate his insightful guidance and dedication.

I would also like to thank my colleagues and friends in the Communications and Signal Processing group for their friendships and they have enriched my life in the journey of my Ph.D research. In particular, I would like to thank Yunhao Liu for countless times of technical discussions that we had.

Next, I am profoundly grateful to my parents who have always given me their unconditional love and supported all my decisions. They have always provided me with constant support and encouragement and without their help I wouldn't have chosen the journey of Ph.D research. Their endless love give me the confidence to tackle all the difficulties during my research.

Last but not the least, I owe a debt of gratitude to my beloved husband Yingnan Sun for his love and support. He has been with me and taking care of me during my full Ph.D life. He has always encouraged me and provided me suggestions when I was stuck during my research. He has also always trying his best to cheer me up when I was unhappy. I am what I am today because of him and I will forever be grateful.

Table of Contents

List of Figures

List of Tables

Publications Related to this Thesis

The following papers[1] were published during the Ph.D.

1. Z. Tang and A. Manikas, "DOA and DOD Channel Estimation in MIMO Access Networks," in *IEEE International Conference on Communications (ICC)*, May 2019, pp. 1–6. [1]

2. Z. Tang and A. Manikas, "Direction-of-Arrival Tracking of Multiple Fast-Moving Sources in Antenna Array based Access Networks," in *IEEE International Conference on Communications (ICC)*, Jun. 2020, pp. 1–6. [2]

3. Z. Tang and A. Manikas, "Multi Direction-of-Arrival Tracking Using Rigid and Flexible Antenna Arrays," *IEEE Transactions on Wireless Communications*, vol. 20, no. 11, pp. 7568-7580, Nov. 2021. [3]

4. Z. Tang and A. Manikas, "DOD-DOA Estimation using MIMO Antenna Arrays with Manifold Extenders," in *IEEE International Symposium on Personal, Indoor and Mobile Radio Communications (PIMRC)*, Sep. 2022, pp. 1-6. [4]

[1] Note that paper [1] is related to Chapter 2, papers [2] and [3] are related to Chapter 4, paper [4] is related to Chapter 3.

Notation

A, a	Scalar
$\underline{A}$, $\underline{a}$	Column vector
$\mathbb{A}, \mathbf{r}$	Matrix
$(\cdot)^T, (\cdot)^H, (\cdot)^*$	Transpose, Hermitian transpose, Complex conjugate
$\mathrm{vec}\,(\mathbb{A})$	Column-wise vectorisation of $\mathbb{A}$
$\exp\,(\underline{A})$	Element by element exponential of $\underline{A}$
$\mathbb{O}_{M\times N}$	Matrix of zeros of size $M \times N$
$\odot$	Hadamard product
$\otimes$	Kronecker product
$\mathcal{E}\,\{\cdot\}$	Expectation operator
$\mathbb{I}_N$	$N \times N$ Identity matrix
$\mathrm{diag}\,(\underline{A})$	Diagonal matrix formed from elements of $\underline{A}$
$\underline{1}_N$, $\underline{0}_N$	Column vector of N ones, N zeros
$\mathcal{R}, \mathcal{C}$	Set of real and complex numbers
∇	Vector differential operator
$\det(\mathbb{A})$	Determinant of matrix $\mathbb{A}$
$\mathrm{triu}(\mathbb{A})$	Upper triangular potion of $\mathbb{A}$
$\mathrm{QR}(\mathbb{A})$	QR decomposition of $\mathbb{A}$
$\mathrm{chol}(\mathbb{A})$	Cholesky factorisation of $\mathbb{A}$

Abbreviations

ADC	Analogue-to-Digital
AIC	Akaike Information Criteria
AWGN	Additive White Gaussian Noise
BS	Base Station
CDMA	Code Division Multiple Access
CRB	Cramer Rao Bound
DAC	Digital-to-Analogue
DOA	Direction of Arrival
DOD	Direction of Departure
DoF	Degrees of Freedom
EKF	Extended Kalman Filter
ESPRIT	Estimation of Signal Parameters via Rotation Invariance Techniques
ISI	Inter Symbol Interference
KR	Khatri-Rao
LMS	Least Mean Squares
LOS	Line of Sight
MAI	Multiple Access Interference
MDL	Minimum Descriptor Length

MIMO	Multiple-Input Multiple-Output
ML	Maximum Likelihood
MSE	Mean Square Error
MUSIC	MUltiple SIgnal Classification
NFR	Near Far Ratio
NLOS	Non-Line of Sight
PN	Pseudo Noise
RADAR	Radio Detection And Ranging
RF	Radio Frequency
RMSE	Root Mean Square Error
SIMO	Single-Input Multiple-Output
SNIR	Signal-to-Noise-plus-Interference Ratio
SNR	Signal-to-Noise Ratio
SONAR	SOund Navigation And Ranging
TDL	Tapped Delay Line
TDMA	Time Division Multiple Access
TOA	Time of Arrival
Tx, Rx	Transmitter, Receiver
UAV	Unmanned Aerial Vehicle
UCA	Uniform Circular Array
UKF	Unscented Kalman Filter
ULA	Uniform Linear Array

Chapter 1

Introduction

Parameter estimation has long been of great research interest due to its importance in a variety of applications including wireless communications, sonar, radar, radio astronomy, and navigation. In the future, the demand for parameter estimation in applications of Internet of Things (IoT) [5], intelligent transportation [6], unmanned aerial vehicle (UAV) [7] and massive multiple-input multiple-output (MIMO) for 5G+ [8] arises. As the applications expanded, accurately estimating temporal and spatial parameters has become increasingly important. In wireless communications, technologies designed based on antenna array systems have been widely used in the current generation wireless systems, in particular, massive MIMO is a promising technology for the next generation wireless systems [9]. The array technologies utilise array of several antennas at the transceiver while the massive MIMO utilises large arrays formed by hundreds or thousands of antennas. The use of antenna arrays improves channel capacity, array (or beamforming) gain, multiplexing gain, diversity, robustness against fading and coverage, therefore, antenna array systems could largely improve the overall performance of the wireless networks. The performance of the antenna array system heavily relies on accurate parameter estimation at the base station (BS) so that the system could provide proper downlink beamforming [10]. Furthermore, the wireless traffic vol-

ume is expected to increase to a large extent in the coming decade as the number of connected devices are rising rapidly [11]. Parameter estimation in the presence of co-channel interference appears to be a challenge, which has to be addressed by designing proper algorithms using array signal processing to ensure its accuracy and reliability. Hence, parameter estimation using array signal processing plays an important role in wireless communications.

1.1 Fundamentals of Array Signal Processing

An antenna array is a collection of antennas distributed in a three-dimensional space working together as a unit. The signal received at the antenna array contains temporal and spatial information of the signal environment. By observing the received signal, the objective of the antenna array system is to solve the following general problems, namely

- The detection problem: this problem is to determine the number of emitting sources in the environment at the time of the observation. Many approaches can be utilised to solve this problem, such as Akaike Information Criterion (AIC) [12] and Minimum description length (MDL) [13], both of which are popular approaches of the solutions.

- The channel estimation problem: this problem is concerned with the estimation of channel parameters associated with the desired sources, such as delays, Direction of Departure (DOD), Direction of Arrival (DOA), velocities, Doppler frequencies, etc. Among these, the DOA is the most important parameter to be estimated in array signal processing. Several DOA estimation approaches have been developed including the MUltiple SIgnal Classification (MUSIC) algorithm [14], and the Estimation of Signal Parameters via Rotational Invariance Technique (ESPRIT) [15].

- The reception problem: this problem is concerned with acquiring the desired signals from particular directions and suppressing undesired signals from all other directions. It involves the weight design at the receiver and/or transmitter to provide high gains to the direction of the desired sources and to eliminate the interferences. Various beamforming approaches have been proposed for resolving the reception problem, such as Capon's beamformer [16] and Wiener-Hopf beamformer [17].

The three aforementioned problems are the major problems in array signal processing and they are interrelated. Extensive research has been carried out to address these problems, including a wide range of solutions in radar, sonar, wireless communications, etc.

Consider an array of N antennas, the locations of these antennas are denoted by

$$\mathbf{r} = [\underline{r}_1, \underline{r}_2, ..., \underline{r}_m ..., \underline{r}_N] = \left[\underline{r}_x, \underline{r}_y, \underline{r}_z\right]^T \in \mathcal{R}^{3\times N} \tag{1.1}$$

where the vector $\underline{r}_m \in \mathcal{R}^{3\times 1}$ denotes the Cartesian coordinates of the m-th antenna and the $N \times 1$ vectors $\underline{r}_x$, $\underline{r}_y$, $\underline{r}_z$ are the Cartesian coordinates of all antennas on the x-axis, y-axis and z-axis, respectively. Consider the array operates in the presence of multiple far field sources. The far field implies that the radius of the propagation is large enough so that the wavefronts are plane wave. The plane wave propagation model is illustrated in Figure 1.1. The propagation delay between the m-th array element and the array reference point can be expressed as a function of the direction of arrival (θ, ϕ) and is obtained as

$$\tau_m = \frac{\underline{r}_m^T \underline{u}\left(\theta, \phi\right)}{c} \tag{1.2}$$

where c is the speed of signal propagation and $\underline{u}\left(\theta, \phi\right)$ denotes the (3×1) unit-norm vector pointing towards the direction (θ, ϕ) given by

$$\underline{u}\left(\theta, \phi\right) = [\cos\theta\cos\phi, \sin\theta\cos\phi, \sin\phi]^T \tag{1.3}$$

The response of an array to a plane wave arriving from the direction (θ, ϕ) is termed as the array manifold vector $\underline{S} \in \mathcal{C}^{N\times 1}$, (or the array response vector), and is formed as a function of the direction-of-arrival (DOA), carrier frequency F_c, velocity of light c and the Cartesian coordinates of the antenna array elements $[\underline{r}_1, \underline{r}_2, ..., \underline{r}_N]$, defined as follows

$$\underline{S} \triangleq \underline{S}(\theta, \phi) = \exp\left(-j\frac{2\pi F_c}{c}\left[\underline{r}_1, \underline{r}_2, ..., \underline{r}_N\right]^T \underline{u}(\theta, \phi)\right) \tag{1.4}$$

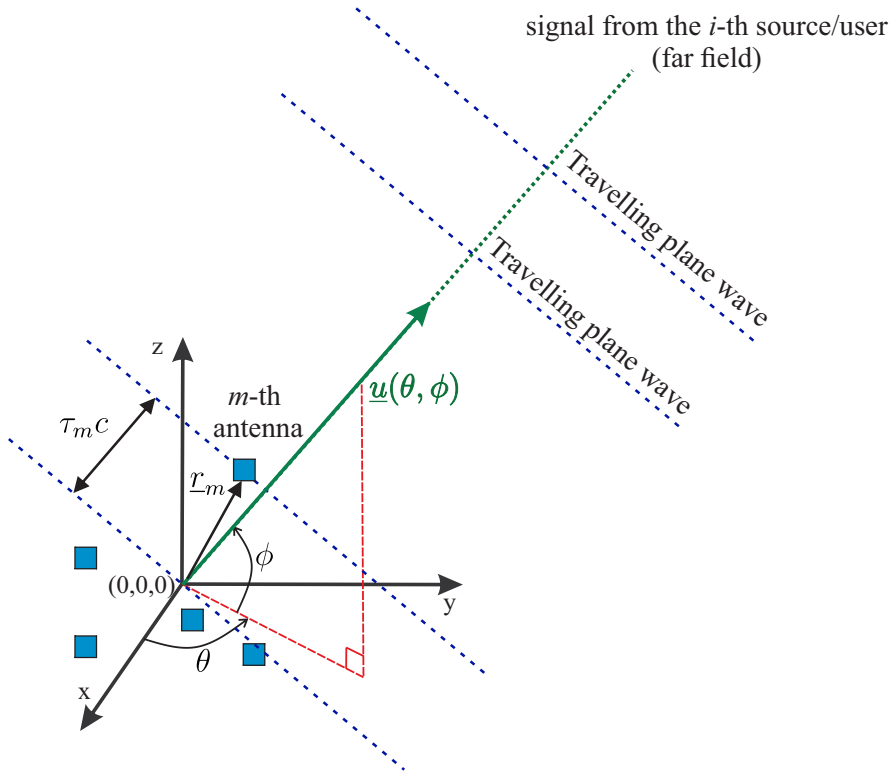

Figure 1.1: Illustration of plane wave propogation from the i-th source/user to a small aperture array.

1.2 The Concept of the Array Manifold

The array manifold vector in Equ 1.4 is generalized to $\underline{S}(p)$ where p is the parameter of interest. The locus of all the array manifold vectors for the range of the

parameter p is defined as the array manifold $\mathcal{A}$ [18], which is given as

$$\mathcal{A} \triangleq \left\{ \underline{S}\left(p\right) \in \mathcal{C}^N, \forall p : p \in \Omega \right\} \tag{1.5}$$

and is illustrated in Figure 1.2, where Ω denotes the parameter space.

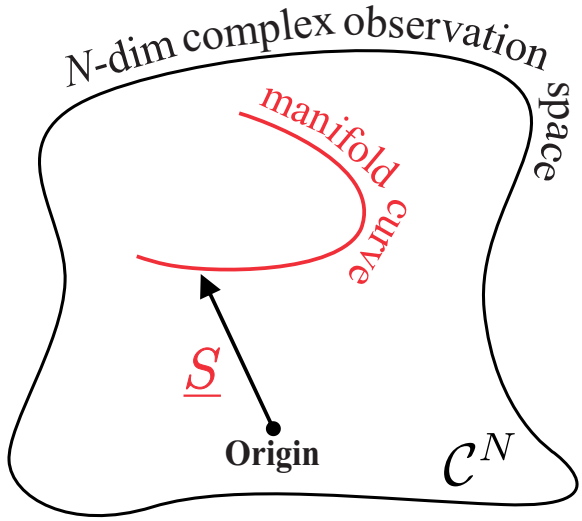

Figure 1.2: Illustration of the array manifold.

The array manifold of an array of sensors (antennas, microphones, etc.) is a mathematical object embedded in a N-dimensional complex Hilbert space shown in Figure 1.2. Note that the array manifold can be a function of more than one parameters. If there is one parameter, i.e. DOA, the array manifold is a curve embedded in an N-dimensional complex space. If there are two parameters, then $p = \underline{p}$, the array manifold is a surface. The array manifold fully characterises any array geometry. In modelling and solving the problems in array signal processing, the concept of the array manifold is of vital significance.

1.3 The Concept of the Manifold Extender

The concept of the "manifold extender" is a complex mapping which maps the "spatial" manifold to the "extended" manifold under certain constraints [19] and it can be visualised in Figure 1.3 illustrating the mapping of the manifold (i.e. the

locus of all manifold vectors $\underline{S}$) to an extended manifold (i.e. the locus of all new extended manifolds vectors $\underline{h}$). In this figure the extended manifold is an "extended curve" and its properties can be analysed as a function $f\{\cdot\}$ of the properties of the original manifold curve, using differential geometry. The proofs can be found in [18], [19] and more explanations can be found in [18, 19, 20, 21]. The "manifold extender" takes into account additional system parameters to extend the dimensionality of the signal observation space, and thus the degrees of freedom can be increased.

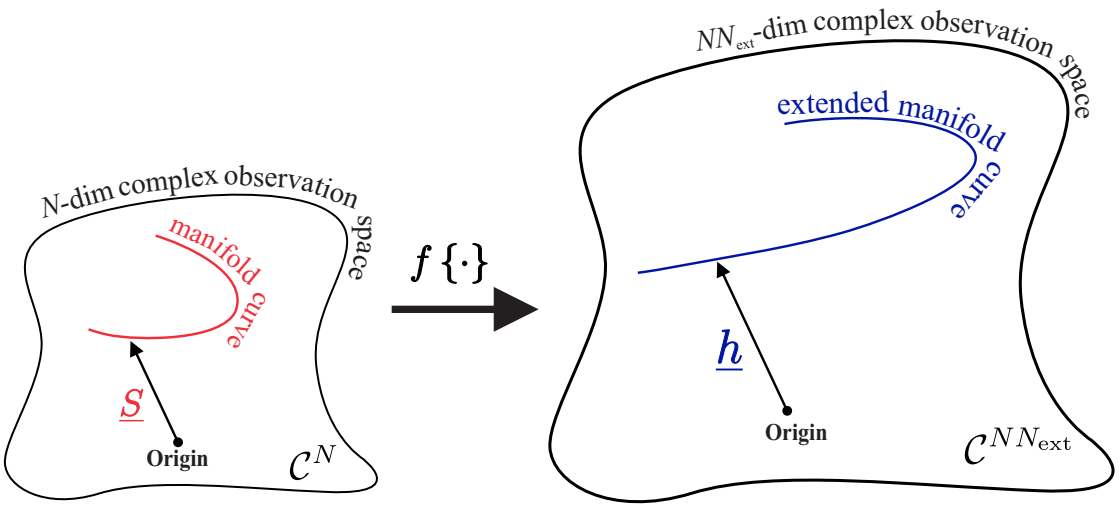

Figure 1.3: Visualisation of the "Manifold Extender".

In this thesis, the concept of the "manifold extender" has been explored in the three technical chapters of this thesis. The "manifold extender" extends the observation space of an array system from N to NN_{ext} where N_{ext} denotes the extended dimension. The value of N_{ext} depends on the algorithms to design the "manifold extender". In this thesis, different "manifold extenders" have been designed and evaluated, and different "extended" manifold vectors obtained by different manifold extenders have been presented and discussed, all of which are functions of the original manifold vector.

1.4 Challenges and Gaps

There are a number of challenges and gaps in multi-source parameter estimation and tracking in wireless communications that have not been fully covered in the literature, the following is the listed problems to be addressed in this thesis.

1. **Multi-source parameter estimation**

   Subspace-based techniques are one of the most widely used techniques in parameter estimation algorithms. However, to achieve desired estimation accuracy, conventional subspace techniques require the signal to noise ratio and the number of snapshot to be high. In addition, it also needs the number of Rx antennas to be larger than the number of signals. In wireless communications, a key challenge is to estimate channel parameters of the desired source whilst providing complete interference cancellation (asymptotically) of the undesired sources, and also to accommodate the number of signals that is much greater than the number of Rx antennas. Thus, it is vital to design algorithms to address the aforementioned issues for the future communication systems, which, forms a contribution of this thesis.

2. **Parametric channel modelling**

   Appropriate channel modelling is of critical importance in designing array processing algorithms in wireless communication systems. Extensive researches have been done to design channel models. However, most of the existing models are "non-parametric", which however are problematic. "Non-parametric" models are described as random matrices $\mathbb{H}$ conformed to specific distributions and they characterise the channel independently of channel parameters such as DOA and ignore the array geometry. The channel estimation using such models would need to estimate a number of variables equal to the number of dimensions of $\mathbb{H}$ (i.e. to estimate all the elements of

$\mathbb{H}$ which are unknown complex numbers). However, with the development of the future communication systems, massive array systems are expected to be widely used, and this will largely increase the size of the channel matrix making the channel estimation complicated and impractical. In addition, measurement campaign in [22] indicates that non-parametric models are not applicable for massive MIMO system as the scattering environment does not show rich. The majority of channel state information (CSI) techniques in various commercial systems employ pilot signals which are spectrum inefficient. Furthermore, in the open literature, it is assumed that the CSI is known and the research is limited on analysing the performance of a system in the presence of partial knowledge of the CSI. This is a serious drawback of the current state of the art and in this thesis novel powerful "blind" and spectrum efficient MIMO channel estimation techniques are proposed.

3. **Enhancing degrees of freedom**

   Future communication systems are expected to operate in very high density signal/user environments with high speeds without sacrificing the quality of service. Using antenna arrays at both the transmitter and receiver allows a multitude of devices and users communicating with each other at the same time on the same frequency band, possibly within small enclosures. Consequently, the biggest challenge for future communication systems is the ability to handle a very large number of co-channel received signals higher than the number of signals in the current generation of communication systems. This drives the requirement for future communication systems to deliver higher number of degrees-of-freedom that will enable the system to detect, resolve and isolate signals from a large number of interfering sources with greater accuracy. Thus, enhancing the degrees of freedom becomes the major objective of this thesis.

4. **Tracking in non-stationary environment**

   Tracking the DOA of multiple moving sources is a significant research topic in array signal processing, due to its wide applications in sonar, radar, air traffic control, mobile communications, remote sensing, etc. For static sources, it is well known that their DOA can be estimated using, for instance, signal-subspace algorithms (e.g. [14]). If the motion of the sources is slow, then small time-frames can be used and, for each time-frame, apply a DOA estimation algorithm (i.e. repetitive DOA estimation) tracking small variations in DOA. However, if the source is moving too fast so that the source cannot be assumed stationary over a small time-frame, these high-resolution algorithms with repetitive DOA estimation begin to exhibit performance degradation. Furthermore, these DOA algorithms suffer from the data association problem. Several approaches have been proposed to avoid this problem by maintaining the order of the DOA estimates for different iterations [23, 24]. However, these approaches suffer from spread array spatial spectrum effects caused by rapid source motion. To remedy the aforementioned problems, various algorithms based on state space models have been proposed. However, these approaches have high computational complexity. In this thesis, the aforementioned problems are addressed.

5. **Tracking with Flexible arrays**

   Using flexible array geometries is an interesting problem in array signal processing for airborne, vehicular, underwater and other applications. The "flexible array" is defined as an antenna array with time varying geometry, i.e. each of the array elements moves independently. If the array geometry is flexible, i.e. the array geometry changes as a function of time, then the majority (if not all) of the array processing algorithms and theory cannot be directly used. Thus, it is important to design approaches that are suitable for

tracking sources in non-stationary environment with flexible arrays, which, constitutes a contribution of this thesis.

1.5 Thesis Scope and Organisation

This thesis is concerned with estimation and tracking of multi-source parameters using antenna arrays. Array signal processing algorithms are designed for estimating and tracking different parameters of multiple sources in presence of co-channel interference and enhancing the degrees of freedom. Both rigid array and flexible array are investigated for simultaneously tracking non-stationary sources and array locations. The performance of the algorithms and approaches for each chapter are evaluated using computer simulation studies. The rest of this thesis is organised as follows:

In Chapter 2, a joint DOD and DOA estimation approach is presented for MIMO system. The proposed approach extends the signal observation space to form the extended manifold vectors and increase the degrees of freedom. Then, by using the extended manifold vectors as well as a superresolution subspace approach, the proposed approach is able to estimate the DOD and DOA of all the paths of the desired user in the presence of multiple access interference.

In Chapter 3, a virtual-spatiotemporal MIMO system is presented which is an extension of the system proposed in Chapter 2 towards the aim of further increasing the degrees of freedom. To achieve this, a virtual-spatiotemporal manifold extender is designed to increase the dimensionality of signal observation space even further. Then, a joint DOD-DOA estimation, delay-Doppler estimation and beamforming algorithms are presented and computer simulation studies show the superiority of the proposed algorithms.

Chapter 4 is concerned with DOA tracking of multiple far-field moving sources in wireless communications using antenna arrays. Two novel approaches are pro-

posed using a rigid array and a flexible array, a spatiotemporal state-space model and a manifold extender for simultaneously tracking multiple DOAs snapshot-by-snapshot. In addition, if the array is flexible, the array locations are also simultaneously tracked with the DOAs. In particular, all the antenna array elements (in a constant or a time varying geometry) work together as one unit. Furthermore, the concept of "manifold extender" is employed which increases the "degrees of freedom" of the system.

Finally, in Chapter 5, the conclusions of the thesis are drawn, the main contributions of the thesis are outlined and the ideas for future works are presented.

Chapter 2

DOA and DOD Channel Estimation

In this chapter, a novel joint DOA and DOD estimation approach is proposed for MIMO systems. In the proposed system, a weight-vector of $\overline{N}$ orthogonal binary signals of length $\mathcal{N}_c$ is employed on the Tx-array where $\overline{N}$ is the number of Tx-array elements, and then used at the Rx-array to extend the observation space of the received signals from N to NN_{ext} where $N_{\text{ext}} = \overline{N}$ by using a "virtual" manifold extender. In the extended observation space the manifold vectors are functions of both the DOA and DOD. The proposed approach uses these extended manifold vectors, in conjunction with a proposed superresolution subspace approach, to find the DOA and DOD of all the multipaths of the desired user in the presence of other multiple-access users, considering that all users transmit at the same time and in the same frequency band. The results show that the proposed approach performs better than conventional MIMO approach in terms of the estimation accuracy.

2.1 Introduction

With an exponential increase in the number of users, it is expected that the wireless traffic will grow a thousand-fold in the next decade [11] so that the wireless communication systems will operate in extremely dense signal environment. To address this problem, massive MIMO array systems have been proposed, which increase the degrees of freedom in order to handle the dense signal environment, suppress co-channel interference and improve channel estimation accuracy. However, there are two main theoretical frameworks for increasing the degrees of freedom:

1. to increase the number of antenna elements [25], i.e. to employ more hardware, and

2. to increase the observation space of the received signals and thus to use the concept of "extended" manifolds [19].

The novel approach proposed in this chapter belongs to the second theoretical framework and increases the degrees-of-freedom using an "extended" manifold which is known as the "virtual array" manifold. It also employs a parametric channel model combined with superresolution subspace based algorithms, to estimate the channel parameters of DOA and DOD with enhanced accuracy.

2.1.1 Channel Modelling

In terms of channel modelling in MIMO systems, the MIMO channel between an $\overline{N}$ element Tx array and an N element Rx array can be modelled in a non-parametric way or in a parametric way. In general, non-parametric channel is modelled as random matrix $\mathbb{H} \in \mathcal{C}^{N \times \overline{N}}$ following certain distributions. Most of the channel estimation approaches in the literature depend on "non-parametric" (statistical) channel models such as the Kronecker-based model [26] which requires rich scattering. However, the practical scattering scenario is not rich enough.

A statistical model presented in [27] models the channel using a virtual spatial matrix and Discrete Fourier Transform (DFT) matrices. However, this model is limited only to uniform linear arrays. Similar model can be found in [28] which uses a unitary basis instead of a Fourier basis. Such model ignores the spatial information of the MIMO systems (i.e. array geometry). A review [29] surveys a variety of statistical channel models. "Non-parametric" models, which characterise the channel independent of the channel parameters, are not suitable in practical scenarios, especially when the number of antennas is large.

Most of the MIMO system approaches assume statistical channel models which are based on the CSI matrix whose elements are complex numbers representing the links from each Tx antenna to each Rx antenna. Thus, the array geometries have been ignored. On the other hand, parametric models characterise the channel on the basis of wave propagation from the Tx array to the Rx array, instead of from each Tx antenna to each Rx antenna. Such models are characterised by tractable parameters such as relative delay, DOA, DOD, array geometries of both Tx and Rx, etc. This kind of model more accurately describe the actual wave propagation environment. With such models, the reconstruction of the channel matrix is independent of the number of antennas.

2.1.2 Parameter Estimation Approaches

Typical parameter estimation approaches are beamforming approaches, subspace-based approaches and maximum likelihood (ML)-based approaches.

Although beamforming approaches are mainly used for receiving the desired signal whilst suppressing the interference, several beamforming approaches can also be used for parameter estimation. In this case, they estimate the parameters by finding the maximum (or minimum) peaks of the constructed spectrum-like functions. The idea is to steer the array to a range of directions and then to

find the estimated directions which give the maximum power. For example, the Bartlett [30] beamformer and the Capon [16] beamformer are typical approaches of this class, but they are limited by the array structure and cannot resolve the paths which are closely spaced.

The ML-based approaches involve multidimensional search of all the parameters based on the underlying signal model [31]. Thus, by considering the modelling of the signal waveform, this class can be classified into either stochastic ML approaches [32] if the signal is assumed Gaussian or deterministic ML approaches [33] if the signal is assumed deterministic and arbitrary. The ML-based approaches in general require to solve nonlinear multidimensional optimization problems which have high computational cost. Several ML approximations have been proposed towards the aim of reducing the computational complexity, such as the Estimate Maximise (EM) algorithm [34] and its extended algorithm space-alternating generalized expectation-maximisation (SAGE) [35].

The subspace-based approaches carry out the estimation by utilising eigendecomposition of the array covariance matrix and use eigenvalues to partition the signal subspace and noise subspace. Typical methods of the subspace-based approaches include MUSIC [14], subspace fitting [36], ESPRIT [15] and Root-MUSIC [37]. The MUSIC and ESPRIT techniques are two widely used subspace-based techniques which can provide high resolution and acceptable computational complexity. However, they require the SNR and the number of snapshots to be relatively high. These problems can be relieved by using subspace fitting methods [36] at the cost of increased computational complexity. The ESPRIT and Root-MUSIC do not require searching, instead they have restrictions on the array geometry. The ESPRIT requires the array to have its identical copy and the Root-MUSIC approach requires the array to be Uniform Linear Array (ULA). A review of the subspace-based approaches can be found in [38]. In this chapter, a novel superresolution subspace-based approach is proposed which provides satisfied estimation

results without the restriction of high SNR, large number of snapshots or specific array geometry, see [19].

2.1.3 DOA and DOD Estimation

In wireless communications, most of the direction finding approaches are concerned with the Direction of Arrival (DOA) estimation problem while the Direction of Departure (DOD) estimation has been ignored. DOA estimation has been an important research area with many applications, including wireless communications, radar, sonar, radio astronomy, etc. On the other hand, only a small number of research has focused on the DOD estimation, with the majority of these approaches designed for radar and sonar applications. Although DOD estimation is also important in wireless communications, it has not yet been extensively investigated.

In the literature, a DOD estimation approach has been proposed in [39] by exploiting the cooperation between the Tx and the Rx. The Tx beamformer rotates its mainlobe then the Rx measures the power level at the output of the Rx beamformer and the DOD is connected to the largest power. Several papers have been proposed for joint estimation of DOD and DOA. For instance, in [40], a Cramer-Rao bound (CRB) based on DOA and DOD using Multi-Mode Antennas is derived, and then a beamformer is presented to estimate the DOA and DOD by minimising this CRB. In [41], the DOD and DOA have been estimated using a Bartlett beamforming method and a SAGE algorithm [42], and it is implemented in a measurement campaign with dual-polarized arrays and assumed a line-of-sight (LoS) environment. In [43], using a single antenna at the transmitter which provides switched transmitting beams, a joint TDOA, DOA-DOD estimation based on a 3D unitary ESPRIT approach is presented. In [44], the transmit and receive auxiliary beam pairs were designed based on a multi-layer pilot structure for estimating DODs and DOAs in dual-polarized MIMO systems. In this chapter,

unlike the systems in [43] and [44] which use pilots, our proposed DOD and DOA estimation algorithm is blind.

The rest of this chapter is organised as follows. In Section 2.2, the MIMO array system is described and the received array signal vector is modelled. This signal is then extended to a "virtual" signal which is embedded in a bigger observation space, allowing the extended manifold vector of the desired signal paths to be a function of both DOA and DOD. Then, a DOA and DOD subspace estimation algorithm based on the proposed virtual manifold vector is presented in Section 2.3. In Section 2.4, the performance of the proposed approach is evaluated via computer simulation studies. Finally, the chapter is summarised in Section 2.5.

2.2 System Model

Consider a MIMO multi-user system with $\overline{N}$-antenna Tx-array and N-antenna Rx-array. Figure 2.1 illustrates the system representation consisting of a transmitter, a channel, a receiver and M co-channel users (the desired plus $M-1$ MAI). With reference to point-A in Figure 2.1, the i-th user transmits a sequence of data symbols $\{\mathrm{a}_i[n], \forall n\}$ with symbol duration T_{cs}. This sequence is then weighted by a weight-code matrix $\mathbb{W}_i$ producing at point-B (during the n-th symbol period) the $\overline{N} \times \mathcal{N}_c$ matrix $\mathbb{W}_i^T \mathrm{a}_i[n]$ where

$$\mathbb{W}_i = \left[\underline{w}_{i1}, \underline{w}_{i2}, ..., \underline{w}_{i\mathrm{j}}, ..., \underline{w}_{i\overline{N}}\right] \in \mathcal{R}^{\mathcal{N}_c \times \overline{N}} \tag{2.1}$$

where $\underline{w}_{i\mathrm{j}} \in \mathcal{R}^{\mathcal{N}_c \times 1}$ denotes the weight-code signal of length $\mathcal{N}_c$ associated with the j-th Tx antenna of the i-th user, which is given as

$$\underline{w}_{i\mathrm{j}} \triangleq \left[w_{i\mathrm{j}}[1], w_{i\mathrm{j}}[2], ..., w_{i\mathrm{j}}[q], ..., w_{i\mathrm{j}}[\mathcal{N}_c]\right]^T \tag{2.2}$$

with $\{w_{i\mathrm{j}}[q] \in \pm 1, q \in [1, \mathcal{N}_c]\}$ and

$$\mathbb{W}_i^T \mathbb{W}_j \simeq \begin{cases} \mathbb{I}_{\overline{N}}, & \text{for } i = j \\ \mathbb{O}_{\overline{N} \times \overline{N}}, & \text{for } i \neq j \end{cases} \tag{2.3}$$

Then, each row (i.e. $\overline{N}$ elements) of this matrix $\mathbb{W}_i^T \mathrm{a}_i[n]$ is driven to a bank of $\overline{N}$ DACs which produces at point-C the baseband transmitted signal vector $\underline{m}_i(t) \in \mathcal{C}^{\overline{N}\times 1}$

$$\underline{m}_i(t) = [m_{i1}(t), m_{i2}(t), ..., m_{i\mathrm{j}}(t), ..., m_{i\overline{N}}(t)]^T \tag{2.4}$$

where $m_{i\mathrm{j}}(t)$ denotes the analogue signal of the i-th user in the j-th Tx antenna modelled as follows

$$m_{i\mathrm{j}}(t) = \sum_{n=1}^{\infty} \mathrm{a}_i[n] \sum_{q=1}^{\mathcal{N}_c} w_{i\mathrm{j}}[q]\, p(t-(n-1)T_{cs}-(q-1)T_c) \tag{2.5}$$

with $T_{cs} = \mathcal{N}_c T_c$, $p(t)$ representing a pulse shaping filter of period T_c and $(n-1)T_{cs} + (q-1)T_c \leq t < (n-1)T_{cs} + qT_c$.

Assuming that the transmitted signal of the i-th user (point-D) arrives at the receiver through K_i multipaths, the MIMO channel in Figure 2.1 will have K_i branches. With reference to the k-th path of the i-th user, the parameter τ_{ik} denotes the delay, the vectors $\underline{\overline{S}}_{ik} \in \mathcal{C}^{\overline{N}\times 1}$ and $\underline{S}_{ik} \in \mathcal{C}^{N\times 1}$ represent the corresponding Tx and Rx manifold vectors, respectively, while $\beta_{ik}(t)$ is the complex path fading coefficient, which is assumed to be a time-varying function in this chapter.

Consequently, with reference to point-E in Figure 2.1, the received signal $\underline{x}(t) \in \mathcal{C}^{N\times 1}$ can be modelled as follows

$$\underline{x}(t) = \sum_{i=1}^{M}\sum_{k=1}^{K_i} \beta_{ik}(t)\, \underline{S}_{ik}\underline{\overline{S}}_{ik}^H \underline{m}_i(t-\tau_{ik}) + \underline{\mathrm{n}}(t) \tag{2.6}$$

where the Tx and Rx array manifold vectors[1] are defined, respectively, as follows:

$$\underline{\overline{S}}_{ik} \triangleq \underline{\overline{S}}(\overline{\theta}_{ik}) = \exp\left(+j\frac{2\pi}{\lambda}\, [\underline{\overline{r}}_1, \underline{\overline{r}}_2, ..., \underline{\overline{r}}_{\overline{N}}]^T \begin{bmatrix} \cos(\overline{\theta}_{ik}) \\ \sin(\overline{\theta}_{ik}) \\ 0 \end{bmatrix} \right) \tag{2.7}$$

[1] With no loss of generality, it is assumed that all users are located on the (x-y) plane so that the elevation angle ϕ_{ik} is equal to zero, $\forall i \& \forall k$, and thus it has been ignored.

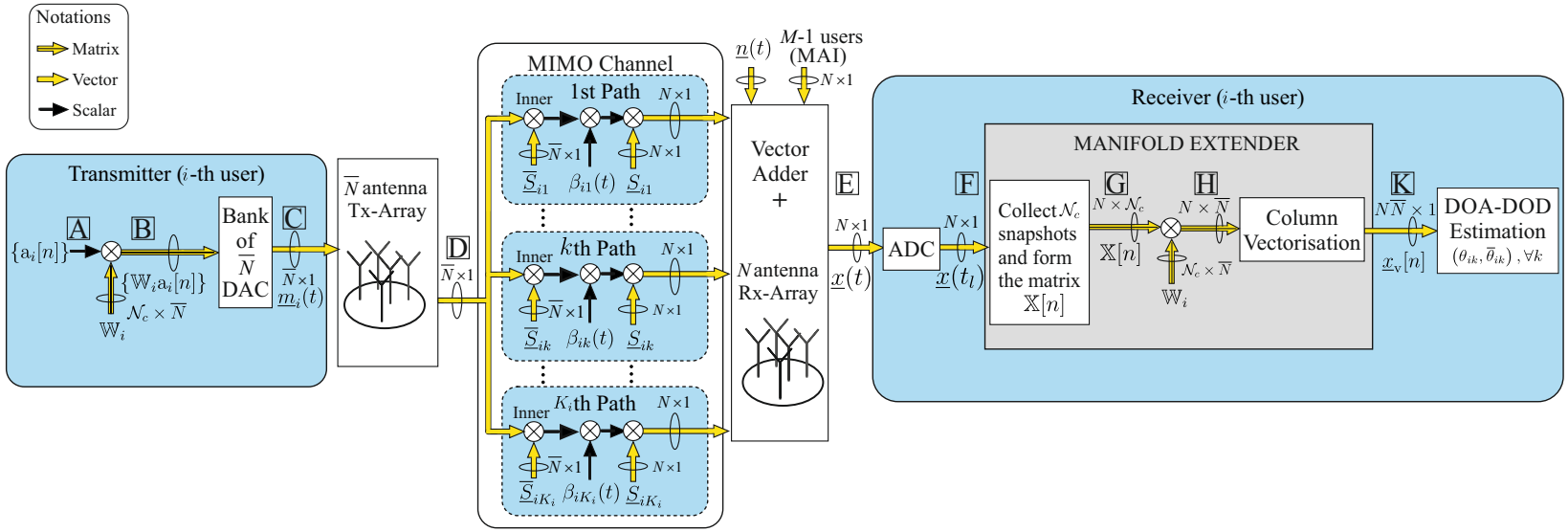

Figure 2.1: Baseband representation of the proposed array system consisting of a transmitter, a channel, a receiver and M co-channel users.

$$\underline{S}_{ik} \triangleq \underline{S}(\theta_{ik}) = \exp\left(-j\frac{2\pi}{\lambda}\left[\underline{r}_1, \underline{r}_2, ..., \underline{r}_N\right]^T \begin{bmatrix} \cos(\theta_{ik}) \\ \sin(\theta_{ik}) \\ 0 \end{bmatrix}\right) \tag{2.8}$$

Note that $\overline{\theta}_{ik}$ denotes the DOD of the k-th path of the i-th user and θ_{ik} denotes the DOA of this path. The matrices $[\underline{\overline{r}}_1, \underline{\overline{r}}_2, ..., \underline{\overline{r}}_{\overline{N}}] \in \mathcal{R}^{3\times\overline{N}}$ and $[\underline{r}_1, \underline{r}_2, ..., \underline{r}_N] \in \mathcal{R}^{3\times N}$ have columns the Cartesian coordinates of the Tx and Rx array elements, respectively. The scalar $\lambda \triangleq c/F_c$ is the wavelength with F_c representing the carrier frequency while c is the velocity of light. Note that without any loss of generality, $\beta_{ik}(t)$ is Gaussian, i.e. the gain $|\beta_{ik}(t)|$ follows a Rayleigh distribution and the phase of $\beta_{ik}(t)$ follows a uniform distribution. The vector $\underline{\mathrm{n}}(t) \in \mathcal{C}^{N\times 1}$ is the complex additive Gaussian noise vector of zero mean and covariance matrix

$$\begin{aligned} \mathbb{R}_{\mathrm{nn}} &= \mathcal{E}\left\{\underline{\mathrm{n}}(t)\underline{\mathrm{n}}^H(t)\right\} \\ &= \sigma_{\mathrm{n}}^2 \mathbb{I}_N \end{aligned} \tag{2.9}$$

where σ_{n}^2 is the unknown noise power.

The received signal $\underline{x}(t)$ at point-E is initially discretised with a sampling period of T_c to provide at point-F the vector $\underline{x}(t_l)$,$\forall l$. Then, the "manifold extender" transforms the $\underline{x}(t_l) \in \mathcal{C}^{N\times 1}$ to $\underline{x}_{\mathrm{v}}[n] \in \mathcal{C}^{N\overline{N}\times 1}$ as follows. Initially, by collecting $\mathcal{N}_c$ snapshot vectors the matrix $\mathbb{X}[n] \in \mathcal{C}^{N\times\mathcal{N}_c}$ corresponding to the n-th symbol interval is formed, which can be modelled as follows

$$\begin{aligned} \mathbb{X}[n] &= \sum_{i=1}^{M}\sum_{k=1}^{K_i} \beta_{ik}[n]\, \underline{S}_{ik}\overline{\underline{S}}_{ik}^H \mathbb{W}_i^T \left(\left(\mathbb{J}^T\right)^{\ell_{ik}} \mathrm{a}_i[n] + \mathbb{J}^{\mathcal{N}_c-\ell_{ik}}\mathrm{a}_i[n-1]\right) \\ &\quad + \mathbb{N}[n] \end{aligned} \tag{2.10}$$

where $\ell_{ik} = \left\lfloor \frac{\tau_{ik}}{T_c} \right\rfloor \mathrm{mod}\, \mathcal{N}_c$ is the discretised delay shown in Figure 2.2. Note that the $\mathcal{N}_c \times \mathcal{N}_c$ matrix $\mathbb{J}$ (or $\mathbb{J}^T$) is the "shifting" matrix defined as

$$\mathbb{J} = \begin{bmatrix} \underline{0}_{\mathcal{N}_c-1}^T, & 0 \\ \mathbb{I}_{\mathcal{N}_c-1}, & \underline{0}_{\mathcal{N}_c-1} \end{bmatrix} \tag{2.11}$$

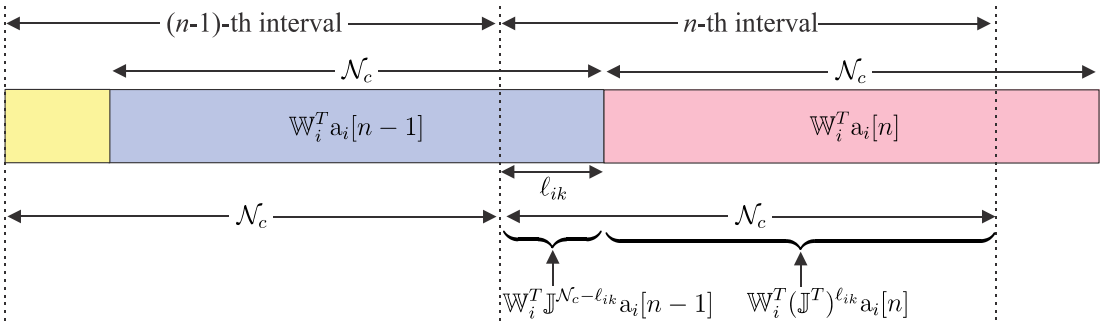

Figure 2.2: Illustration of the delay ℓ_{ik} and the modelling of the data symbols received during the n-th time-interval.

and the power ℓ of $\mathbb{J}$ (or $\mathbb{J}^T$) when applied to a matrix $\mathbb{Z} \in \mathcal{C}^{\overline{N}\times\mathcal{N}_c}$, i.e. $\mathbb{Z}\mathbb{J}^\ell$ $\left(\text{or } \mathbb{Z}\left(\mathbb{J}^T\right)^\ell\right)$, leftshifts (or rightshifts) the matrix $\mathbb{Z}$ by ℓ elements.

In Equ 2.10, at the n-th time interval, the scalar $\beta_{ik}[n]$ denotes the complex path fading coefficient of the k-th path of the i-th user and the matrix $\mathbb{N}[n] \in \mathcal{C}^{N\times\mathcal{N}_c}$ represents the noise matrix with columns the discretised noise snapshots.

In this chapter, with no loss of generality, the first user is assumed to be the desired user. By multiplying the received data matrix $\mathbb{X}[n]$ in Equ 2.10 with the matrix $\mathbb{W}_1$, the matrix $\mathbb{X}[n]\mathbb{W}_1$ is formed at point-H. Then, at the output of the manifold extender (point-K), the virtual snapshot vector is formed as follows

$$\underline{x}_{\mathrm{v}}[n] = \mathrm{vec}\left(\mathbb{X}[n]\,\mathbb{W}_1\right) \tag{2.12}$$

which can be expanded as

$$\begin{aligned}\underline{x}_{\mathrm{v}}[n] = &\underbrace{\sum_{k=1}^{K_1} \beta_{1k}[n]\,\mathbb{A}_{1k}[n]\,\overbrace{\left(\overline{\underline{S}}_{1k}^{*} \otimes \underline{S}_{1k}\right)}^{\underline{S}_{\mathrm{v},1k}}}_{\text{Desired term}} \\ &+ \underbrace{\sum_{i=2}^{M}\sum_{k=1}^{K_i} \beta_{ik}[n]\,\mathbb{A}_{ik}[n]\,\overbrace{\left(\overline{\underline{S}}_{ik}^{*} \otimes \underline{S}_{ik}\right)}^{\underline{S}_{\mathrm{v},ik}}}_{\text{MAI term}} \\ &+ \underbrace{\underline{\mathrm{n}}_{\mathrm{v}}[n]}_{\text{Noise}}\end{aligned} \tag{2.13}$$

where the matrix $\mathbb{A}_{ik}[n] \in \mathcal{C}^{N\overline{N}\times N\overline{N}}$ (for $i = 1, 2, ..., M$) is given[2] as

$$\begin{aligned}\mathbb{A}_{ik}[n] &= \overbrace{\left(\left(\mathbb{W}_1^T \mathbb{J}^{\ell_{ik}} \mathbb{W}_i\right) \otimes \mathbb{I}_N\right)}^{\mathbb{T}_{ik}} \mathrm{a}_i[n] \\ &+ \overbrace{\left(\left(\mathbb{W}_1^T \left(\mathbb{J}^T\right)^{\mathcal{N}_c - \ell_{ik}} \mathbb{W}_i\right) \otimes \mathbb{I}_N\right)}^{\mathbb{T}_{ik,\mathrm{ISI}}} \mathrm{a}_i[n-1] \end{aligned} \tag{2.14}$$

In addition, the vector $\underline{\mathrm{n}}_{\mathrm{v}}[n] \in \mathcal{C}^{N\overline{N}\times 1}$ denotes the virtual noise vector given by

$$\underline{\mathrm{n}}_{\mathrm{v}}[n] = \mathrm{vec}\left(\mathbb{N}[n]\,\mathbb{W}_1\right) \tag{2.15}$$

In Equ 2.13, the virtual snapshot vector $\underline{x}_{\mathrm{v}}[n]$ is expressed as a function of a virtual manifold vector $\underline{S}_{\mathrm{v},ik} \triangleq \underline{S}_{\mathrm{v}}(\overline{\theta}_{ik}, \theta_{ik}) \in \mathcal{C}^{N\overline{N}\times 1}$ of the k-th path of the i-th user, as follows

$$\underline{S}_{\mathrm{v},ik} = \overline{\underline{S}}_{ik}^{*} \otimes \underline{S}_{ik} \tag{2.16}$$

Finally, it is important to point out that the theoretical covariance matrix (second order statistics) $\mathbb{R}_{x_{\mathrm{v}}x_{\mathrm{v}}} \in \mathcal{C}^{N\overline{N}\times N\overline{N}}$ of the virtual array signal $\underline{x}_{\mathrm{v}}[n]$ is as follows

$$\mathbb{R}_{x_{\mathrm{v}}x_{\mathrm{v}}} = \mathcal{E}\left\{\underline{x}_{\mathrm{v}}[n]\,\underline{x}_{\mathrm{v}}^H[n]\right\} \tag{2.17}$$

which in practice, assuming L symbols, can be expressed as

$$\mathbb{R}_{x_{\mathrm{v}}x_{\mathrm{v}}} \simeq \frac{1}{L}\sum_{n=1}^{L} \underline{x}_{\mathrm{v}}[n]\,\underline{x}_{\mathrm{v}}^H[n] \tag{2.18}$$

By observing the $\underline{x}_{\mathrm{v}}[n]$ or its covariance matrix $\mathbb{R}_{x_{\mathrm{v}}x_{\mathrm{v}}}$, it is clear that the dimensionality of the complex "observation" space is $N\overline{N}$ while the dimensionality of a conventional MIMO system is N (number of Rx array elements). This indicates that the proposed array system has more degrees of freedom so that it is more suitable for any future dense access communication networks. In addition, the proposed system does not cause "latency".

[2] The second term in Equ 2.14 is the "Inter-Symbol Interference" (ISI) effects and is related to the delay ℓ_{ik} (if ℓ_{ik}=0 then the second term is a zero matrix).

2.3 DOA and DOD Estimation Algorithm using the Virtual Array Manifold (Manifold Extender)

In this chapter, we focus on the estimation of the parameters (DOD, DOA) of all the multipaths of the desired user, i.e. $\left(\overline{\theta}_{1k}, \theta_{1k}\right) \forall k$, assuming that L symbols are collected at the output of the "manifold extender" at the receiver. Based on the eigen-decomposition of Equ 2.17, the $N\overline{N}$ complex observation space can be partitioned into the signal-subspace and the noise-subspace, and the projection operator $\mathbb{P}_{\mathrm{n_v}}$ onto the noise subspace can be formed. The estimation problem can be addressed by exploiting the orthogonality between the noise-subspace and the signal-subspace formed by the virtual manifold vectors associated with the desired user. Therefore, the DOD and DOA of the desired user's paths can be estimated by solving the following optimization problem

$$(\underline{\overline{\theta}}, \underline{\theta}) = \arg \max_{\forall\left(\overline{\theta},\theta\right)} \xi(\overline{\theta}, \theta) \tag{2.19}$$

where the cost function $\xi(\overline{\theta}, \theta)$ is defined as follows

$$\xi(\overline{\theta}, \theta) \triangleq \sum_{k=1}^{K_1} \frac{\left(\underline{\overline{S}}^* \left(\overline{\theta}\right) \otimes \underline{S}\left(\theta\right)\right)^H \mathbb{T}_{1k}^H \mathbb{T}_{1k} \left(\underline{\overline{S}}^* \left(\overline{\theta}\right) \otimes \underline{S}\left(\theta\right)\right)}{\left(\underline{\overline{S}}^* \left(\overline{\theta}\right) \otimes \underline{S}\left(\theta\right)\right)^H \mathbb{T}_{1k}^H \mathbb{P}_{\mathrm{n_v}} \mathbb{T}_{1k} \left(\underline{\overline{S}}^* \left(\overline{\theta}\right) \otimes \underline{S}\left(\theta\right)\right)} \tag{2.20}$$

However, Equ 2.20 includes

$$\mathbb{T}_{1k} = \left(\mathbb{W}_1^T \mathbb{J}^{\ell_{1k}} \mathbb{W}_1\right) \otimes \mathbb{I}_N \tag{2.21}$$

where although the matrix $\mathbb{W}_1$ is known, the delays ℓ_{1k} for $k = 1, 2, ..., K_1$ are unknown. These delays (integers) can be pre-estimated using one-dimensional search for the peaks $[\ell_{11}, \ell_{12}, ..., \ell_{1K_1}]$ of the function

$$\xi\left(\ell\right) = \frac{\det\left(\left(\left(\mathbb{J}^\ell + \left(\mathbb{J}^T\right)^{\mathcal{N}_c - \ell}\right) \mathbb{W}_1\right)^H \left(\left(\mathbb{J}^\ell + \left(\mathbb{J}^T\right)^{\mathcal{N}_c - \ell}\right) \mathbb{W}_1\right)\right)}{\det\left(\left(\left(\mathbb{J}^\ell + \left(\mathbb{J}^T\right)^{\mathcal{N}_c - \ell}\right) \mathbb{W}_1\right)^H \mathbb{P}_{\mathrm{n}} \left(\left(\mathbb{J}^\ell + \left(\mathbb{J}^T\right)^{\mathcal{N}_c - \ell}\right) \mathbb{W}_1\right)\right)}, \forall \ell \tag{2.22}$$

where $\mathbb{P}_{\mathrm{n}}$ is the projection operator onto the noise subspace of the following covariance matrix

$$\mathbb{R} = \frac{1}{NL}\left[\mathbb{X}^T[1], \mathbb{X}^T[2], ..., \mathbb{X}^T[L]\right]\left[\mathbb{X}^T[1], \mathbb{X}^T[2], ..., \mathbb{X}^T[L]\right]^H \tag{2.23}$$

Thus, by estimating firstly the integers $[\ell_{11}, \ell_{12}, ..., \ell_{1K_1}]$, the solutions of Equ 2.19 will provide all the (DOD, DOA) of the desired user's paths.

2.4 Computer Simulation Studies

The performance of the proposed approach has been evaluated using computer simulation studies and the results are given in this section. The Tx and Rx arrays are assumed to be uniform circular arrays (UCAs) with the Tx-array consisting of 9 elements and the Rx-array consisting of 5 elements. Without any loss of generality, the Tx and the Rx array geometries are shown together in Figure 2.3 although they are far away from each other (far field). The signal to noise ratio (SNR) is set to 20 dB and there are $M = 3$ users (i.e. desired user plus 2 multiple-access-interfering users) with 3 paths per user. The system simulation parameters are listed in Table 2.1.

Table 2.1: System parameters

Parameter	Symbol	Value
Rx Array	N	5
Tx Array	$\overline{N}$	9
Code Period	T_c	0.1 ms
Length of weight code	$\mathcal{N}_c$	31
Number of users	M	3
Number of paths per user	$K_1 = K_2 = K_3$	3
Number of symbols	L	200

The pairs of (DOD, DOA) of the desired user associated with its three paths are $(40°, 270°)$, $(120°, 180°)$ and $(150°, 70°)$ and their corresponding delays are $6T_c$,

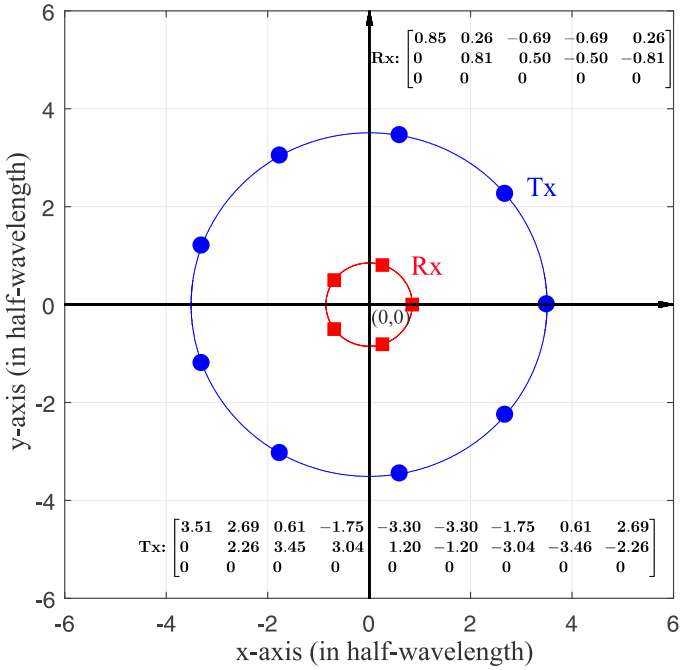

Figure 2.3: The array geometry of the transmitter (blue marker) and the receiver (red marker).

$12T_c$ and $21T_c$. Figure 2.4 shows the delay estimation of all the paths of the desired user. Then, Figure 2.5 shows the results of the joint estimation of the DOD and DOA of all the paths of the desired user. It is clearly illustrated that the peaks occur at the correct directions.

Next, consider a case that two of the paths of the desired user are close together in space. For example, consider the (DOD, DOA) of the first two paths are $(100°, 134°)$ and $(102°, 132°)$ while the third path remains at $(150°, 70°)$. As shown in Figure 2.6, the peaks of these two paths are clearly resolved and their values are correctly estimated illustrating the superresolution capabilities of the proposed approach. Consider again the simulation environment in Figure 2.5 where two of the three paths are co-directional, i.e. the DOA of the two paths are 270°. The results are shown in Figure 2.7 indicating that the proposed algorithms are still able to distinguish the two paths and estimate their associated parameters. However, in such case, conventional MIMO non-virtual MIMO system may not able to

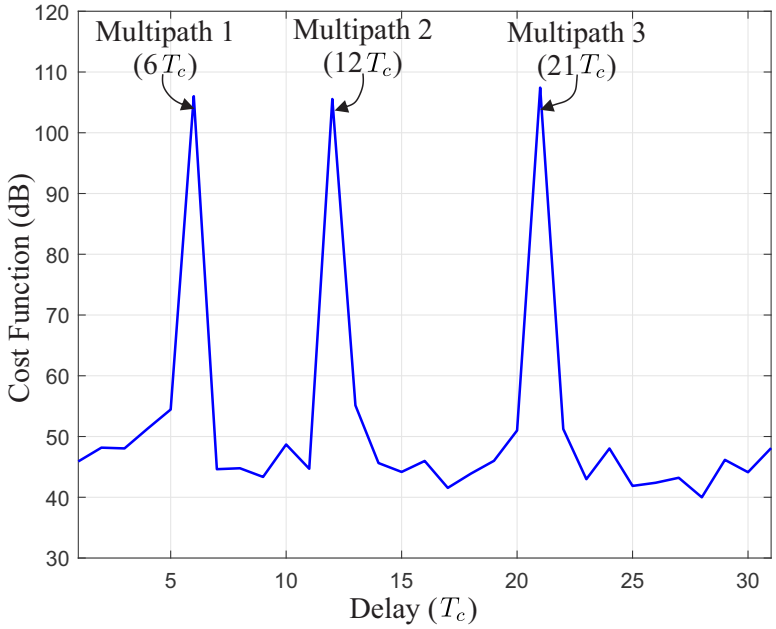

Figure 2.4: Delay estimation for three paths of the desired user.

resolve the two paths as they have no means to estimate DODs.

Furthermore, using the parameters given in Table 2.1, the performance of the proposed approach is evaluated in terms of the root mean square estimation error (RMSE) of the DOAs and DODs as a function of the SNR. Based on 1000 Monte-Carlo simulations, the results are shown in Figure 2.8. Then, the performance of the proposed approach is also evaluated in terms of the number of snapshot for a fixed SNR and the results are shown in Figure 2.9. Figures 2.8 and 2.9 indicate that the RMSE of the estimated DOD and DOA is low even when the SNR is equal to -10 dB or the number of snapshots is equal to 50. The estimation error of the DOD and DOA decreases when the SNR increases or the number of snapshots increases which are expected by any signal-subspace type algorithm. In addition, better resolution can be achieved[3] by either increasing the SNR or the number of snapshots (i.e. the "observation" interval).

Finally, the proposed system is compared with a conventional non-virtual MIMO system (that is without the manifold extender block) with the same Tx and

[3]see Chapter 8 of [18].

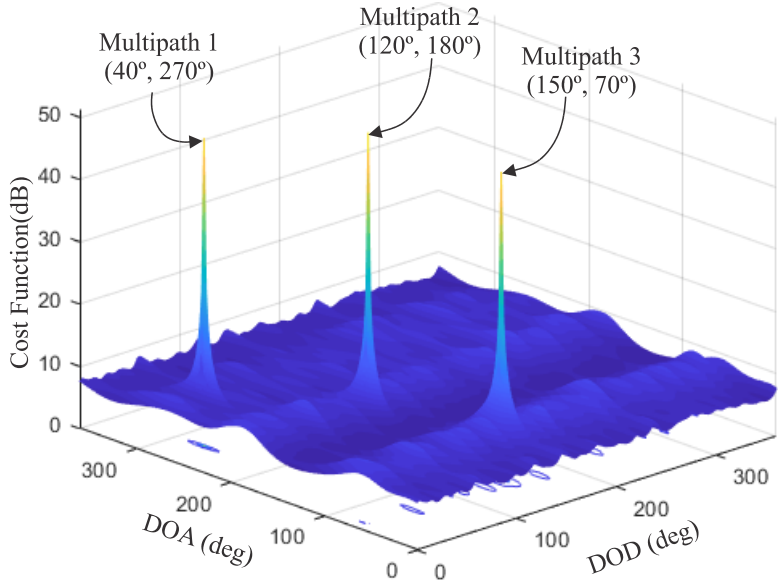

Figure 2.5: Proposed MIMO: Joint estimation of DOD and DOA for three paths of the desired user.

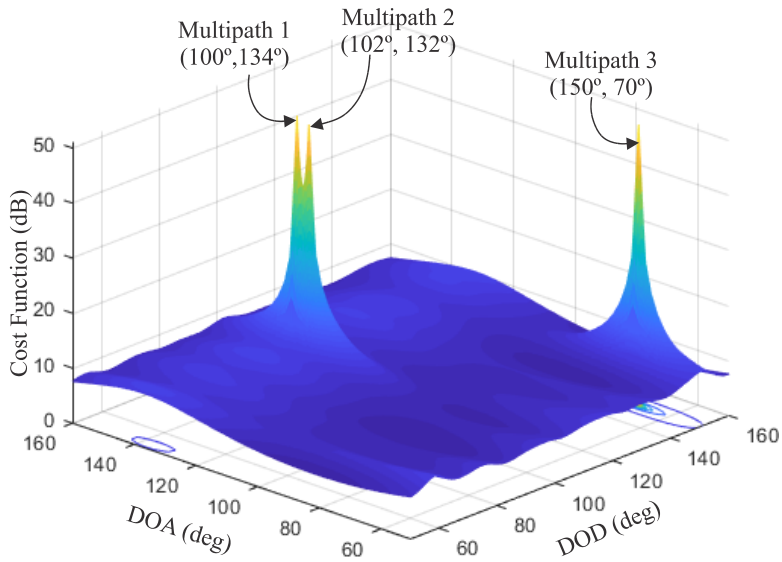

Figure 2.6: An example of the superresolution capabilities of the proposed approach where the directions of the paths 1 and 2, which are close together in space, are properly resolved.

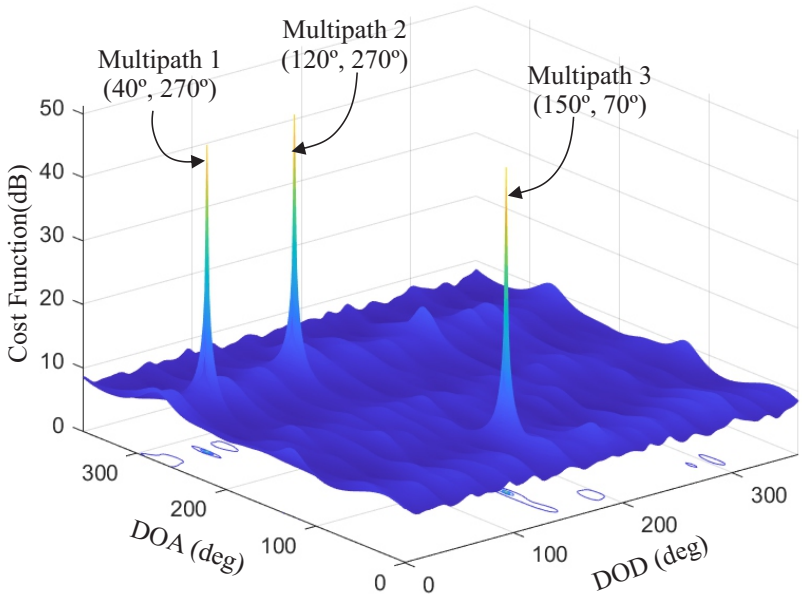

Figure 2.7: Joint estimation of DOD and DOA for three paths of the desired user where two paths of the desired user are co-directional.

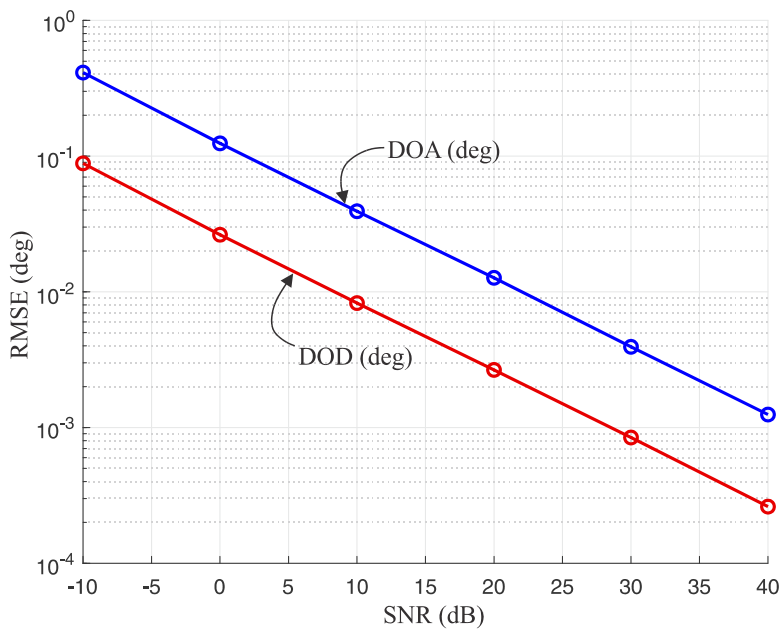

Figure 2.8: RMSE of the DOD and DOA estimation versus SNR in the proposed MIMO system. The number of snapshots L is fixed at 200 (1000 realisations).

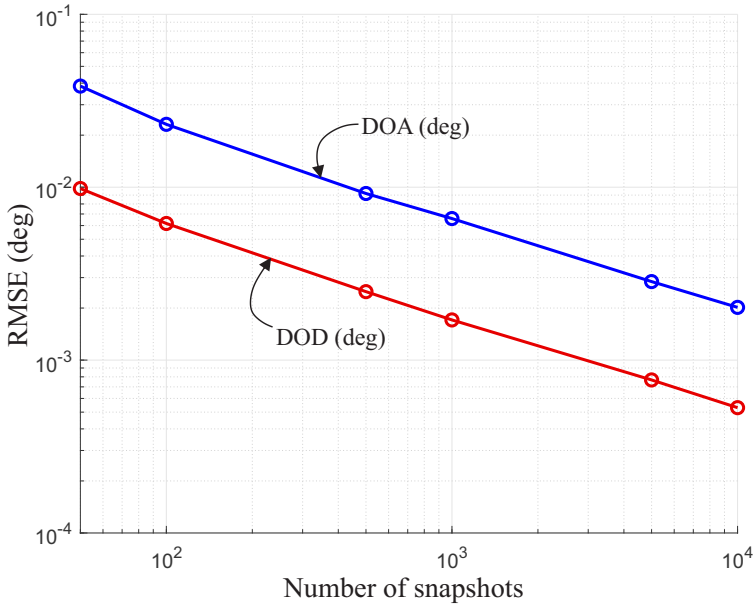

Figure 2.9: RMSE of the DOD and DOA estimation versus the number of snapshots in the proposed MIMO system. The SNR is fixed at 20 dB (1000 realisations).

Rx array geometries and under the same simulation environment as the proposed array system with the manifold extender. However, for the parameters given in Table 2.1, the channel estimation algorithm for the conventional system fails due to insufficient degrees-of-freedom (9 signals in a 5-dimensional observation space). Thus, to enable the channel estimation algorithm to work for the conventional system, both the number of users and paths per user are reduced to $M=2$ and $K_1=K_2=2$ (i.e. 4 signals in a 5-dimensional observation space) whilst the other parameters in Table 2.1 remain the same. Figure 2.10 shows the RMSE of the proposed approach based on the virtual array system, as well as the RMSE of the conventional MIMO system (i.e. without the manifold extender) as a function of the SNR over 5000 realisations. Similarly, Figure 2.11 shows the comparison results as a function of the number of snapshots. Note that the RMSE of the DOD estimation is not plotted in Figures 2.10 and 2.11 for comparison since the conventional system cannot estimate the DOD, as the Tx geometrical information (contained in the Tx manifold vector $\overline{\underline{S}}$) is reduced to a scalar factor and it cannot

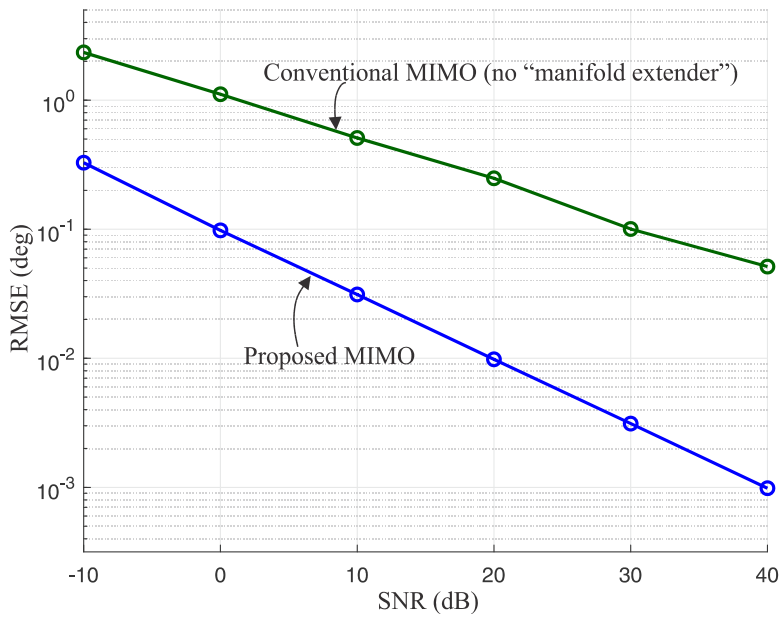

Figure 2.10: Comparison of the RMSE of the DOA estimation versus SNR between the proposed MIMO system and the conventional MIMO system. The number of snapshots L is fixed at 200 (5000 realisations).

be extracted and employed by the receiver. Figures 2.10 and 2.11 clearly illustrated that the proposed system is more accurate than the conventional MIMO system. This is because the proposed system extends the degrees-of-freedom from N to $N\overline{N}$, thus enhancing the channel estimation accuracy.

2.5 Summary

In this chapter, a MIMO communication system is proposed which increases the degrees-of-freedom and is capable of jointly estimating the DOA and DOD of all the paths of the desired user in the presence of multiple access interference. The proposed approach was evaluated with varying noise levels and varying number of snapshots, and then it was compared with the conventional MIMO system. Computer simulation studies show the accuracy of the proposed approach and its superresolution capabilities.

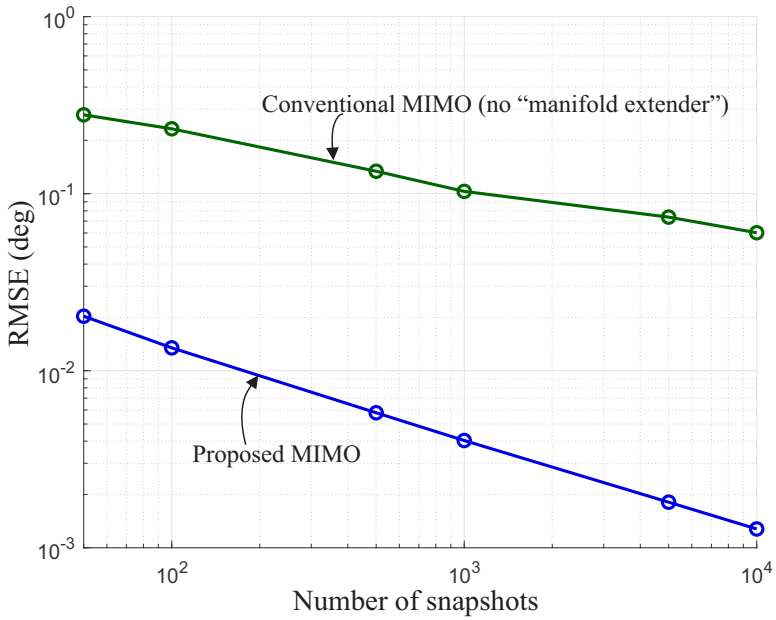

Figure 2.11: Comparison of the RMSE of the DOA estimation versus the number of snapshots between the proposed MIMO system and the conventional MIMO system. The SNR is fixed at 20 dB (5000 realisations).

2.6 Appendix of Derivation of the Proposed Virtual Snapshot Vector in Equ 2.13

In this appendix, the identity

$$\mathrm{vec}\left(\mathbb{A}\mathbb{B}\right) = \left(\mathbb{B}^T \otimes \mathbb{I}_k\right) \mathrm{vec}\left(\mathbb{A}\right) \tag{2.24}$$

will be used, where the dimensions of the matrices $\mathbb{A}$ and $\mathbb{B}$ are $k \times l$ and $l \times m$, respectively.

Recall Equ 2.12, we have

$$
\begin{aligned}
\underline{x}_{\mathrm{v}}[n] &= \mathrm{vec}\left(\mathbb{X}[n]\,\mathbb{W}_1\right) \\
&= \mathrm{vec}\Bigg\{\Bigg(\sum_{i=1}^{M}\sum_{k=1}^{K_i}\beta_{ik}[n]\,\underline{S}_{ik}\overline{\underline{S}}_{ik}^{H}\mathbb{W}_i^T \\
&\quad\times\left(\left(\mathbb{J}^T\right)^{\ell_{ik}}\mathrm{a}_i[n]+\mathbb{J}^{\mathcal{N}_c-\ell_{ik}}\mathrm{a}_i[n-1]\right)+\mathbb{N}[n]\Bigg)\mathbb{W}_1\Bigg\} \\
&= \mathrm{vec}\Bigg\{\sum_{i=1}^{M}\sum_{k=1}^{K_i}\beta_{ik}[n]\,\underline{S}_{ik}\overline{\underline{S}}_{ik}^{H}\mathbb{W}_i^T \\
&\quad\times\left(\left(\mathbb{J}^T\right)^{\ell_{ik}}\mathrm{a}_i[n]+\mathbb{J}^{\mathcal{N}_c-\ell_{ik}}\mathrm{a}_i[n-1]\right)\mathbb{W}_1\Bigg\} \\
&\quad+\mathrm{vec}\left\{\mathbb{N}[n]\,\mathbb{W}_1\right\} \\
&= \sum_{i=1}^{M}\sum_{k=1}^{K_i}\beta_{ik}[n]\left(\left[\mathbb{W}_i^T\left(\left(\mathbb{J}^T\right)^{\ell_{ik}}\mathrm{a}_i[n]+\mathbb{J}^{\mathcal{N}_c-\ell_{ik}}\mathrm{a}_i[n-1]\right)\mathbb{W}_1\right]^T\otimes\mathbb{I}_N\right) \\
&\quad\times\mathrm{vec}\left\{\underline{S}_{ik}\overline{\underline{S}}_{ik}^{H}\right\}+\underline{\mathrm{n}}_{\mathrm{v}}[n] \\
&= \sum_{i=1}^{M}\sum_{k=1}^{K_i}\beta_{ik}[n]\underbrace{\left(\left[\mathbb{W}_1^T\left(\mathbb{J}^{\ell_{ik}}\mathrm{a}_i[n]+\left(\mathbb{J}^T\right)^{\mathcal{N}_c-\ell_{ik}}\mathrm{a}_i[n-1]\right)\mathbb{W}_i\right]\otimes\mathbb{I}_N\right)}_{=\mathbb{A}_{ik}[n]} \\
&\quad\times\mathrm{vec}\left\{\underline{S}_{ik}\overline{\underline{S}}_{ik}^{H}\right\}+\underline{\mathrm{n}}_{\mathrm{v}}[n] \\
&= \sum_{i=1}^{M}\sum_{k=1}^{K_i}\beta_{ik}[n]\,\mathbb{A}_{ik}[n]\left(\overline{\underline{S}}_{ik}^{*}\otimes\underline{S}_{ik}\right)+\underline{\mathrm{n}}_{\mathrm{v}}[n]
\end{aligned}
$$

or, equivalently,

$$
\begin{aligned}
\underline{x}_{\mathrm{v}}[n] = &\underbrace{\sum_{k=1}^{K_1}\beta_{1k}[n]\,\mathbb{A}_{1k}[n]\overbrace{\left(\overline{\underline{S}}_{1k}^{*}\otimes\underline{S}_{1k}\right)}^{\underline{S}_{\mathrm{v},1k}}}_{\text{Desired term}} \\
&+\underbrace{\sum_{i=2}^{M}\sum_{k=1}^{K_i}\beta_{ik}[n]\,\mathbb{A}_{ik}[n]\overbrace{\left(\overline{\underline{S}}_{ik}^{*}\otimes\underline{S}_{ik}\right)}^{\underline{S}_{\mathrm{v},ik}}}_{\text{MAI term}} \\
&+\underbrace{\underline{\mathrm{n}}_{\mathrm{v}}[n]}_{\text{Noise}}
\end{aligned}
$$

Chapter 3

DOD-DOA Delay-Doppler Estimation and Beamforming

In this chapter, a novel virtual-spatiotemporal MIMO system is proposed that extends the system presented in Chapter 2 by incorporating the temporal domain of the system towards the objective of increasing the degrees of freedom of the communication system even further. In this system, a joint DOD-DOA estimation, delay-Doppler estimation, and beamforming algorithms are presented. This is achieved by using the proposed subspace type algorithms and the proposed virtual-spatiotemporal manifold extender which increases the dimensionality of the observation space from N to NN_{ext}, and thus the degrees of freedom is increased from N to NN_{ext} where $N_{\text{ext}} = 2\mathcal{N}_c\overline{N}$. The proposed system is able to resolve multipath effect, estimate multi parameters accurately, provide high beamforming gain, suppress multiple access interference, and it is also applicable for arbitrary array geometries. The performance of the channel parameter estimator and the beamformer is evaluated against the existing spatial-only and spatiotemporal receivers using different performance metrics by computer simulation studies and the results show the superiority of the proposed approaches.

3.1 Introduction

With increasing demands on capacity and heightened user density, it is imperative to propose approaches that utilise and exploit all possible degrees of freedom of a MIMO system. The degrees of freedom is defined in [45] as the coefficient of the logarithm of the SNR (for high SNR). In [46] it is equivalent to the multiplexing gain and in [47] it is considered as the number of sources that the system can resolve. In any case, the degrees of freedom scales with the number of dimensions of the system, and increasing the degrees of freedom maps to a number of objectives, namely

1. ability to deliver highly pointed beams towards "desired" users and "nulls" in the directions of "unwanted" users leading to increased interference cancellation,
2. increased channel estimation accuracy,
3. ability to accommodate increased number of users.

All the aforementioned objectives are achieved in this chapter. This chapter presents an extended work based on Chapter 2. To address the requirements of future communication systems, a novel parametric approach (suitable for arbitrary array geometry) is presented. Given a fixed number of antennas, it is capable of delivering higher degrees of freedom, consequently increasing channel estimation accuracy and beamforming capability. It is also able to handle multipath effect and suppress high interference in dense signal environment.

There has been considerable research in the literature that refer to increasing the number of the degrees of freedom. For instance, the minimum redundancy arrays (MRA) were proposed in [48]. The designed arrays reduce redundant inter-element spacings given a fixed number of array elements to maximise resolution accuracy. Although such arrays increase the resolution accuracy, they does not

increase the degrees of freedom. In [49] and [50], the MRAs were improved by constructing an augmented covariance matrix, however, the constructed augmented covariance matrix is not positive semidefinite for finite number of snapshots. The aforementioned approaches that rely on the MRAs have no closed-form expression for array geometry and involve exhaustive search for finding the array positions.

Another approach is to employ fourth order cumulants rather than just employing second order statistics [51][52]. However, the approach is restricted to non-Gaussian sources and the computation of fourth order cumulants is expensive in terms of computations. The Khatri-Rao (KR)-based approach [53] is also used for increasing the DoF by constructing a difference coarray. For this method, quasi stationary sources are required, which is not applicable to stationary sources.

Inspired by the concept of the difference coarray, another approach increases the degrees of freedom by utilising sparse arrays to form "virtual arrays". The sparse arrays are arrays with non-uniform inter-element spacing, in general, there are two typical types of the sparse arrays: Coprime arrays [54] and nested arrays [47]. A coprime array generally comprises two uniform linear arrays (ULAs) with adjacent spacing larger than half wavelength and the variants of coprime arrays include generalized coprime array [55], thinned coprime array (TCA) [56], complementary coprime array (CCP) [57], and relocating extended coprime array (RECA) [58]. A typical nested array is constructed by a dense ULA and a sparse ULA, and the variants of the nested array include super nested arrays (SNA) [59], augmented nested arrays (ANA) [60], generalized nested arrays [61], inter-element spacing constraint (MISC) arrays [62], and Cantor arrays [63]. However, these techniques using sparse arrays are limited to linear array geometries. These papers involve linear sub-arrays of the Rx array and none of these approaches made use of the Tx array geometry.

Furthermore, the concept of the "virtual array" has been extensively explored in MIMO radar systems to increase the degrees of freedom. This is achieved by

taking the advantage of the knowledge of the transmitted radar signal, which can be directly exploited by the radar's receiver (see [64], [65], [66]), something that cannot be easily done in communication systems.

The remainder of this chapter is organised as follows. In Section 3.2, an overview of the parametric approaches for extending the degrees of freedom is provided. In Section 3.3, the transmitter and channel models of the proposed system are presented. Then, the receiver model is proposed and the antenna array received signal is modelled as a function of a virtual-spatiotemporal manifold extender. Based on this modelling, two joint estimation algorithms (Doppler-Delay and DOA-DOD) and a beamforming algorithm are proposed in Section 3.4. This is followed in Section 3.5, by computer simulation studies and the chapter is summarised in Section 3.6.

3.2 Expanding the DoF in a Multi-Antenna Communication System

There are two typical class of approaches of expanding the DoF in multi-antenna communication system: *Extended Manifold* approaches and *Massive MIMO* approaches. The *Extended Manifold* approach can be visualised in Figure 3.1 which illustrates the baseband blocks of a MIMO communication system consisting of its three main blocks: the transmitter, the channel and the receiver. The transmitter employs an antenna array of $\overline{N}$ elements and it is followed by a noisy channel. The receiver also employs an antenna array of N elements and includes a "manifold extender", a channel estimator and a weight formation for beamforming.

At point-D in Figure 3.1, the $N \times 1$ vector signal $\underline{x}(t) \in \mathcal{C}^{N\times 1}$ can be expressed in terms of the manifold vector $\underline{S} \in \mathcal{C}^{N\times 1}$ of the receiver's array which is a function of the DOA, carrier frequency F_c, velocity of light and the Cartesian coordinates

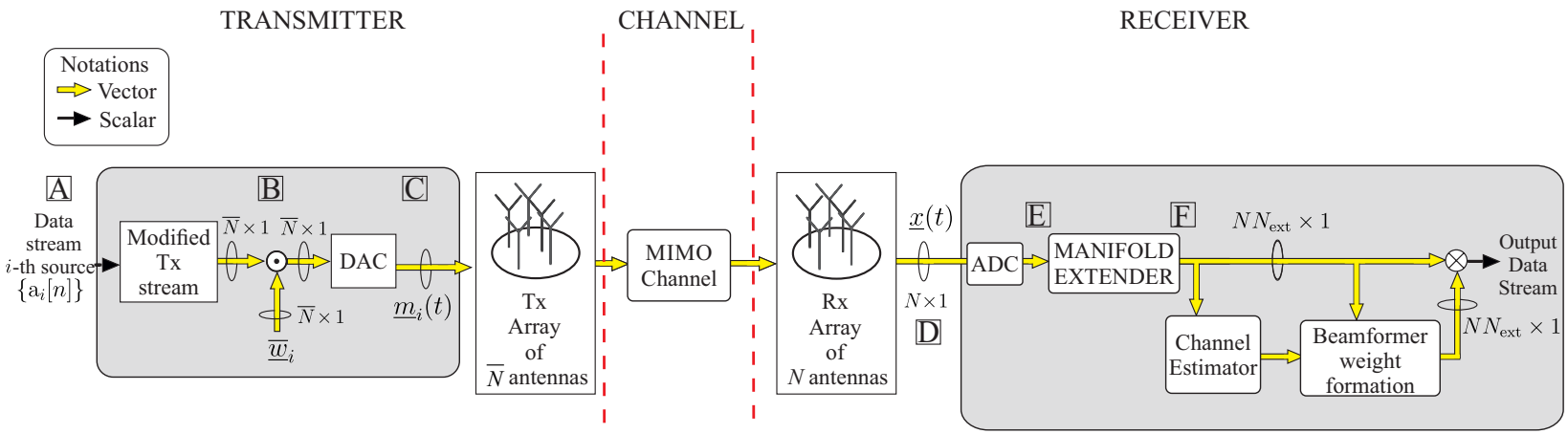

Figure 3.1: Block diagram representation of the transmitter, channel and receiver blocks of the proposed scheme for extending the degrees of freedom.

of the Rx antenna array elements $[\underline{r}_1, \underline{r}_2, ..., \underline{r}_N]$. At the output of the "manifold extender" (i.e. point-F in Figure 3.1), the signal $\underline{x}[n]$ is an $NN_{\text{ext}} \times 1$ vector signal and this can be expressed as a function of the "extended" manifold vector $\underline{h} \in \mathcal{C}^{NN_{\text{ext}} \times 1}$ which, in addition to the Cartesian coordinates of the Rx antenna, may also include other system parameters, such as Doppler, polarisation, PN-codes, Cartesian coordinates of the Tx antenna array elements $[\underline{\overline{r}}_1, \underline{\overline{r}}_2, ..., \underline{\overline{r}}_N]$, etc.

The *Massive MIMO* approaches attempt to increase the DoF of the system by increasing the number of Rx antennas N to a large value in the order of 100s-1000s [25]. However, the downside of the massive MIMO approach is the requirement of more hardware (massive number of RF unit set). On the other hand, the class of MIMO approach based on the concept of *manifold extender* attempt to increase the number of dimensions of the system by keeping the hardware fixed (i.e. the number of Rx antennas N fixed) and increase computational complexity by creating long observation vectors of dimensionality of $NN_{\text{ext}} \times 1$. In array processing, the complexity is mainly related to the dimensionality of the vectors and matrices. That is, the longer the vectors, the more computationally complex is the system. This increases the "degrees-of-freedom" to NN_{ext} and consequently improves the capabilities of the overall system. Note that

1. if N = very large and $N_{\text{ext}} = 1$ then this is a standard massive MIMO with massive DoF.

2. if N = small but fix and N_{ext} = very large then this is a spatiotemporal MIMO with massive DoF.

3. if N = very large and N_{ext} = very large then this is a spatiotemporal massive MIMO with super massive DoF.

In this chapter, to address the requirements of future communication systems, a novel parametric approach (suitable for any geometry) is presented which is based

on the concept of the "manifold extender". In the next sections, the design of the proposed virtual-spatiotemporal system is presented.

3.3 Transmitter and Channel Model

With reference to a MIMO communication system of M co-channel users, Figure 3.2 illustrates the baseband blocks of the i-th user consisting of the transmitter and the channel. As shown in Figure 3.2, M co-channel users including the desired user plus the $M-1$ MAI (point C_1) operate at the same time on the same frequency band. The data stream of the i-th user denoted by $\{\mathrm{a}_i[n]\}$ (see point-A), with a symbol period of T_{cs}, is weighted (see point-B) by the known code vector sequence $\{\underline{c}_i[q] \odot \underline{\overline{w}}_i\}$ where $\underline{c}_i^T[q]$ is the q-th row of the code matrix $\mathbb{C}_i \in \mathcal{R}^{\mathcal{N}_c \times \overline{N}}$ having columns weight codes of $\pm 1'$s of length $\mathcal{N}_c$, as this is shown in Figure 3.3.

In Figure 3.3, the elements of the code matrix $\mathbb{C}_i$ are denoted as $\alpha_{im}[q] \in \{+1, -1\}$, $\forall m \in \left[1, \overline{N}\right]$, $\forall q \in [1, \mathcal{N}_c]$. The vector $\underline{c}_{im}$ denotes the m-th column of $\mathbb{C}_i$ representing the code applied to the m-th Tx antenna and $\underline{c}_i[q]$ denotes the column version of the q-th row of $\mathbb{C}_i$ which is applied to all Tx antennas at the q-th period T_c with $T_{cs} = \mathcal{N}_c T_c$. The vector $\underline{\overline{w}}_i \in \mathcal{C}^{\overline{N} \times 1}$ is a known Tx beamforming weight vector and it may be designed based on the feedback of the receiver. The vector $\underline{\overline{w}}_i$ may also be a vector of 1s in which case this can be ignored from the system's description. However, the precise design of $\underline{\overline{w}}_i$ (Tx beamforming) is beyond the scope of this chapter. To maintain the integrity of the system model, the Tx weight is assumed to be a steering vector beamformer with its mainlobe towards arbitrary degrees. Then, at point-B in Figure 3.2, The sequence corresponding to the n-th symbol of the i-th user transmitted across $\overline{N}$ antennas is denoted by the matrix $\mathbb{M}_i[n] \in \mathcal{C}^{\overline{N} \times \mathcal{N}_c}$ and can be written as

$$\mathbb{M}_i[n] = \mathbb{C}_i^T \odot \left(\underline{\overline{w}}_i \underline{1}_{\mathcal{N}_c}^T\right) \mathrm{a}_i[n] \tag{3.1}$$

Finally, using a DAC, the message symbols of Equ 3.1 become the analogue base-

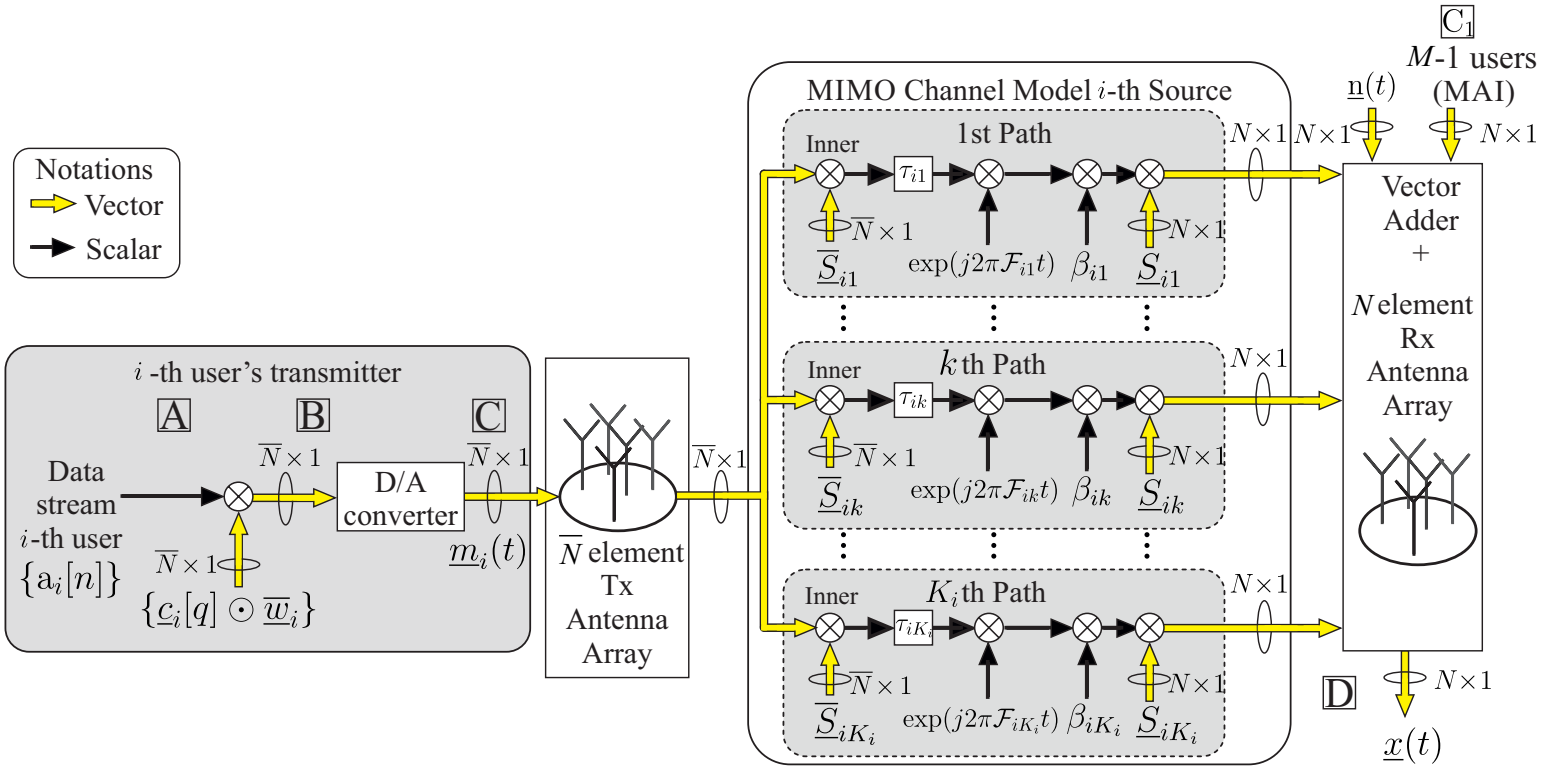

Figure 3.2: Baseband representation of the MIMO transmitter and the MIMO channel for M co-channel users ("desired" plus (M-1) MAI users).

$$\mathbb{C}_i = \begin{bmatrix} \alpha_{i1}[1] & \alpha_{i2}[1] & \dots & \alpha_{im}[1] & \dots & \alpha_{i\overline{N}}[1] \\ \alpha_{i1}[2] & \alpha_{i2}[2] & \dots & \alpha_{im}[2] & \dots & \alpha_{i\overline{N}}[2] \\ \vdots & \vdots & & \vdots & & \vdots \\ \alpha_{i1}[q] & \alpha_{i2}[q] & \dots & \alpha_{im}[q] & \dots & \alpha_{i\overline{N}}[q] \\ \vdots & & & & & \\ \alpha_{i1}[\mathcal{N}_c] & \alpha_{i2}[\mathcal{N}_c] & \dots & \alpha_{im}[\mathcal{N}_c] & \dots & \alpha_{i\overline{N}}[\mathcal{N}_c] \end{bmatrix} \leftarrow \underline{c}_i^T[q]$$

$$\uparrow \underline{c}_{im}$$

Figure 3.3: The code matrix $\mathbb{C}_i$ with elements ± 1s.

band signal $\underline{m}_i(t) \in \mathcal{C}^{\overline{N}\times 1}$ at point-C in Figure 3.2. The $\underline{m}_i(t)$ vector signal is transmitted via a multipath channel of K_i paths, as this is shown in Figure 3.2 where the k-th path of the i-th user includes:

- the manifold vector $\underline{\overline{S}}_{ik}$ of the Tx,
- the delay τ_{ik},
- the Doppler frequency $\mathcal{F}_{ik}$,
- the path gain β_{ik},
- the manifold vector $\underline{S}_{ik}$ of the Rx.

The manifold vectors $\underline{S}_{ik}$ and $\underline{\overline{S}}_{ik}$ can be expressed as a function of the Cartesian coordinates of the Rx and Tx arrays $[\underline{r}_1, \underline{r}_2, ..., \underline{r}_N] \in \mathcal{R}^{3\times N}$ and $[\underline{\overline{r}}_1, \underline{\overline{r}}_2, ..., \underline{\overline{r}}_{\overline{N}}] \in \mathcal{R}^{3\times \overline{N}}$ as follows

$$\underline{S}_{ik} \triangleq \underline{S}(\theta_{ik}) = \exp(-j\,[\underline{r}_1, \underline{r}_2, ..., \underline{r}_N]^T\,\underline{k}(\theta_{ik})) \tag{3.2a}$$

$$\underline{\overline{S}}_{ik} \triangleq \underline{\overline{S}}(\overline{\theta}_{ik}) = \exp(j\,[\underline{\overline{r}}_1, \underline{\overline{r}}_2, ..., \underline{\overline{r}}_{\overline{N}}]^T\,\underline{k}(\overline{\theta}_{ik})) \tag{3.2b}$$

with $\underline{k} \triangleq \underline{k}(\theta_{ik})$ and $\underline{\overline{k}} \triangleq \underline{k}(\overline{\theta}_{ik})$ denoting the wavenumber vectors defined as

$$\underline{k} = \frac{2\pi F_c}{c}\,[\cos\theta_{ik},\ \ \sin\theta_{ik},\ \ 0]^T \tag{3.3a}$$

$$\underline{\overline{k}} = \frac{2\pi F_c}{c}\,[\cos\overline{\theta}_{ik},\ \ \sin\overline{\theta}_{ik},\ \ 0]^T \tag{3.3b}$$

where θ_{ik} and $\overline{\theta}_{ik}$ denote the DOA and the DOD of the i-th user's k-th path, respectively. In addition, F_c denotes the carrier frequency and c is the velocity of light. This parametric channel model allows the modelling of the received array vector $\underline{x}(t)$ at point-D in Figure 3.2 to be expressed as a function of channel parameters as

$$\underline{x}(t) = \sum_{i=1}^{M}\sum_{k=1}^{K_i}\beta_{ik}\exp(j2\pi\mathcal{F}_{ik}t)\underline{S}_{ik}\overline{\underline{S}}_{ik}^{H}\underline{m}_i\left(t-\tau_{ik}\right)+\underline{\mathrm{n}}(t) \tag{3.4}$$

where $\underline{\mathrm{n}}(t)$ is the noise vector which is assumed to be white, zero mean complex additive Gaussian noise with covariance matrix $\sigma_{\mathrm{n}}^2\mathbb{I}_N$ where σ_{n}^2 is unknown and represents the noise power.

3.4 Receiver Model: Virtual-Spatiotemporal Manifold Extender

The proposed receiver model is illustrated in Figure 3.4 which consists of the manifold extender, channel estimation and beamforming weight formation blocks. At point-D in Figure 3.4, the received signal $\underline{x}(t)$ (given by Equ 3.4) is firstly discretised with sampling period equal to T_c producing at point-E the discrete vector $\underline{x}(t_l)$ where t_l denotes the l-th snapshot. Then, these snapshots are fed into a "manifold extender" which transforms the discretised vector $\underline{x}(t_l) \in \mathcal{C}^{N\times 1}$ to a longer snapshot $\underline{x}\,[n] \in \mathcal{C}^{2N\overline{N}\mathcal{N}_c\times 1}$ which we call it a virtual-spatiotemporal snapshot. The structure of the manifold extender is illustrated in Figure 3.5 and the data processing within the manifold extender is visualised in Figure 3.6.

Firstly, as shown in the block between point-E and point-E$_1$ in Figure 3.5, the "manifold extender" includes a bank of N Tapped delay lines (TDLs) which collects at its input (point-E) $2\mathcal{N}_c$ snapshots $\underline{x}(t_l)$ and, for the n-th time interval, forms a vector $\underline{x}_{\mathrm{st}}[n] \in \mathcal{C}^{2N\mathcal{N}_c\times 1}$ (point-E$_1$). To be specific, at point-E the sampled snapshots $\underline{x}(t_l)$ pass through the bank of TDLs of length $2\mathcal{N}_c$. Then, these

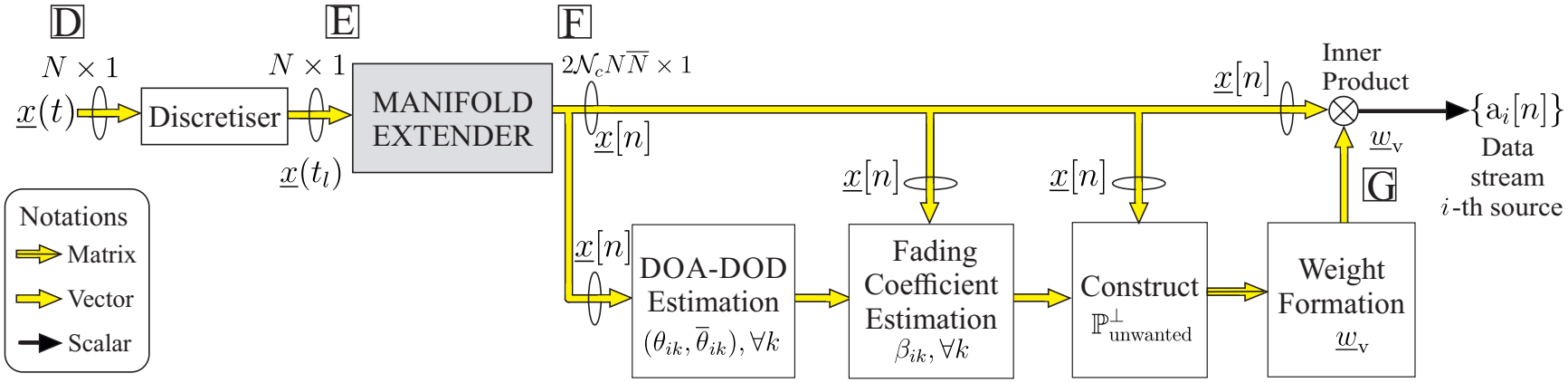

Figure 3.4: Baseband representation of the receiver of the i-th source.

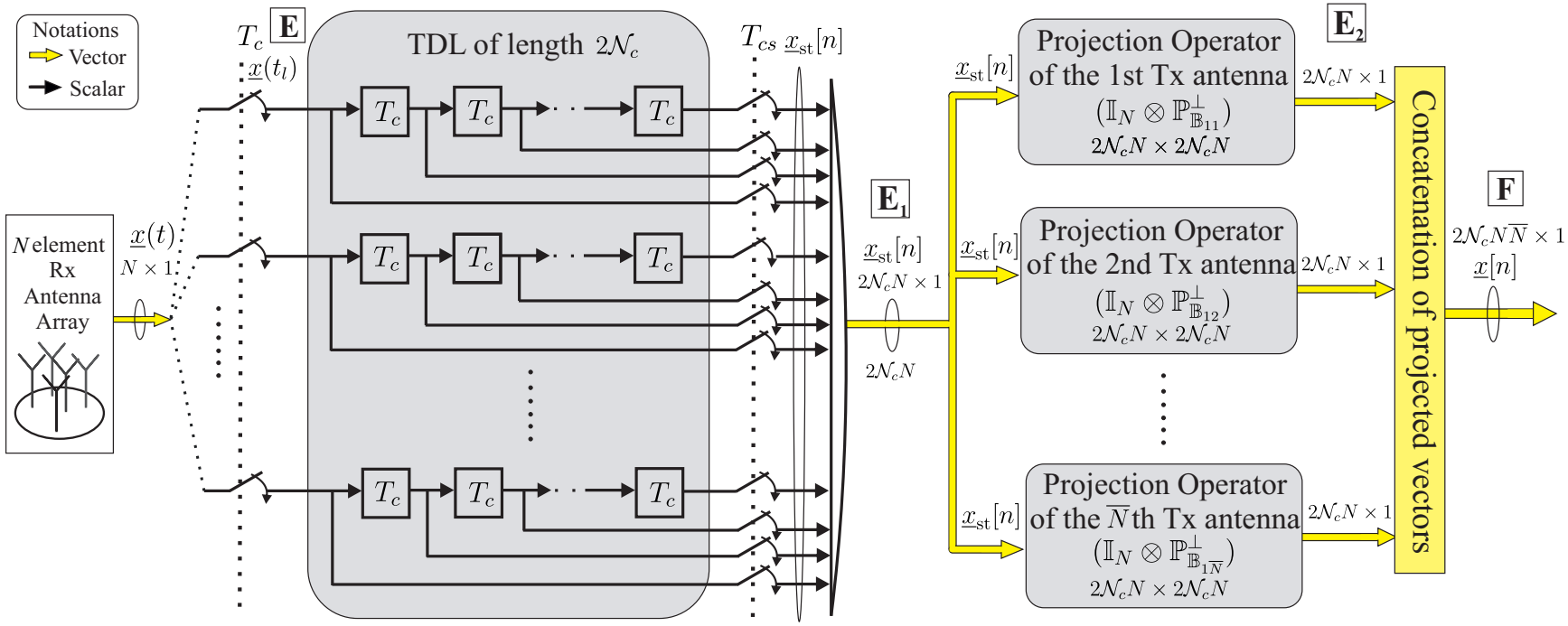

Figure 3.5: Illustration of the structure of the manifold extender of the proposed virtual-spatiotemporal system.

snapshots are sampled with a sampling period T_{cs} (note that $T_{cs} = \mathcal{N}_c T_c$) and $2\mathcal{N}_c$ snapshots are collected at the nT_{cs} period. Thus, the $2\mathcal{N}_c$ snapshots contain the contribution of the current n-th symbol, some information of the previous $(n-1)$-th and the next $(n+1)$-th symbols. These snapshots are expressed in the form of an $N \times 2\mathcal{N}_c$ matrix $\mathbb{X}[n]$. The matrix $\mathbb{X}[n]$ can be visualised as the n-th slice of the 3D cube shown in Figure 3.6(a) and modelled as follows (Note that with no loss of generality, the first user is considered to be the desired user.)

$$\mathbb{X}[n] = \underbrace{\sum_{k=1}^{K_1} \beta_{1k} \exp\left(j2\pi\mathcal{F}_{1k} n T_{cs}\right) \underline{S}_{1k} \underline{\overline{S}}_{1k}^H \mathrm{diag}\left(\underline{\overline{w}}_1\right) \mathbb{T}_{1k}^T \mathrm{a}_1[n]}_{\text{Desired term}} \tag{3.5}$$

$$+\mathbb{X}_{\mathrm{ISI}} + \mathbb{X}_{\mathrm{MAI}} + \mathbb{N}[n] \tag{3.6}$$

where $\mathbb{X}_{\mathrm{ISI}}$ denotes the Inter-Symbol Interference (ISI) and $\mathbb{X}_{\mathrm{MAI}}$ denotes the multiple access interference (MAI), both are expressed as follows

$$\begin{aligned}\mathbb{X}_{\mathrm{ISI}} = & \sum_{k=1}^{K_1} \beta_{1k} \underline{S}_{1k} \underline{\overline{S}}_{1k}^H \mathrm{diag}\left(\underline{\overline{w}}_1\right) \mathbb{T}_{1k}^T \times \\ & \Big\{ \mathbb{J}^{\mathcal{N}_c} \exp\left(j2\pi\mathcal{F}_{1k}(n-1) T_{cs}\right) \mathrm{a}_1[n-1] \\ & + \left(\mathbb{J}^T\right)^{\mathcal{N}_c} \exp\left(j2\pi\mathcal{F}_{1k}(n+1) T_{cs}\right) \mathrm{a}_1[n+1] \Big\}\end{aligned} \tag{3.7}$$

$$\begin{aligned}\mathbb{X}_{\mathrm{MAI}} = & \sum_{i=2}^{M} \sum_{k=1}^{K_i} \beta_{ik} \underline{S}_{ik} \underline{\overline{S}}_{ik}^H \mathrm{diag}\left(\underline{\overline{w}}_i\right) \mathbb{T}_{ik}^T \times \\ & \Big\{ \exp\left(j2\pi\mathcal{F}_{ik} n T_{cs}\right) \mathrm{a}_i[n] \\ & + \mathbb{J}^{\mathcal{N}_c} \exp\left(j2\pi\mathcal{F}_{ik}(n-1) T_{cs}\right) \mathrm{a}_i[n-1] \\ & + \left(\mathbb{J}^T\right)^{\mathcal{N}_c} \exp\left(j2\pi\mathcal{F}_{ik}(n+1) T_{cs}\right) \mathrm{a}_i[n+1] \Big\}\end{aligned} \tag{3.8}$$

In Equ 3.5, $\mathbb{T}_{ik} \in \mathcal{C}^{2\mathcal{N}_c \times \overline{N}}$ contains the temporal information of the received signal, which is given as

$$\mathbb{T}_{ik} = \mathbb{J}^{l_{ik}} \begin{bmatrix} \mathbb{C}_i \\ \mathbb{O}_{\mathcal{N}_c \times \overline{N}} \end{bmatrix} \odot \left(\underline{\mathcal{F}}_{ik} \underline{1}_{\overline{N}}^T\right) \tag{3.9}$$

with

- $\underline{\mathcal{F}}_{ik} \in \mathcal{C}^{2\mathcal{N}_c \times 1}$ representing the Doppler shift vector, i.e.

$$\underline{\mathcal{F}}_{ik} = \exp\left(j2\pi\mathcal{F}_{ik}\left[0,\ldots,2\mathcal{N}_c-1\right]^T T_c\right) \tag{3.10}$$

- $\mathbb{J}$ (or $\mathbb{J}^T$) is a $2\mathcal{N}_c \times 2\mathcal{N}_c$ matrix defined as follows[1]:

$$\mathbb{J} = \begin{bmatrix} \underline{0}^T_{2\mathcal{N}_c-1}, & 0 \\ \mathbb{I}_{2\mathcal{N}_c-1}, & \underline{0}_{2\mathcal{N}_c-1} \end{bmatrix} \tag{3.11}$$

- $l_{ik} = \left\lfloor \frac{\tau_{ik}}{T_c} \right\rfloor \mathrm{mod}\mathcal{N}_c$ denoting the discretised delay shown in Figure 3.7,
- $\mathbb{N}[n]$ representing the noise contribution.

Secondly, at point-E$_1$ in Figure 3.5, the vector $\underline{x}_{\mathrm{st}}[n] \in \mathcal{C}^{2N\mathcal{N}_c \times 1}$ is formed by vectorising the matrix $\mathbb{X}[n]$, given as follows

$$\underline{x}_{\mathrm{st}}[n] = \mathrm{vec}\left(\mathbb{X}^T[n]\right) \tag{3.12}$$

which is called "spatiotemporal snapshot" and it can also be visualised as in Figure 3.6(b).

Thirdly, at point-E$_2$ in Figure 3.5, the spatiotemporal snapshot vector $\underline{x}_{\mathrm{st}}[n]$ is projected by a set of $\overline{N}$ projection operators. The projection operator set $\mathbb{P}^{\perp}_{\mathbb{B}_{im}} \in \mathcal{C}^{2\mathcal{N}_c \times 2\mathcal{N}_c}$, $\forall m = 1, 2, ..., \overline{N}$ is defined to isolate the signal corresponding to the m-th antenna of the i-th user, given as follows

$$\mathbb{P}^{\perp}_{\mathbb{B}_{im}} = \mathbb{I}_{2\mathcal{N}_c} - \mathbb{B}_{im}\left(\mathbb{B}^H_{im}\mathbb{B}_{im}\right)^{-1}\mathbb{B}^H_{im} \tag{3.13}$$

where $\mathbb{B}_{im} \in \mathcal{C}^{2\mathcal{N}_c \times K_i(\overline{N}-1)}$ is obtained as follows

$$\begin{aligned} \mathbb{B}_{im} \quad = \quad & \left[\mathbb{J}^{l_{i1}}\begin{bmatrix} \mathbb{C}_{im} \\ \mathbb{O}_{\mathcal{N}_c \times \left(\overline{N}-1\right)} \end{bmatrix} \odot \underline{\mathcal{F}}_{i1}\underline{1}^T_{\overline{N}-1}, \ldots \right. \\ & \left. \ldots, \mathbb{J}^{l_{iK_i}}\begin{bmatrix} \mathbb{C}_{im} \\ \mathbb{O}_{\mathcal{N}_c \times \left(\overline{N}-1\right)} \end{bmatrix} \odot \underline{\mathcal{F}}_{iK_i}\underline{1}^T_{\overline{N}-1}\right] \end{aligned} \tag{3.14}$$

[1] The power l of $\mathbb{J}$ (or $\mathbb{J}^T$) when applied to a vector $\underline{z} \in \mathcal{C}^{\mathcal{N}_c \times 1}$ or matrix $\mathbb{Z}$, i.e. $\mathbb{J}^l\underline{z}$ $\left(\text{or } \left(\mathbb{J}^T\right)^l\underline{z}\right)$ and $\mathbb{J}^l\mathbb{Z}$ $\left(\text{or } \left(\mathbb{J}^T\right)^l\mathbb{Z}\right)$, downshifts (or upshifts) the vector $\underline{z}$ or matrix $\mathbb{Z}$ by l elements.

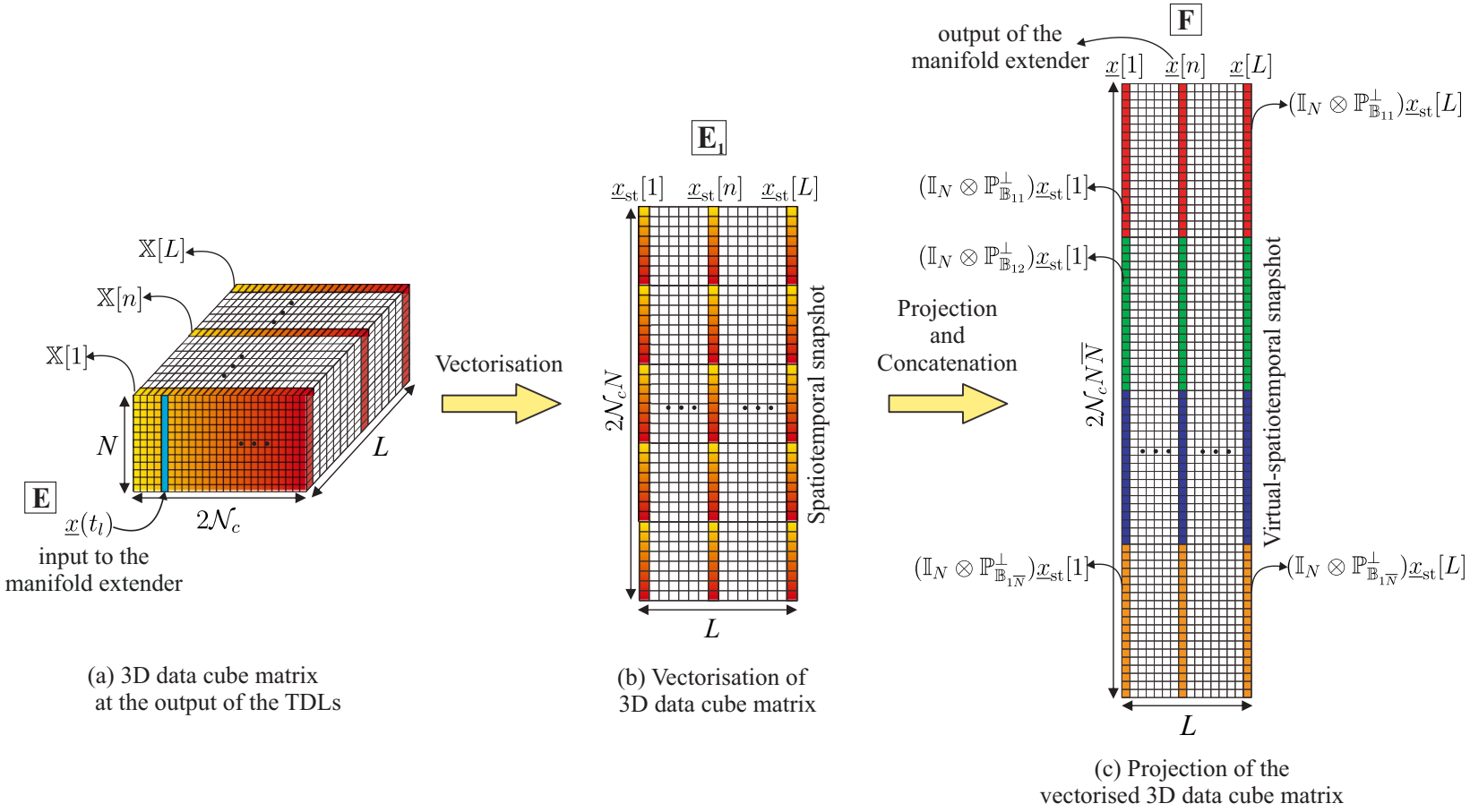

(a) 3D data cube matrix at the output of the TDLs

(b) Vectorisation of 3D data cube matrix

(c) Projection of the vectorised 3D data cube matrix

Figure 3.6: Illustration of the received data processing at the manifold extender for the proposed virtual-spatiotemporal system. The received data cube matrices in (a) are first vectorised to get spatiotemporal snapshots in (b), and then each spatiotemporal snapshot is projected by $\overline{N}$ projection operators to form virtual-spatiotemporal snapshot in (c). Different colors in (c) represent different projection operators.

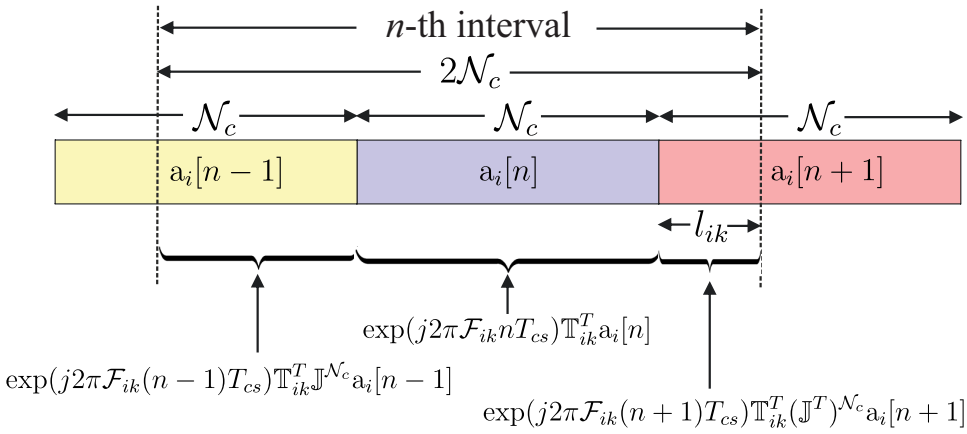

Figure 3.7: Illustration of the delay l_{ik} and the modelling of the data symbols received during the n-th time-interval.

where $\mathbb{C}_{im} \in \mathcal{R}^{\mathcal{N}_c \times \overline{N}-1}$ is formed by the codes of the i-th user with the m-th code removed, this is given as

$$\mathbb{C}_{im} = \left[\underline{c}_{i1}, \ldots, \underline{c}_{i(m-1)}, \underline{c}_{i(m+1)}, \ldots, \underline{c}_{i\overline{N}}\right] \tag{3.15}$$

Then, the projection matrix $\mathbb{P}_{\mathbb{B}_1}^{\perp}$ encloses the projection operators of all Tx antennas of the desired user is given as

$$\mathbb{P}_{\mathbb{B}_1}^{\perp} = \begin{bmatrix} \mathbb{I}_N \otimes \mathbb{P}_{\mathbb{B}_{11}}^{\perp}, & \mathbb{O}_{2N\mathcal{N}_c}, & \ldots, & \mathbb{O}_{2N\mathcal{N}_c} \\ \mathbb{O}_{2N\mathcal{N}_c}, & \mathbb{I}_N \otimes \mathbb{P}_{\mathbb{B}_{12}}^{\perp}, & \cdots, & \mathbb{O}_{2N\mathcal{N}_c} \\ \vdots & \vdots & \ddots & \vdots \\ \mathbb{O}_{2N\mathcal{N}_c}, & \mathbb{O}_{2N\mathcal{N}_c}, & \cdots, & \mathbb{I}_N \otimes \mathbb{P}_{\mathbb{B}_{1\overline{N}}}^{\perp} \end{bmatrix} \tag{3.16}$$

Finally, at point-F in Figure 3.5, all the projected vectors are concatenated to form a longer vector $\underline{x}[n] \in \mathcal{C}^{2N\overline{N}\mathcal{N}_c \times 1}$ (see also in Figure 3.6(c)) as follows

$$\underline{x}[n] = \begin{bmatrix} \left(\mathbb{I}_N \otimes \mathbb{P}_{\mathbb{B}_{11}}^{\perp}\right) \underline{x}_{\mathrm{st}}[n] \\ \left(\mathbb{I}_N \otimes \mathbb{P}_{\mathbb{B}_{12}}^{\perp}\right) \underline{x}_{\mathrm{st}}[n] \\ \vdots \\ \left(\mathbb{I}_N \otimes \mathbb{P}_{\mathbb{B}_{1\overline{N}}}^{\perp}\right) \underline{x}_{\mathrm{st}}[n] \end{bmatrix} \tag{3.17}$$

and this is the "virtual-spatiotemporal snapshot". Equ 3.17 can also be written in a more compact form as follows

$$\underline{x}[n] = \underbrace{\sum_{k=1}^{K_1} \beta_{1k} \exp\left(j2\pi\mathcal{F}_{1k} n T_{cs}\right) \mathbb{P}_{\mathbb{B}_1}^{\perp}\left(\underline{h}_{1k} \odot \left(\overline{\underline{w}}_1 \otimes \underline{1}_{2N\mathcal{N}_c}\right)\right) \mathrm{a}_1[n]}_{\text{Desired term}} + \underline{x}_{\text{ISI}} + \underline{x}_{\text{MAI}} + \text{noise} \tag{3.18}$$

which contains the desired symbol, the ISI, the MAI and the noise. The ISI term, MAI term and the noise term are expressed as follows, respectively

$$\begin{aligned}\underline{x}_{\text{ISI}} = & \sum_{k=1}^{K_1} \beta_{1k} \mathbb{P}_{\mathbb{B}_1}^{\perp}\left(\underline{h}_{1k} \odot \left(\overline{\underline{w}}_1 \otimes \underline{1}_{2N\mathcal{N}_c}\right)\right) \\ & \Big\{ \left(\mathbb{I}_{N\overline{N}} \otimes \left(\mathbb{J}^T\right)^{\mathcal{N}_c}\right) \exp\left(j2\pi\mathcal{F}_{1k}(n-1)T_{cs}\right) \mathrm{a}_1[n-1] \\ & + \left(\mathbb{I}_{N\overline{N}} \otimes \mathbb{J}^{\mathcal{N}_c}\right) \exp\left(j2\pi\mathcal{F}_{1k}(n+1)T_{cs}\right) \mathrm{a}_1[n+1] \Big\}\end{aligned} \tag{3.19}$$

$$\begin{aligned}\underline{x}_{\text{MAI}} = & \sum_{i=2}^{M} \sum_{k=1}^{K_i} \beta_{ik} \mathbb{P}_{\mathbb{B}_1}^{\perp}\left(\underline{h}_{ik} \odot \left(\overline{\underline{w}}_i \otimes \underline{1}_{2N\mathcal{N}_c}\right)\right) \\ & \Big\{ \exp\left(j2\pi\mathcal{F}_{ik} n T_{cs}\right) \mathrm{a}_i[n] \\ & + \left(\mathbb{I}_{N\overline{N}} \otimes \left(\mathbb{J}^T\right)^{\mathcal{N}_c}\right) \exp\left(j2\pi\mathcal{F}_{ik}(n-1)T_{cs}\right) \mathrm{a}_i[n-1] \\ & + \left(\mathbb{I}_{N\overline{N}} \otimes \mathbb{J}^{\mathcal{N}_c}\right) \exp\left(j2\pi\mathcal{F}_{ik}(n+1)T_{cs}\right) \mathrm{a}_i[n+1] \Big\}\end{aligned} \tag{3.20}$$

$$\text{noise} = \underbrace{\mathbb{P}_{\mathbb{B}_1}^{\perp}\left(\underline{1}_{\overline{N}} \otimes \text{vec}\left(\mathbb{N}^T[n]\right)\right)}_{\underline{\mathrm{n}}[n]} \tag{3.21}$$

It is clear that the virtual-spatiotemporal snapshot $\underline{x}[n]$ in Equs 3.18-3.21 is a function of the extended manifold vector $\underline{h}_{ik} \in \mathcal{C}^{2N\overline{N}\mathcal{N}_c \times 1}$, which is written as

$$\boxed{\underline{h}_{ik} = \left(\overline{\underline{S}}_{ik}^{*} \otimes \underline{S}_{ik}\right) \otimes \left(\mathbb{J}^{l_{ik}} \underline{c}_i \odot \underline{\mathcal{F}}_{ik}\right)} \tag{3.22}$$

and called as virtual-spatiotemporal manifold vector. The word "virtual" has been used because the Tx manifold vector $\overline{\underline{S}}_{ik}$ and Rx manifold vector $\underline{S}_{ik}$ form the "virtual" manifold vector $\overline{\underline{S}}_{ik}^{*} \otimes \underline{S}_{ik}$. In Equ 3.22, the vector $\underline{c}_i \in \mathcal{R}^{2\mathcal{N}_c \times 1}$ representing the sum of the weight code vector associated with each Tx antenna

of the i-th user shown as

$$\underline{c}_i = \begin{bmatrix} \mathbb{C}_i \\ \mathbb{O}_{\mathcal{N}_c \times \overline{N}} \end{bmatrix} \underline{1}_{\overline{N}} \tag{3.23}$$

It is important to point out that, the theoretical covariance matrix $\mathbb{R}_{xx} \in \mathcal{C}^{2N\overline{N}\mathcal{N}_c \times 2N\overline{N}\mathcal{N}_c}$ of $\underline{x}[n]$ is

$$\begin{aligned}
\mathbb{R}_{xx} &= \mathcal{E}\left\{\underline{x}[n]\,\underline{x}^H[n]\right\} \\
&= \underbrace{\mathbb{G}_1 \mathrm{diag}\left\{\underline{\beta}_1 \odot \underline{\beta}_1^*\right\} \mathbb{G}_1^H}_{\mathbb{R}_{\mathrm{des}}} \\
&+ \underbrace{\mathbb{G}_1^{\mathrm{shift}} \left(\mathbb{I}_2 \otimes \mathrm{diag}\left\{\underline{\beta}_1 \odot \underline{\beta}_1^*\right\}\right) \left(\mathbb{G}_1^{\mathrm{shift}}\right)^H}_{\mathbb{R}_{\mathrm{ISI}}} \\
&+ \underbrace{\sum_{i=2}^{M} \left[\mathbb{G}_i^{\mathrm{shift}}, \mathbb{G}_i\right] \left(\mathbb{I}_3 \otimes \mathrm{diag}\left\{\underline{\beta}_i \odot \underline{\beta}_i^*\right\}\right) \left[\mathbb{G}_i^{\mathrm{shift}}, \mathbb{G}_i\right]^H}_{\mathbb{R}_{\mathrm{MAI}}} \\
&+ \underbrace{\sigma_{\mathrm{n}}^2 \mathbb{P}_{\mathbb{B}_1}^{\perp}}_{\mathbb{R}_{\mathrm{nn}}}
\end{aligned} \tag{3.24}$$

with the following assumptions

$$\begin{cases}
\mathcal{E}\left\{\mathrm{a}_i[n]\,\mathrm{a}_i^H[n]\right\} = 1 \\
\mathcal{E}\left\{\underline{f}_i[n]\,\underline{f}_i^H[n]\right\} = \mathbb{I}_{K_i} \\
\mathcal{E}\left\{\underline{\mathrm{n}}[n]\,\underline{\mathrm{n}}^H[n]\right\} = \sigma_{\mathrm{n}}^2 \mathbb{I}_{2N\overline{N}\mathcal{N}_c}
\end{cases} \tag{3.25}$$

and the vector $\underline{\beta}_i$ contains the path coefficient β_{ik} of K_i paths, the matrix $\mathbb{G}_i$ contains $\underline{g}_{ik}$ of K_i paths and $\mathbb{G}_i^{\mathrm{shift}}$ is its shifted matrix, given as follows

$$\underline{\beta}_i = \left[\beta_{i1}, \beta_{i2}, \ldots, \beta_{ik}, \ldots, \beta_{iK_i}\right]^T \in \mathcal{C}^{K_i \times 1} \tag{3.26}$$

$$\mathbb{G}_i = \left[\underline{g}_{i1}, \underline{g}_{i2}, \ldots, \underline{g}_{ik}, \ldots, \underline{g}_{iK_i}\right] \in \mathcal{C}^{2N\overline{N}\mathcal{N}_c \times K_i} \tag{3.27}$$

$$\mathbb{G}_i^{\mathrm{shift}} = \left[\left(\mathbb{I}_{N\overline{N}} \otimes \left(\mathbb{J}^T\right)^{\mathcal{N}_c}\right) \mathbb{G}_i, \left(\mathbb{I}_{N\overline{N}} \otimes \mathbb{J}^{\mathcal{N}_c}\right) \mathbb{G}_i\right] \in \mathcal{C}^{2N\overline{N}\mathcal{N}_c \times 2K_i} \tag{3.28}$$

where $\underline{g}_{ik}$ is given as

$$\underline{g}_{ik} = \mathbb{P}_{\mathbb{B}_1}^{\perp}\left(\underline{h}_{ik} \odot \left(\underline{\overline{w}}_i \otimes \underline{1}_{2N\mathcal{N}_c}\right)\right) \tag{3.29}$$

In practice, over an observation interval of L symbols (see Figure 3.6(c)), this matrix can be expressed as follows

$$\mathbb{R}_{xx} \simeq \frac{1}{L} \sum_{n=1}^{L} \underline{x}\left[n\right] \underline{x}^{H}\left[n\right] \tag{3.30}$$

In summary, by observing $\underline{x}\left[n\right]$ or $\mathbb{R}_{xx}$, the "manifold extender" increases the dimensionality of the signal observation space from N to $2N\overline{N}\mathcal{N}_c$ so that the degrees of freedom has been increased.

3.4.1 Manifold Extender Comparison

In this chapter, two other extended manifold vectors obtained by different manifold extenders are presented, all of which are functions of the original manifold vector, and their performance is evaluated in computer simulation studies.

With reference to [1] and Chapter 2, a virtual manifold extender is presented which extends the signal observation space from N to $N\overline{N}$ and its equivalent extended manifold vector is known as the virtual manifold vector $\underline{S}_{\mathrm{v},ik} \in \mathcal{C}^{N\overline{N}\times 1}$ given as

$$\boxed{\underline{S}_{\mathrm{v},ik} = \overline{\underline{S}}^{*}_{ik} \otimes \underline{S}_{ik}} \tag{3.31}$$

It is clear that the virtual-spatiotemporal manifold vector in Equ 3.22 is shown as a function of the virtual manifold vector in Equ 3.31. Thus, the virtual-spatiotemporal manifold extender can be considered as an extension of the virtual manifold extender. This, in effect, increases the number of dimensions of the virtual array system from $N\overline{N}$ to $2N\overline{N}\mathcal{N}_c$ in the proposed virtual-spatiotemporal system, and thus the degrees of freedom is further increased.

Furthermore, with reference to [21], the spatiotemporal manifold vector is expressed as

$$\boxed{\underline{\mathfrak{h}}_{ik} = \underline{S}_{ik} \otimes \left(\mathbb{J}^{l_{ik}} \underline{c}_i \odot \underline{\mathcal{F}}_{ik}\right)} \tag{3.32}$$

and it can also be clearly noted in Equ 3.22 that the virtual-spatiotemporal manifold vector is an extension of the spatiotemporal manifold vector. In this case,

the number of system dimensions increases from $2N\mathcal{N}_c$ to $2N\overline{N}\mathcal{N}_c$ in the proposed virtual-spatiotemporal system. Note that for a SIMO system ($\overline{N} = 1$), the virtual-spatiotemporal manifold vector becomes equivalent to the spatiotemporal manifold vector.

3.4.2 Joint Delay-Doppler Estimation

The delay and Doppler frequency associated with all the multipaths of the desired user can be estimated by the cost function $\xi(l, \mathcal{F})$ as

$$\xi\left(l, \mathcal{F}\right) = \frac{\det\left(\mathbb{T}^H \mathbb{T}\right)}{\det\left(\mathbb{T}^H \mathbb{P}_{\mathrm{n}} \mathbb{T}\right)} \tag{3.33}$$

where $\mathbb{T} \triangleq \mathbb{T}(l, \mathcal{F})$ is given by

$$\mathbb{T} = \mathbb{J}^l \begin{bmatrix} \mathbb{C}_1 \\ \mathbb{O}_{\mathcal{N}_c \times \overline{N}} \end{bmatrix} \odot \left(\underline{\mathcal{F}} \underline{1}_{\overline{N}}^T\right) \tag{3.34}$$

By maximising (2D search) Equ 3.33, the peak values $(l_1, \mathcal{F}_1), (l_2, \mathcal{F}_2), ..., (l_{K_1}, \mathcal{F}_{K_1})$ can be obtained that correspond to the desired user's delay and Doppler frequency of all paths respectively. Note that $\mathbb{P}_{\mathrm{n}}$ in Equ 3.33 is the projection operator spanned by noise eigenvectors $\mathbb{E}_{\mathrm{n}}$ of the covariance matrix $\mathbb{R}_{\mathbb{Y}\mathbb{Y}}$ of $\mathbb{Y}$ where

$$\mathbb{Y} = \left[\mathbb{X}^T[1], \mathbb{X}^T[2], \ldots, \mathbb{X}^T[n], \ldots, \mathbb{X}^T[L]\right] \tag{3.35}$$

which is a $2N\mathcal{N}_c \times NL$ matrix with $\mathbb{X}[n]$ denoting the n-th slide of the 3D data cube.

3.4.3 Joint DOA-DOD Estimation

With the estimated pairs of delays and Doppler frequencies, the projection matrix $\mathbb{P}_{\mathbb{B}_1}^{\perp}$ is constructed. Then, the virtual-spatiotemporal snapshot $\underline{x}[n]$ is formed based on Equ 3.17. Towards this, the projection operator $\mathbb{P}_{\mathrm{n_v}}$ onto the subspace spanned by noise eigenvectors of the covariance matrix $\mathbb{R}_{xx}$ can be formed. We

now employ the virtual-spatiotemporal manifold vector associated with the desired user as given by Equ 3.22 in conjunction with the following cost function to yield the DOA and DOD corresponding to every pair of $(l_k, \mathcal{F}_k)$

$$(\underline{\theta}, \underline{\overline{\theta}}) = \arg\max_{\forall(\theta,\overline{\theta})} \xi(\theta, \overline{\theta})|_{(l_k,\mathcal{F}_k)}, \forall k \tag{3.36}$$

where $\xi(\theta, \overline{\theta})$ is defined as follows

$$\xi(\theta, \overline{\theta}) = \frac{\left(\mathbb{P}^{\perp}_{\mathbb{B}_1} \underline{h}(\theta, \overline{\theta}) \odot (\underline{\overline{w}}_1 \otimes \underline{1}_{2N\mathcal{N}_c})\right)^H (\mathbb{P}^{\perp}_{\mathbb{B}_1} \underline{h}(\theta, \overline{\theta}) \odot (\underline{\overline{w}}_1 \otimes \underline{1}_{2N\mathcal{N}_c}))}{\left(\mathbb{P}^{\perp}_{\mathbb{B}_1} \underline{h}(\theta, \overline{\theta}) \odot (\underline{\overline{w}}_1 \otimes \underline{1}_{2N\mathcal{N}_c})\right)^H \mathbb{P}_{\mathrm{n_v}} (\mathbb{P}^{\perp}_{\mathbb{B}_1} \underline{h}(\theta, \overline{\theta}) \odot (\underline{\overline{w}}_1 \otimes \underline{1}_{2N\mathcal{N}_c}))} \tag{3.37}$$

This is easy to be optimised by using a 2D search where the peaks of the cost function $\xi(\theta, \overline{\theta})$ correspond to the DOA and DOD of all paths of the desired user respectively.

3.4.4 Design of the Rx Virtual-Spatiotemporal Beamformer Weights

In this subsection, by using the estimated channel parameters of the desired user in Sections 3.4.2 and 3.4.3 together with path fading coefficients, the design of the virtual-spatiotemporal beamformer weights are proposed that receives the desired signal whilst suppress co-channel interference. The design procedure is described as follows

1. The unwanted subspace $\mathbb{R}_{\text{unwanted}}$ is constructed by removing the contribution of the desired signal from the received signal covariance matrix $\mathbb{R}_{xx}$, given by

$$\mathbb{R}_{\text{unwanted}} = \mathbb{R}_{xx} - \mathbb{G}_1 \text{diag}\left\{\underline{\beta}_1\right\} \mathbb{G}_1^H \tag{3.38}$$

   where $\mathbb{R}_{xx}$ is given by Equ 3.24 and $\mathbb{G}_1$ is obtained by substituting all the estimated channel parameters into Equ 3.27.

2. By performing an eigendecomposition of $\mathbb{R}_{\text{unwanted}}$, the unwanted signal subspace spanned by the significant eigenvector matrix $\mathbb{E}_s$ can be obtained to

construct a projection operator towards the space spanned by the desired user shown as

$$\mathbb{P}^{\perp}_{\text{unwanted}} = \mathbb{I}_{2N\overline{N}\mathcal{N}_c} - \mathbb{E}_s \left(\mathbb{E}_s^H \mathbb{E}_s\right)^{-1} \mathbb{E}_s^H \tag{3.39}$$

Thus, the virtual-spatiotemporal subspace beamformer weight $\underline{w}_{\text{v}}^{\text{sub}} \in \mathcal{C}^{2N\overline{N}\mathcal{N}_c \times 1}$ (point-G in Figure 3.4) may be obtained as

$$\underline{w}_{\text{v}}^{\text{sub}} = \mathbb{P}^{\perp}_{\text{unwanted}} \mathbb{G}_1 \left\{\mathbb{G}_1^H \mathbb{P}^{\perp}_{\text{unwanted}} \mathbb{G}_1\right\}^{-1} \underline{\beta}_1 \tag{3.40}$$

In addition, for the sake of completeness, the virtual-spatiotemporal RAKE beamformer weight introduced in [67] is also employed here

$$\underline{w}_{\text{v}}^{\text{RAKE}} = \mathbb{G}_1 \underline{\beta}_1 \tag{3.41}$$

3.5 Computer Simulation Studies

In this section the performance of the proposed algorithms is evaluated using computer simulation studies. Without loss of generality, the Tx and Rx antenna array geometries to be used are given (without any loss of generality) by Equs 3.42 and 3.43, respectively. These are two uniform circular arrays (UCAs) on the (x, y) plane with $\overline{N} = 7$ antennas on the Tx's side and $N = 9$ antennas on the Rx's side. In the reception studies, a uniform linear array (ULA) and a cross-shaped array with $\overline{N} = 7$ antennas are also considered at the Tx to evaluate the receiver performance in terms of different Tx array geometries. The three different Tx array geometries under consideration are plotted in Figure 3.8. Furthermore, an observation interval of $L = 200$ transmitted symbols is assumed. Table 3.1 provides

$$[\underline{\overline{r}}_1, \underline{\overline{r}}_2, ..., \underline{\overline{r}}_{\overline{N}}] = \begin{bmatrix} 1.13, & 0.55, & -0.45, & -1.11, & -0.94, & -0.06, & 0.86 \\ 0.20, & 1.01, & 1.06, & 0.31, & -0.67, & -1.15, & -0.76 \\ 0.00, & 0.00, & 0.00, & 0.00, & 0.00, & 0.00, & 0.00 \end{bmatrix} \tag{3.42}$$

$$[\underline{r}_1, \underline{r}_2, ..., \underline{r}_N] = \begin{bmatrix} 1.46, & 1.12, & 0.25, & -0.73, & -1.37, & -1.37, & -0.73, & 0.25, & 1.12 \\ 0.00, & 0.94, & 1.44, & 1.27, & 0.50, & -0.50, & -1.27, & -1.44, & -0.94 \\ 0.00, & 0.00, & 0.00, & 0.00, & 0.00, & 0.00, & 0.00, & 0.00, & 0.00 \end{bmatrix} \tag{3.43}$$

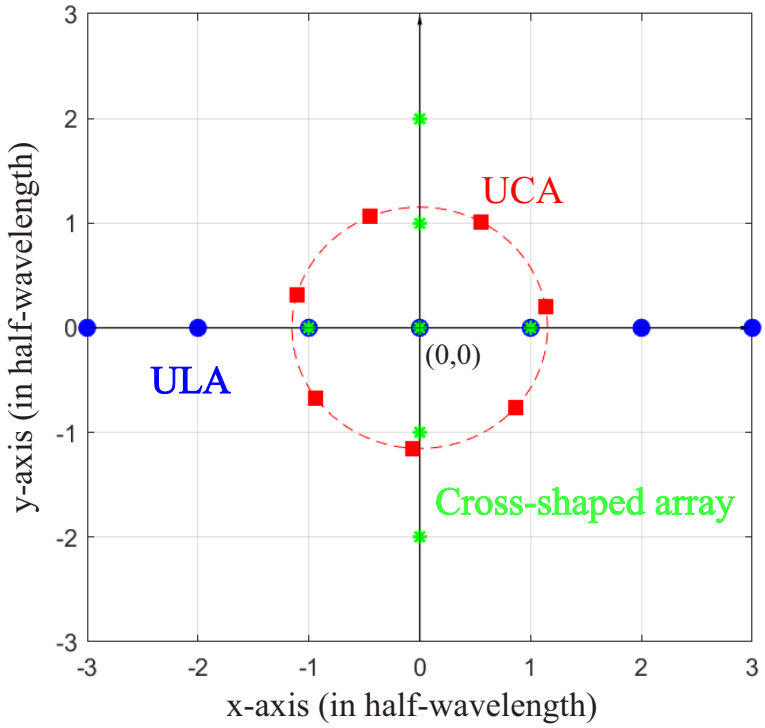

Figure 3.8: The three Tx array geometries: UCA (red marker), ULA (blue marker) and cross-shaped array (green marker).

some additional system simulation parameters. The channel parameters to be estimated are assumed to be randomly selected following uniform distributions in their respective intervals.

Table 3.1: Simulation parameters

Parameter	Value	Parameter	Value
M	4	$\mathcal{N}_c$	31 chips
K	3	$\bar{N}$	7
T_c	0.1 ms	N	9

3.5.1 Estimation Studies

In this subsection, the performance of the channel estimation of the proposed virtual-spatiotemporal system is evaluated. As indicated in Table 3.1, there are $M = 4$ users, which implies that the desired user operates in the presence of three

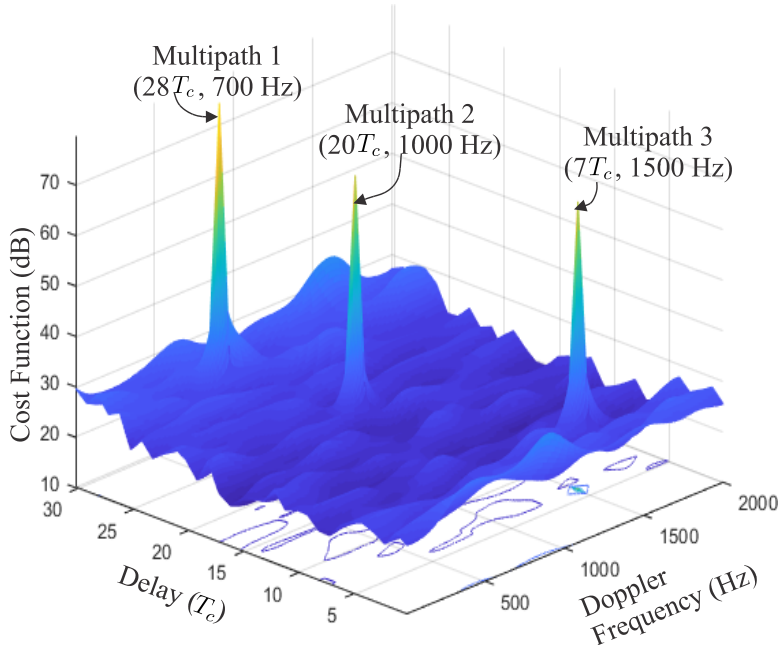

Figure 3.9: Joint estimation of delay and Doppler frequency corresponding to the three multipaths of the desired user.

other co-channel interferers with $K = 3$ multipaths per user. Therefore, it is assumed that the channel parameters to be estimated are displayed in Table 3.2. Figure 3.9 and Figure 3.10 show the results of the joint delay-Doppler frequency estimation and joint DOA-DOD estimation respectively. It can be clearly seen that the peaks occur at the wanted parameters of the desired user.

Table 3.2: Channel parameters

Path index	delay (T_c)	Doppler frequency (Hz)	DOA (deg)	DOD (deg)
1st path	28	700	280	30
2nd path	20	1000	200	110
3rd path	7	1500	60	140

Consider again the simulation environment in Figure 3.10, now it is assumed two of the three paths of the desired user have directions close together in space. That is, the DOA and DOD values of three paths are $(92°, 90°, 60°)$ and $(68°, 70°, 90°)$. The result is illustrated in Figure 3.11 and it shows that the estimation peaks are still very sharp and distinguishable, indicating the superresolution capabilities of

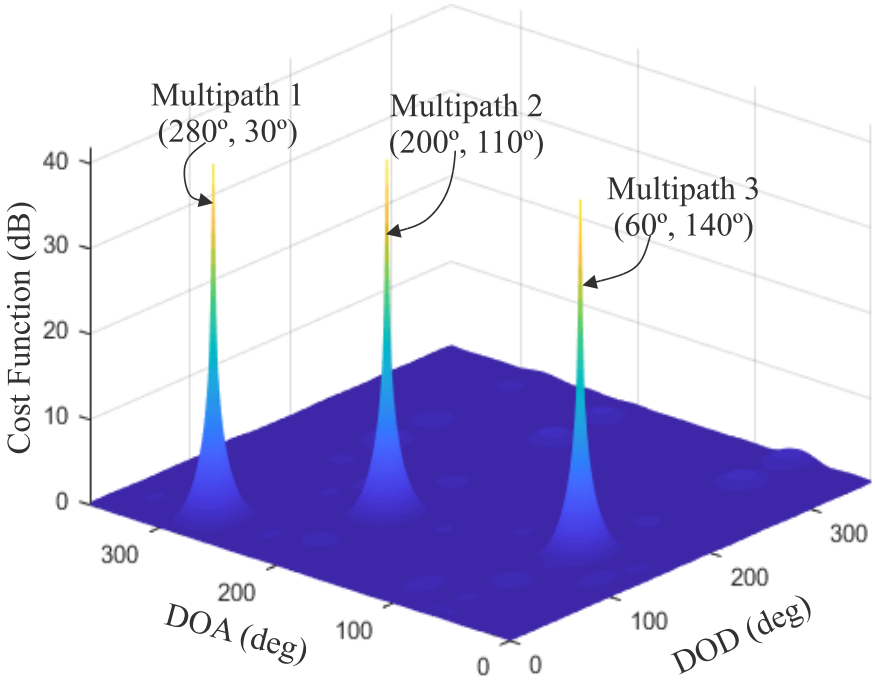

Figure 3.10: Joint estimation of DOA and DOD corresponding to the three multipaths of the desired user.

the proposed algorithm.

Furthermore, the performance of the estimation algorithms presented in Subsections 3.4.2 and 3.4.3 is evaluated in terms of the root mean square error (RMSE) of the Doppler frequency, DOD and DOA as a function of the SNR. The results are shown in Figure 3.12 indicating that estimation error decreases with an increase in SNR.

A key performance parameter for subspace based estimation approaches is the number of the virtual-spatiotemporal snapshots L required to achieve a certain RMSE at a specified SNR. Figure 3.13 illustrates the performance of the proposed estimation algorithms in terms of the RMSE of the estimated parameters versus the number of the virtual-spatiotemporal snapshots L with the SNR fixed at 20 dB. As expected (see Chapter 8 in [18]), the error in the estimation of Doppler frequency, DOA and DOD decreases with an increase in the number of snapshots[2].

[2]The delay estimation error is not presented as it remains zero through the total range of SNR or number of snapshots.

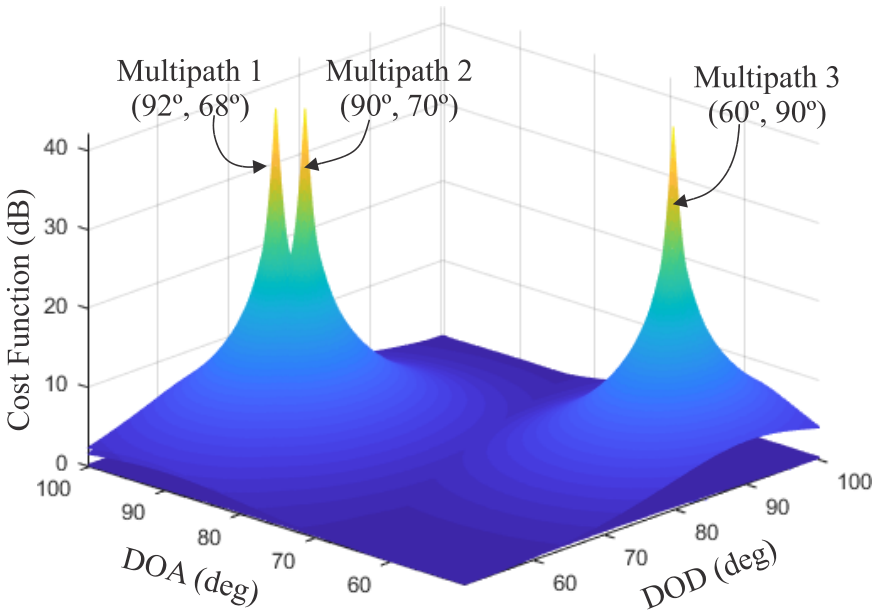

Figure 3.11: Joint Estimation of DOA and DOD when the signals from path 1 and path 2 of the desired user are closely spaced.

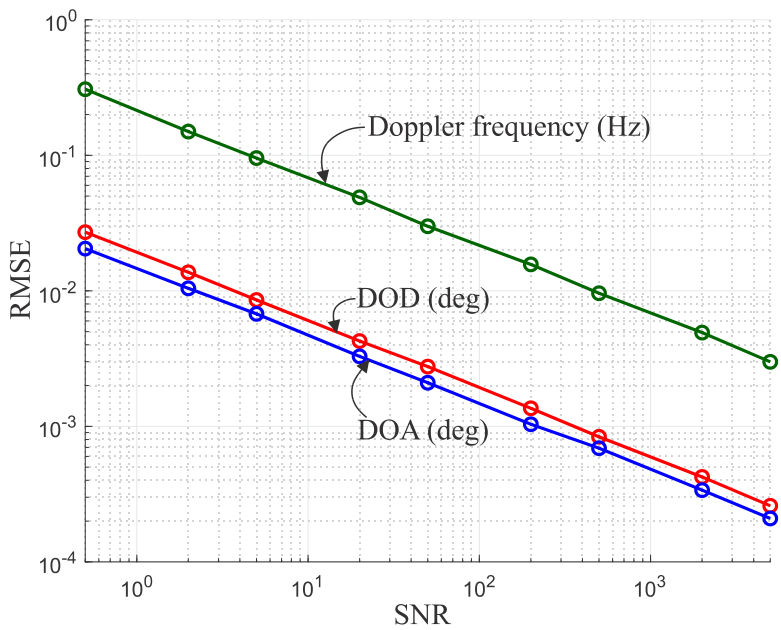

Figure 3.12: RMSE of the different parameters being estimated versus the SNR. (300 realisations)

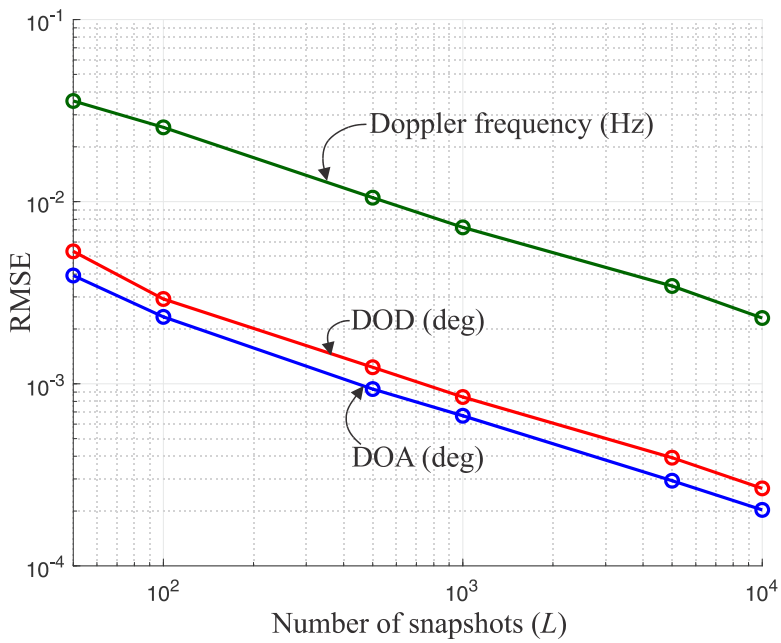

Figure 3.13: RMSE of the different parameters being estimated versus the number of the virtual-spatiotemporal snapshot L. (300 realisations)

Thus, when the SNR is low, a high number of snapshots may be needed to resolve two transmitters which are close together in space.

Finally, the proposed virtual-spatiotemporal system is compared with the virtual system in [1], the spatiotemporal system in [21] and the conventional spatial-only system with the same Tx and Rx array geometries and under the same simulation environment. However, the channel estimation algorithm for the space-only system fails due to insufficient degrees of freedom (12 signals in a 9-dimensional observation space). Thus, to enable the space-only system to work properly, the number of multipath per user is reduced to 2 with all DODs equal to 0°. The algorithm of the virtual system and the spatiotemporal system is provided in [1] and [21], respectively. Figure 3.14 and Figure 3.15 show the RMSE of the DOD and DOA estimation versus the (SNR$\times L$) using the aforementioned system approaches. Note that the DOD estimation for the spatial-only system and the spatiotemporal system are not plotted in Figure 3.14 because such systems cannot estimate the DODs as their Tx information cannot be exploited by the receiver.

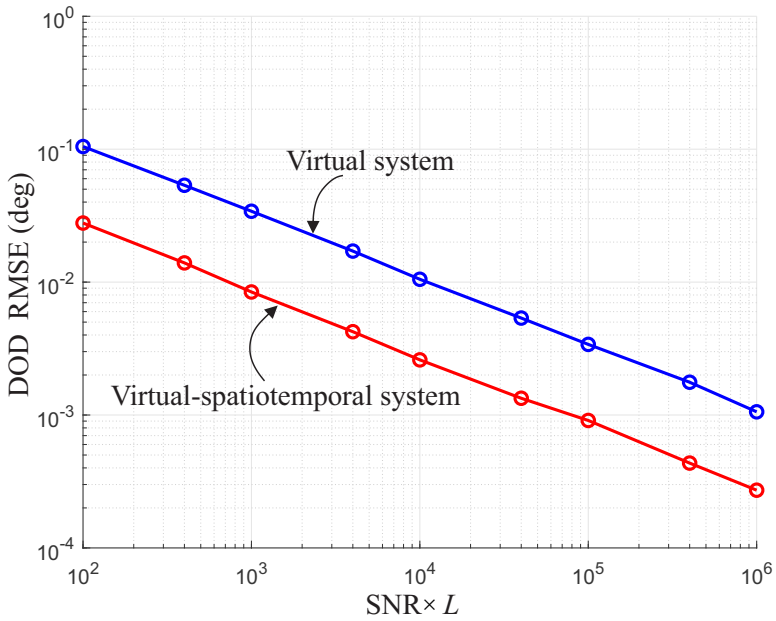

Figure 3.14: RMSE of DOD estimation for the virtual and virtual-spatiotemporal systems. (300 realisations)

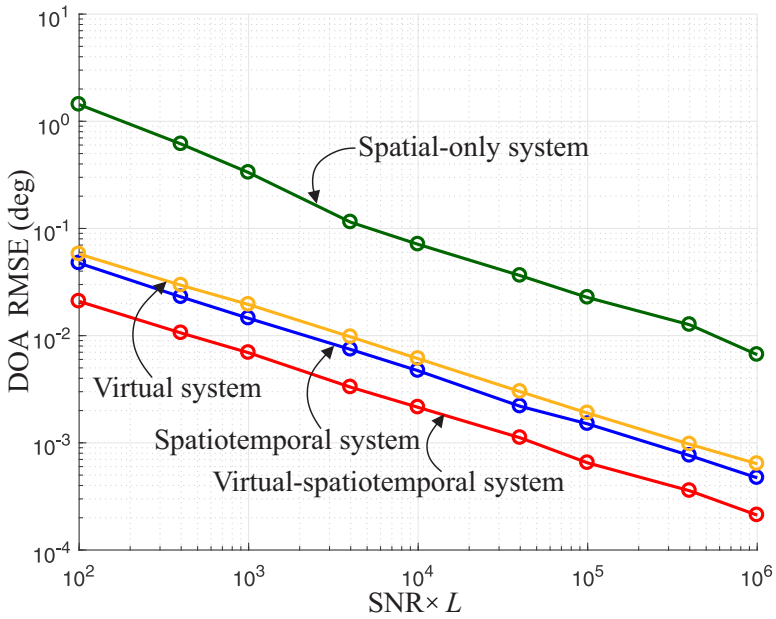

Figure 3.15: RMSE of DOA estimation for the spatial-only, spatiotemporal, virtual and virtual-spatiotemporal systems. (100 realisations)

In this simulation, the number of snapshots L is fixed at 200 and the SNR varies from -3 dB to 36 dB. As illustrated in Figures 3.14 and 3.15, the proposed virtual-spatiotemporal system has superior channel estimation accuracy, which indicates that this system has the most degrees of freedom. It is also proven that the estimation accuracy is related to the dimensionality of the system (or degrees of freedom) since the dimensionality for the proposed virtual-spatiotemporal system, the spatiotemporal system, the virtual system and the spatial-only system is $2N\overline{N}\mathcal{N}_c > 2N\mathcal{N}_c > N\overline{N} > N$, based on the parameter value in Table 3.1. This illustrates the superiority[3] of the virtual-spatiotemporal MIMO system in terms of the receiver resolution capability.

3.5.2 Reception Studies

In this subsection, the performance of the proposed virtual-spatiotemporal subspace beamformer is evaluated by comparing with the spatial-only and the spatiotemporal [21] beamformers. The metric used for comparison is the output signal-to-noise plus interference ratio ($\mathrm{SNIR}_{\mathrm{out}}$) given as

$$\mathrm{SNIR}_{\mathrm{out}} = \frac{\underline{w}^H \mathbb{R}_{\mathrm{des}} \underline{w}}{\underline{w}^H \left(\mathbb{R}_{\mathrm{MAI}} + \mathbb{R}_{\mathrm{ISI}} + \mathbb{R}_{\mathrm{nn}}\right) \underline{w}} \tag{3.44}$$

where $\underline{w}$ denotes the beamforming weight employed at the receiver, $\mathbb{R}_{\mathrm{des}}$ denotes the covariance matrix of the desired signal, $\mathbb{R}_{\mathrm{MAI}}$ denotes the covariance matrix of the multiple access interference signal, $\mathbb{R}_{\mathrm{ISI}}$ denotes the covariance matrix of the inter symbol interference signal of the desired user, and $\mathbb{R}_{\mathrm{nn}}$ represents the noise covariance matrix. Evidently, the value of the SNIR output depends on the design of receiver weight being employed at the receiver.

A conventional non-subspace beamformer weight design algorithm such as the RAKE given by Equ 3.41 is introduced here for the beamformer performance comparison. The proposed virtual-spatiotemporal subspace beamformer is compared

[3] It is important to point out that spatiotemporal systems perform better than massive MIMO systems (see [21]).

against the spatiotemporal subspace beamformer, the spatial-only subspace beamformer, and the RAKE-type beamformers for the three systems. All the systems being compared utilise identical resources i.e. identical Tx and Rx antenna arrays and sampling frequency at the receiver (i.e. bandwidth). The DODs of the desired user for all receivers are set to 45° and the transmit weight is assumed to be steering vector beamformer directed to 90°. Figure 3.16 illustrates a comparison of $\mathrm{SNIR}_{\mathrm{out}}$ for the subspace-type and RAKE-type steering vector beamformers for varying levels of interference power (i.e. the near-far ratio (NFR)). As expected, the performance of all the RAKE steering vector beamformers steadily declines with increasing interference levels because the RAKE beamformer is unable to provide sufficient levels of interference cancellation. It can also be observed that the virtual-spatiotemporal subspace beamformer provides a constant higher gain than the other beamformers in this situation and this gain in the $\mathrm{SNIR}_{\mathrm{out}}$ is attributed to the extension of the array manifold to incorporate the Tx spatial domain and temporal domain resulting in an increase in system dimensions to $2\overline{N}N\mathcal{N}_c$. The increase in the system dimensions enables the beamformer to reconstruct the signal and noise subspaces with increased accuracy, resulting in heightened interference cancellation, and thus more degrees of freedom.

It is illustrated in Figure 3.16 that subspace beamformers exhibit nearly constant performance for NFR levels ranging from 0 to 60 dB. Therefore, the interference term maybe completely cancelled and Equ 3.44 may be simplified to the following

$$\mathrm{SNIR}_{\mathrm{out}} = G_{\mathrm{dim}}\mathrm{SNR}_{\mathrm{in}} \tag{3.45}$$

where G_{dim} denotes the array gain and $\mathrm{SNR}_{\mathrm{in}}$ denotes the desired signal to noise ratio at the input of the receiver which is given by

$$\mathrm{SNR}_{\mathrm{in}} = \frac{P_s}{\sigma_{\mathrm{n}}^2} \tag{3.46}$$

where P_s denotes the power of the desired signal at the receiver. It is assumed

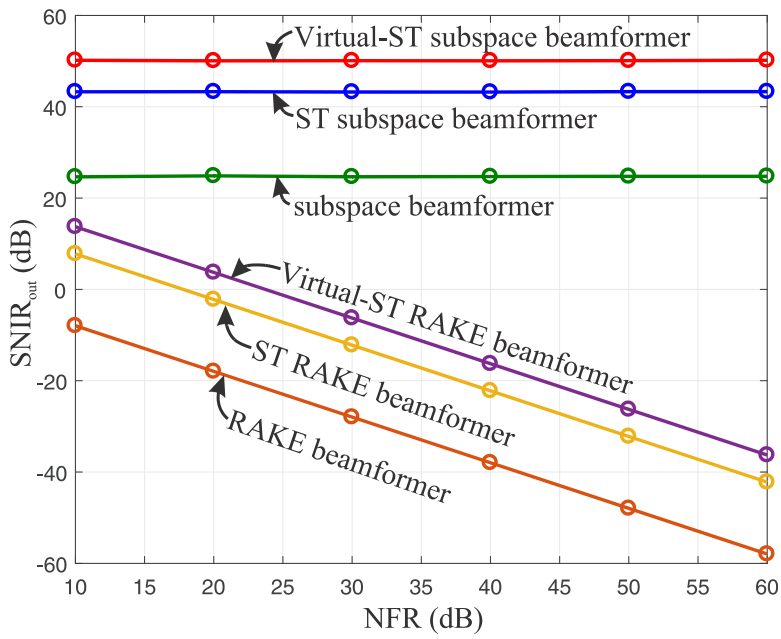

Figure 3.16: Comparison of output SNIR versus the near far ratio for three different RAKE and subspace receivers namely spatial-only, spatiotemporal (ST) and the proposed virtual-spatiotemporal (virtual-ST) receivers (50 realisations).

that the power of the desired signal at the transmitter is unity, equivalently, Equ 3.45 can be simplified to the followings for the spatial-only, spatiotemporal and virtual-spatiotemporal beamformers

$$\mathrm{SNIR}_{\mathrm{out}} = N\mathrm{SNR}_{\mathrm{in}} = N\frac{G_{Tx}}{\sigma_{\mathrm{n}}^2} \tag{3.47a}$$

$$\mathrm{SNIR}_{\mathrm{out}}^{\mathrm{ST}} = N\mathcal{N}_c\mathrm{SNR}_{\mathrm{in}} = N\mathcal{N}_c\frac{G_{Tx}}{\sigma_{\mathrm{n}}^2} \tag{3.47b}$$

$$\mathrm{SNIR}_{\mathrm{out}}^{\mathrm{vST}} = N\overline{N}\mathcal{N}_c\mathrm{SNR}_{\mathrm{in}} = N\overline{N}\mathcal{N}_c\frac{1}{\sigma_{\mathrm{n}}^2} \tag{3.47c}$$

where G_{Tx} denotes the gain caused by Tx beamforming. It can be observed from the aforementioned equations that the output SNIR in the spatial-only and spatiotemporal systems is variable which depends on the Tx beamforming, i.e. the Tx array geometry, the DOD and the transmit weight. Note that the spatial-only and spatiotemporal beamformers cannot estimate DODs, thus the beamformer cannot utilise this parameter which means that the array gain should be considered a variable. The output SNIR in terms of the DOD is illustrated in Figures 3.17 -

3.19 where the proposed beamformer is compared with the spatial-only and spatiotemporal beamformers for three sets of Tx array geometries as shown in Figure 3.8. The DOD of the desired user varies from 0° to 180°, and for simplicity, all the paths of the desired user are assumed to have identical DODs. The transmit weight is assumed to be a steering vector beamformer with its mainlobe towards 90°. The NFR is set to 10 dB and the SNR is set to 20 dB.

It is shown in Figures 3.17 - 3.19 that the SNIR output of the spatiotemporal and spatial-only receivers varies depending on the DOD and the Tx array geometry, and the best SNIR output for each receiver occurs when the DOD is equal to the direction of the mainlobe of the Tx steering vector beamformer. These beamformers cannot estimate (and thus utilise) DOD which is arbitrary and unknown. Consequently, the SNIR output varies with DOD. On the contrary, the proposed virtual-spatiotemporal beamformer shows a high steady SNIR output when the DOD or the Tx array geometry varies indicating that the performance of the proposed virtual-spatiotemporal system is independent of the DOD and the Tx array geometry. This is because the beamformer is capable of estimating the DOD and utilise this parameter together with the Tx array geometry to enhance the system performance. Furthermore, the proposed system is applicable for arbitrary array geometries.

Finally, Figure 3.20 illustrates a comparative study of the output SNIR for the spatial-only, spatiotemporal, and virtual-spatiotemporal beamformers with an increasing number of signals in the system. Note that these signals are equivalent to an increasing number of users and/or multipaths. In this figure, the number of users varies and the number of multipaths per user is fixed at 6. Figure 3.20 shows that the output SNIR of the spatial-only system drops to a very low value when the system is required to support a large number of signals, as the dimension of the covariance matrix is insufficient to construct the interference space and therefore interference cannot be fully eliminated. The output SNIR of the spatiotemporal

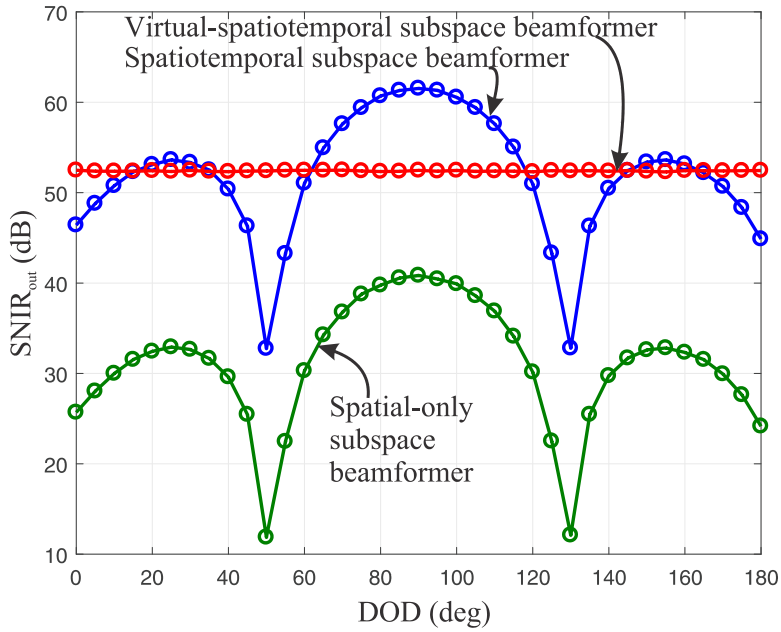

Figure 3.17: Comparison of output SNIR versus the DOD between the spatial-only, spatiotemporal, virtual-spatiotemporal subspace beamformers with a UCA being employed at the transmitter (50 realisations).

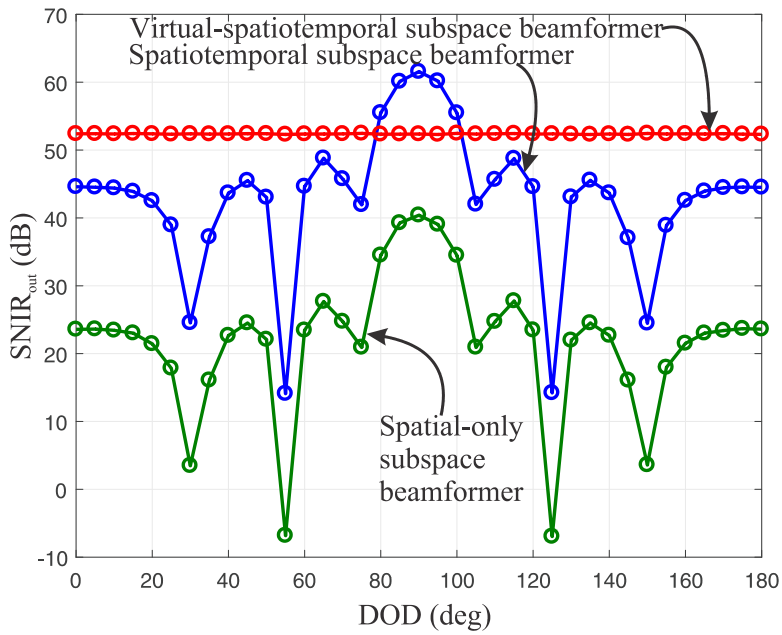

Figure 3.18: Comparison of output SNIR versus the DOD between the spatial-only, spatiotemporal, virtual-spatiotemporal subspace beamformers with a ULA being employed at the transmitter (50 realisations).

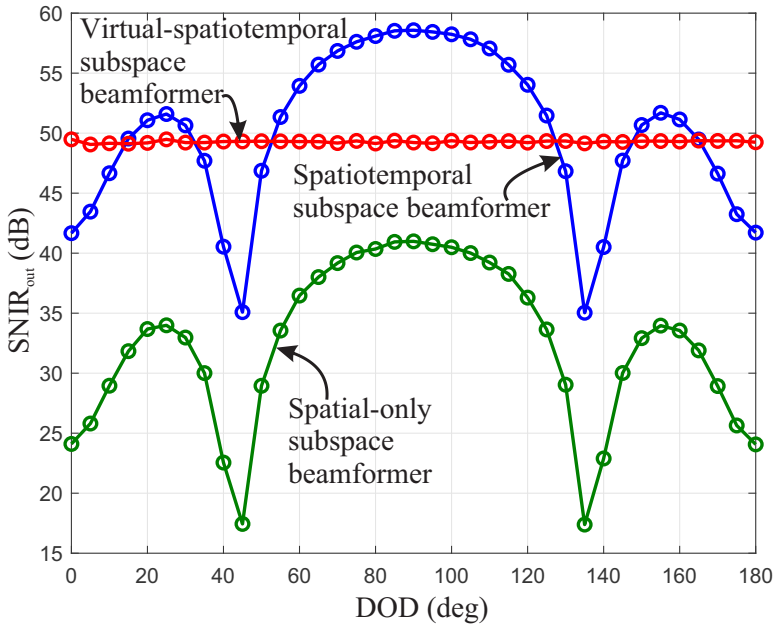

Figure 3.19: Comparison of output SNIR versus the DOD between the spatial-only, spatiotemporal, virtual-spatiotemporal subspace beamformers with a cross-shaped array being employed at the transmitter (50 realisations).

beamformer also starts to steadily decline and drops to unacceptable values when there are 160 signals in the system. However, the proposed virtual-spatiotemporal system provides a steady output SNIR even beyond 180 signals in the system, illustrating that the increase in DoF is achieved by the proposed system. Precisely, considering the inter symbol interference of each distinct signal is also contributed to the system, the spatial-only system can only accommodate $\frac{N}{3}$ distinct signals and the spatiotemporal system provides an ability to accommodate $\frac{2N\mathcal{N}_c}{3}$ distinct signals while the proposed virtual-spatiotemporal system can accommodate $\frac{2\overline{N}N\mathcal{N}_c}{3}$ distinct signals.

Thus, the proposed virtual-spatiotemporal system offers very high degrees of freedom for a system operating in a highly scattering environment or an extremely dense user scenario. If the proposed algorithm is applied to massive MIMO systems, super massive signal observation space will be obtained leading to super massive degrees of freedom. In addition, the proposed algorithm also ensures that

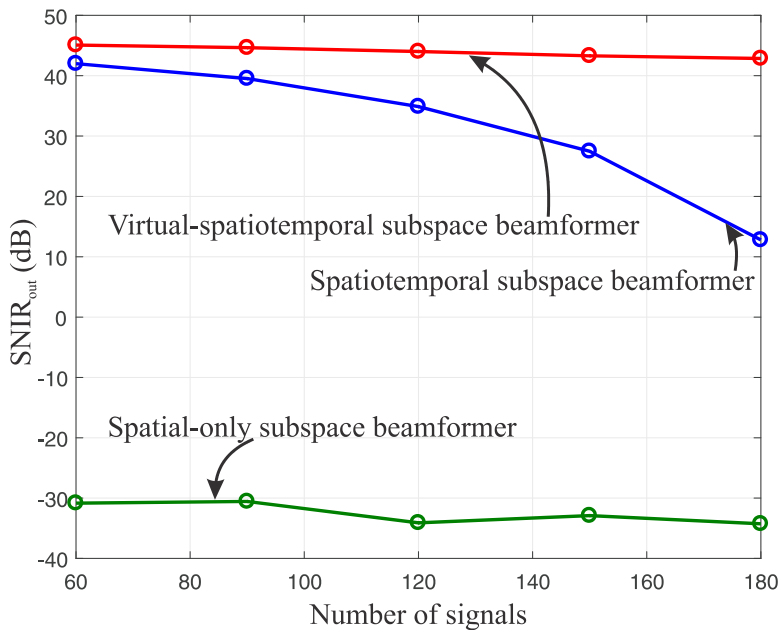

Figure 3.20: Comparison of output SNIR versus the number of signals for the spatial, spatiotemporal and virtual-spatiotemporal beamformer with subspace beamformer weights employed at the receiver. (50 realisations).

system performance remains independent of the Tx array geometry, the DOD and the design of the transmit weight.

3.6 Summary

In this chapter, a novel MIMO antenna array system was proposed which incorporates a virtual-spatiotemporal manifold extender to perform a joint estimation of Doppler-delay and DOD-DOA of all paths of the desired user, in the presence of multiple access co-channel interference, and also to form a beamformer that suppresses the multiple access co-channel interference. The proposed approach can largely increase the degrees of freedom and it was evaluated and compared against other techniques that also attempt to increase the degrees of freedom of the system. Computer simulation studies showed that the proposed approach outperforms the existing techniques in different aspects such as

- heightened interference cancellation,
- increased channel estimation accuracy,
- SNIR output performance independent of the Tx array geometry, the DOD and the transmit weight

as well as the ability to support a higher number of signals in the system.

Chapter 4

Multi DOA Tracking using Rigid and Flexible Antenna Arrays

This chapter is concerned with the problem of simultaneously tracking the DOA of far-field multiple moving sources/users in wireless communications using the vector-signal received by an antenna array of N elements. The antenna array can be rigid (fixed array locations) or flexible (time-varying array locations), and it is used in conjunction with a "manifold extender", a spatiotemporal state-space model and a Kalman-type tracking approach for non-stationary wireless channels. In particular, two tracking approaches are proposed. The first is based on an arrayed Extended Kalman Filter (arrayed-EKF) algorithm and the second on an arrayed Unscented Kalman Filter (arrayed-UKF) algorithm. Furthermore, if the array is rigid the spatiotemporal state-space model incorporates the DOAs and the angular velocities of the sources, while if it is flexible it also includes the array locations in the set of state-variables. The performance of the two approaches using both rigid and flexible arrays is evaluated using computer simulation studies and compared with a subspace tracking algorithm and a particle filter method under the same conditions.

4.1 Introduction

In the previous chapters, the source parameters to be estimated are assumed stationary, i.e. do not change with time. However, in many cases the source parameters are non-stationary and thus the estimation of such parameters are called source tracking. In particular, DOA tracking of multiple moving sources/users using an array has been an important research area with a wide range of applications in sonar, radar, air traffic control, wireless communications, remote sensing, etc. There has been considerable array processing techniques related to the DOA tracking. However, the majority of array processing techniques assume by default that the array geometry is rigid. On the other hand, using flexible array geometries is an interest problem in array signal processing for airborne, vehicular, underwater and other applications [68].

In this chapter, both "rigid array" and "flexible array" are presented for simultaneously tracking multiple DOAs snapshot-by-snapshot. The proposed algorithms in this chapter have many applications, including UAV communications. For instance, a rigid antenna array may be deployed on a single UAV platform[1] for tracking multiple users. Furthermore, a number of UAVs (a swarm of UAVs), each equipped with a single antenna having its own propulsion system, can be used as a flexible array for multi-user tracking (e.g. [69]). In this case, each UAV is equipped with a GPS-clock so that the array system will have a common clock to keep the system coherent.

4.1.1 DOA Tracking using Rigid Arrays

DOA tracking techniques can be classified into *probabilistic* and *parametric*. For instance, in [70], a probabilistic DOA tracking approach is presented which is based on a probability hypothesis density filter with a likelihood function expressed as a

[1] Except the UAV platform, the rigid array may be deployed in aircraft, automobile, shipboard as well as in Node-B, eNode-B or gNode-B in an access network.

complex Wishart random matrix. In [71], the tracking of DOAs is also *probabilistic* and is based on the sparse approximation technique LASSO. One of the main tracking families of *parametric* techniques is the "subspace tracking" [8, 72, 73, 74], In [8], a cross-correlation based 2D DOA tracking algorithm is proposed using an automatic pair-matching batch method which, however, is restricted to only L-shape array geometries. Some "subspace tracking" techniques are based on various decomposition forms such as Singular Value Decomposition (SVD) [72], URV decomposition [73] and cross RV decomposition (CRV) [74].

However, many DOA tracking techniques assume that the sources are stationary over a small time frame (observation interval) and for each time frame a DOA subspace estimation algorithm like multiple signal classification (MUSIC) [14] can be applied. In these type of techniques the tracking is based on repetitive DOA estimation (or, in general, repetitive localization) where the set of consecutive estimates provide the tracking trajectory (e.g. [75]). However, in non-stationary environments, repetitive high-resolution estimation algorithms for DOA source trajectory tracking exhibit serious performance degradation. In addition, these techniques suffer from the data association problem and several algorithms have been proposed to avoid this problem. In [23], the authors minimise the norm of an error matrix based on the covariance matrix of the received array output. A repetitive DOA source tracking algorithm is proposed in [24] which uses the most recent received data to update the existing DOA estimates using the MUSIC algorithm. Both [23] and [24] avoid data association by preserving the order of the estimated DOAs over certain iterations, which however suffer from spread array spatial spectrum effects caused by the source motion. Alternatively, state-space model based approaches have been proposed which are combined with various tracking algorithms (e.g. [76, 77, 78, 79]). In [76], multiple target states (MTS) are defined to describe the source motion, followed by a ML algorithm for updating the MTS and tracking the DOAs. In [77], a bank of linear combiner matrices are formed

as state variables, and then they are updated adaptively by an H-infinity filter to track the noise subspaces and consequently the DOAs. Furthermore, some Bayesian state-space models have been used in [78], [79] which incorporate the source motion and the likelihood of received measurements based on the source's state. Then, a particle filter is used to track the source state to obtain the DOA of the sources. The particle filter has also been used in [80] and [81] for target tracking in radar system. However, in radar literature, "active" radar tracking approaches have been employed where both system architectures and assumptions are different than those used in communications.

Another family of approaches for repetitive DOA estimation are based on Kalman Filter (KF). Since the standard Kalman filter requires the measurement model to be linear, all the approaches that use standard Kalman filter need to pre-estimate the DOA and view the DOA estimates as "measurement". Then the pre-estimated DOA is refined by the Kalman filter. For example, the Kalman filter has been used for multiple DOA tracking which are pre-estimated by a least squares (LS) estimator [82], or a Maximum Likelihood (ML) estimator [83], [84]. In [85], the proposed algorithm improves the algorithm in [24] by employing a source movement model and a Kalman filter. The Kalman filter has also been used in [86] for tracking signal subspace towards the objective of tracking single target. However, it is important to point out that the above KF approaches require the overall observation interval to be divided into small intervals over which the DOAs can be assumed to be stationary. Consequently, they will suffer from serious performance degradation when this assumption is not valid.

In addition to KF, the Extended Kalman filter (EKF) and the Unscented Kalman Filter (UKF) are suitable for the case that the measurement model is non-linear. For instance, the EKF has been employed in [87] for trajectory tracking of moving sources using a large aperture rigid array and in [2] for DOA tracking of moving sources using a small aperture rigid array. In [88], the EKF is combined

with a particle filter forming an EKPF algorithm. However, to the best of our knowledge, there are not many papers for DOA tracking using EKF and the majority of these papers are for single DOA tracking. In addition, the UKF has been rarely used and in [89], [90] it has been used for single DOA tracking. In general, the EKF and UKF algorithms have equal computational complexity but they are conceptually different. The EKF linearizes nonlinear transformations by using Taylor series expansions and then uses these linear transformations in standard Kalman filter. Whereas the UKF involves the unscented transformation which essentially selects a set of points (sigma points) via a deterministic sampling approach, and then propagates these points to the true nonlinear function which are then exploited to form the mean and covariance of the estimation [91], [92]. In this chapter, both the EKF and UKF are employed to track multiple DOAs in non-stationary environment and our paper [3] is the first paper to employ UKF for multi-DOA tracking.

4.1.2 DOA Tracking using Flexible Arrays

Several approaches have been proposed for solving source tracking problem with time varying arrays but for static sources. For example, the ML estimator has been employed in [93, 94, 95]. However, in these cases, a multi-dimensional search is required which is computationally prohibitive. In [96], two eigenstructure-based algorithms based on the concept of array interpolation and focusing matrices are proposed with faster approximations to the ML estimators. However, these algorithms need relatively large Signal to Noise Ratio (SNR) levels to maintain satisfactory performance. In [97], the authors use noncoherent time-varying arrays that are a collection of coherent subarrays with stationary covariance matrices. Then, the functions of the covariance matrices of the subarrays are derived to find source locations. As it was stated before, all these approaches ([93, 94, 95, 96, 97])

are designed for static sources. In [98], a dynamic radar network is proposed which is related with a swarm of UAVs working independently for tracking the location of a single target. It uses a Markovian state space model and employs a two-step EKF algorithm. However, this approach is not related with flexible arrays as the UAVs work independently and this scenario belongs to radar applications.

This chapter is concerned with tracking the DOA of multiple sources in non-stationary wireless communications using both rigid and flexible arrays. In addition to [69] in the current literature, to the best of our knowledge, there are only two papers [99], [100] that deal with the tracking using time-varying arrays. [99] is concerned with tracking stationary sources using an array of hydrophones. This is a "towed-array" - towed behind a submarine or a surface ship on a cable – where the hydrophones are placed at specific/constant distances along the cable. This is also a flexible array because when the ship turns this line becomes curvy and there are small but very restricted changes in the overall shape. However, [99] deals with DOA estimation of stationary acoustic sources using Maximum Likelihood (ML) followed by a second estimation of the shape of the array using Kalman filtering. Reference [100] is a "probabilistic" approach for non-stationary channels which completely ignores the parameterisation in terms of the array manifold vector and array geometry. It recursively estimates a conditional probability density function (Bayesian filtering) by following the EKF iterative steps, although this is not an EKF approach, while its performance is compared with that of a particle-filter method.

In the proposed approaches, all the sources and the array locations are tracked in a unified way which is suitable for tracking even of fast moving sources using antenna array systems. In particular, two novel approaches are proposed based on an arrayed-EKF and an arrayed-UKF using

- a rigid array and a flexible array,

- a spatiotemporal state-space model and
- a "manifold extender"

for simultaneously tracking multiple DOAs snapshot-by-snapshot. In our proposed approaches, both "rigid" and "flexible" arrays as well as arrayed-EKF and arrayed-UKF are presented in a unified way. Furthermore, the concept of "manifold extender" (see [19]) is employed which increases the "degrees of freedom" of the system by integrating the spatial and the temporal domains. This is used in the spatiotemporal state-space model. If the array is flexible, apart from tracking multiple DOAs, the array locations are also simultaneously tracked as they change arbitrarily with time. Therefore, we developed our array processing algorithms (arrayed-EKF/UKF), based on fixed or time-varying array geometry, where all the antenna array elements (in a constant or a time varying geometry) work together as one unit for solving the problem of trajectory tracking of moving sources. The integration of all the above forms our proposed "arrayed-EKF" and "arrayed-UKF" algorithms.

The remainder of this chapter is organised as follows. In Section 4.2, the array system and the received vector-signal model are presented. In Section 4.3, the mobility model of the multiple sources is described. Then, the extended mobility model is presented. In the case of flexible arrays, the mobility model of the array elements is also discussed. In Section 4.4, the proposed approaches are introduced based on arrayed-EKF and arrayed-UKF for both rigid and flexible arrays. In Section 4.5, the performance of the proposed approaches is evaluated using computer simulation studies. Finally, this chapter is concluded in Section 4.6.

4.2 System Model

Consider an array system for tracking multiple users with a receiver array of N antennas. Figure 4.1 shows the baseband representation of the array system model consisting of M far-field transmitters/users, a wireless channel and an array receiver[2]. With reference to Figure 4.1, at Point-A, the transmitted data sequence of symbols of the i-th user $\{\mathrm{a}_i[n]\}$ (with a symbol duration of T_{cs}) where each symbol is weighted by a $\mathcal{N}_c \times 1$ weight-code vector given by

$$\underline{w}_i \triangleq [w_i[1], w_i[2], ..., w_i[q], ..., w_i[\mathcal{N}_c]]^T \tag{4.1}$$

with

$$w_i[q] \in \pm 1, q \in [1, \mathcal{N}_c] \tag{4.2}$$

Then, at Point-B, the weighted data symbol sequence $\{\underline{w}_i \mathrm{a}_i[n]\}$ is driven to a Digital-to-Analog Converter (DAC) to produce a baseband transmitted signal $m_i(t)$ at Point-C.

At the receiver, an antenna array of N antennas is employed with locations

$$\begin{aligned} \mathbf{r} &= [\underline{r}_1, \underline{r}_2, ..., \underline{r}_m ..., \underline{r}_N] \\ &= \left[\underline{r}_x, \underline{r}_y, \underline{r}_z\right]^T \in \mathcal{R}^{3\times N} \end{aligned} \tag{4.3}$$

where the vector $\underline{r}_m \in \mathcal{R}^{3\times 1}$ denotes the Cartesian coordinates of the m-th antenna and the $N \times 1$ vectors $\underline{r}_x$, $\underline{r}_y$, $\underline{r}_z$ are the Cartesian coordinates of all antennas on the x-axis, y-axis and z-axis, respectively. In this chapter, we also consider the scenario where the array locations (and thus the array geometry) change due to any unknown forces. In this case, the array is flexible with time-varying geometry, re-modelled as function of time as follows

$$\begin{aligned} \mathbf{r}(t) &= [\underline{r}_1(t), \underline{r}_2(t), ..., \underline{r}_m(t) ..., \underline{r}_N(t)] \\ &= \left[\underline{r}_x(t), \underline{r}_y(t), \underline{r}_z(t)\right]^T \in \mathcal{R}^{3\times N} \end{aligned} \tag{4.4}$$

[2]The M narrowband far-field users operate at the same time and on the same frequency band.

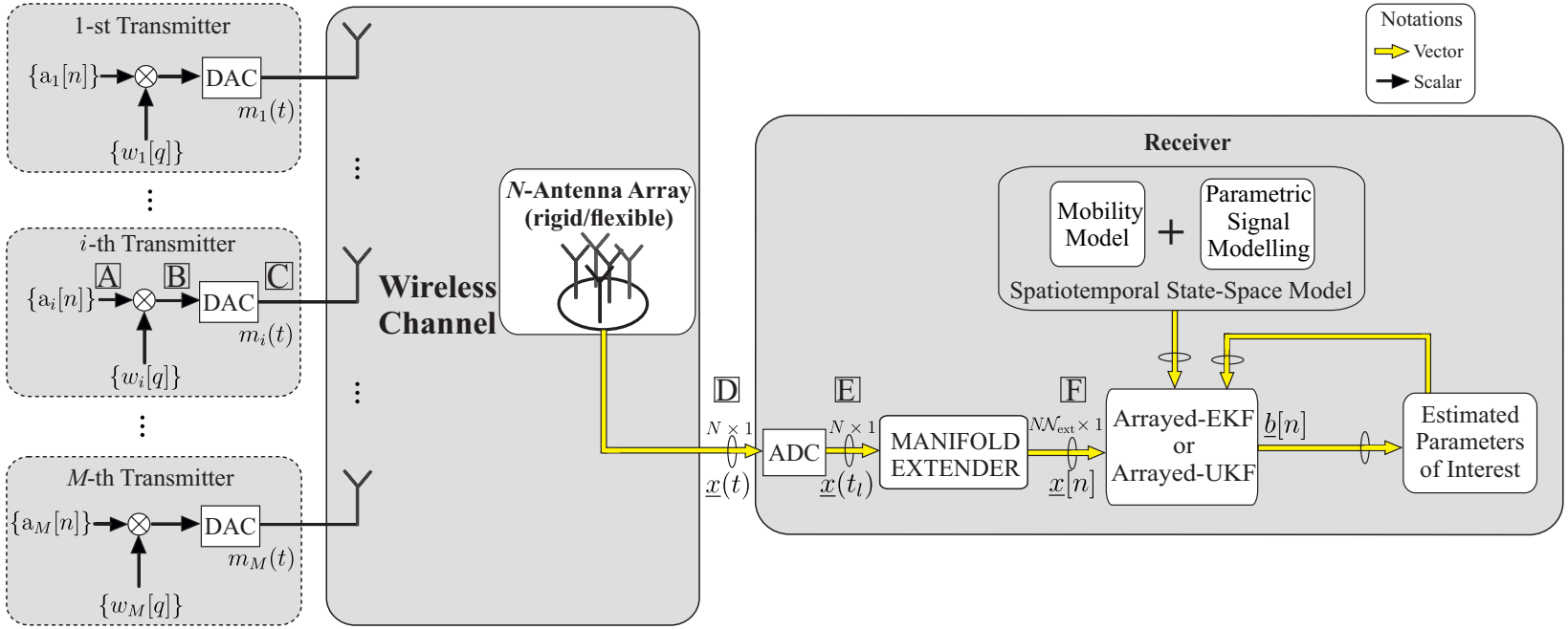

Figure 4.1: Baseband representation of the array system model consisting of M transmitters, a SIMO multiuser wireless channel and an array receiver. The array can be rigid or flexible.

Thus, at Point-D in Figure 4.1, the received baseband vector signal $\underline{x}(t) \in \mathcal{C}^{N\times 1}$ can be modelled as follows

$$\underline{x}(t) = \sum_{i=1}^{M} \beta_i(t) \exp(j2\pi\mathcal{F}_i t)\underline{S}_i(t) m_i(t) + \underline{\mathrm{n}}(t) \tag{4.5}$$

where, for the i-th user, $\beta_i(t)$ denotes the path fading coefficient, $\mathcal{F}_i$ represents the Doppler frequency and the vector $\underline{\mathrm{n}}(t) \in \mathcal{C}^{N\times 1}$ denotes the additive white complex Gaussian noise of zero mean and covariance matrix given by

$$\mathbb{R}_{\mathrm{nn}} = \sigma_{\mathrm{n}}^2 \mathbb{I}_N \tag{4.6}$$

with σ_{n}^2 denoting the noise power. In Equ 4.5, $\underline{S}_i(t) \in \mathcal{C}^{N\times 1}$ denotes the time-varying manifold vector which is given as follows

$$\underline{S}_i(t) = \begin{cases} \exp\left(-j\frac{2\pi F_c}{c}\mathbf{r}^T \underline{u}_i(t)\right) & \text{for rigid array} \\ \exp\left(-j\frac{2\pi F_c}{c}\mathbf{r}(t)^T \underline{u}_i(t)\right) & \text{for flexible array} \end{cases} \tag{4.7}$$

where F_c is the carrier frequency, c denotes the speed of light and $\underline{u}_i(t)$ is given by

$$\underline{u}_i(t) = \begin{bmatrix} \cos\theta_i(t)\cos\phi_i(t) \\ \sin\theta_i(t)\cos\phi_i(t) \\ \sin\phi_i(t) \end{bmatrix} \tag{4.8}$$

with $\theta_i(t)$ and $\phi_i(t)$ representing the azimuth and the elevation angles of the i-th source. In general, the vector $\underline{u} = \underline{u}(\theta, \phi)$ denotes the (3×1) unit-norm vector pointing towards the direction (θ, ϕ), as illustrated in Figure 4.2. In this chapter, with no loss of generality, the elevation angle is assumed to be zero (i.e. $\phi_i(t) = 0$). Equ 4.5 can also be rewritten in a more compact form as follows

$$\underline{x}(t) = \mathbb{S}(t)\underline{m}(t) + \underline{\mathrm{n}}(t) \tag{4.9}$$

where $\mathbb{S}(t) \in \mathcal{C}^{N\times M}$ is the matrix with columns the array manifold vectors, i.e.

$$\mathbb{S}(t) = [\underline{S}_1(t), \underline{S}_2(t), ..., \underline{S}_i(t), \ldots, \underline{S}_M(t)] \tag{4.10}$$

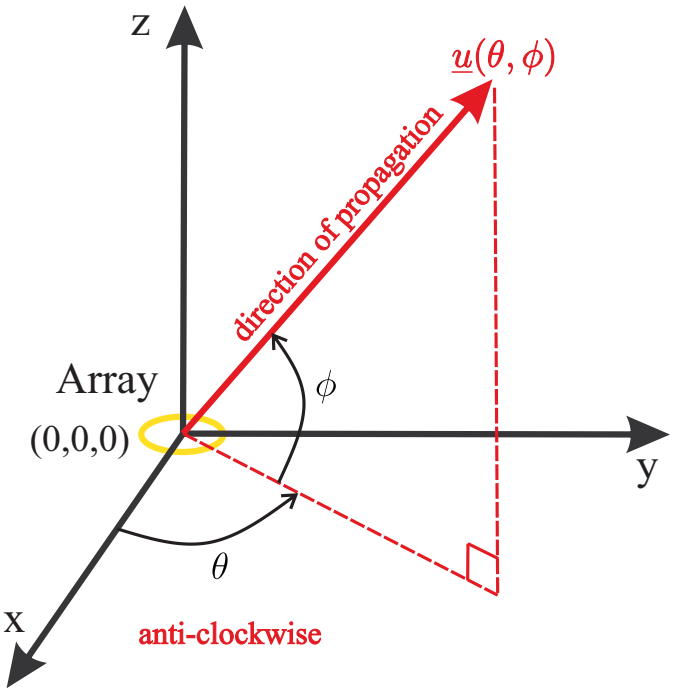

Figure 4.2: The array's Cartesian coordinate system and the unit-norm vector $\underline{u}(\theta, \phi)$ in terms of the azimuth angle θ and elevation angle ϕ.

and $\underline{m}(t) \in \mathcal{C}^{M\times 1}$ is expressed to include, in addition to the M baseband message signals, the Doppler frequencies and the path coefficients as follows

$$\underline{m}(t) = \begin{bmatrix} \beta_1(t)\exp(j2\pi\mathcal{F}_1 t)m_1(t) \\ \beta_2(t)\exp(j2\pi\mathcal{F}_2 t)m_2(t) \\ \vdots \\ \beta_M(t)\exp(j2\pi\mathcal{F}_M t)m_M(t) \end{bmatrix} \tag{4.11}$$

with its covariance matrix $\mathbb{R}_{mm}$ defined as

$$\mathbb{R}_{mm} = \mathcal{E}\left\{(\underline{m}(t) - \mathcal{E}\{\underline{m}(t)\})(\underline{m}(t) - \mathcal{E}\{\underline{m}(t)\})^H\right\} \tag{4.12}$$

With reference to Figure 4.1, the $(N \times 1)$ vector signal $\underline{x}(t)$ is firstly discretised (see Point-E). Then, at Point-F the $(N\mathcal{N}_{\text{ext}} \times 1)$ vector signal $\underline{x}[n]$ can be expressed

as follows

$$\underline{x}\,[n] = \sum_{i=1}^{M} \underbrace{(\underline{S}_i[n] \otimes \underline{w}_i)}_{\underline{h}_i[n]} \overbrace{\beta_i\,[n] \exp(j2\pi\mathcal{F}_i nT)\mathrm{a}_i\,[n]}^{m_i[n]} + \underline{\mathrm{n}}\,[n] \tag{4.13a}$$

$$= \sum_{i=1}^{M} \underline{h}_i[n] m_i[n] + \underline{\mathrm{n}}\,[n] \tag{4.13b}$$

$$= \mathbb{H}[n]\underline{m}[n] + \underline{\mathrm{n}}[n] \tag{4.13c}$$

where the vector $\underline{\mathrm{n}}\,[n] \in \mathcal{C}^{N\mathcal{N}_{\text{ext}}\times 1}$ denotes the discretised "extended" noise (i.e. the noise at Point-F in Figure 4.1) and the matrix $\mathbb{H}\,[n] \in \mathcal{C}^{N\mathcal{N}_{\text{ext}}\times M}$ is given by

$$\mathbb{H}\,[n] = [\underline{h}_1\,[n]\,, \underline{h}_2\,[n]\,, ..., \underline{h}_i\,[n]\,, \ldots, \underline{h}_M\,[n]] \tag{4.14}$$

with its i-th column $\underline{h}_i\,[n] \in \mathcal{C}^{N\mathcal{N}_{\text{ext}}\times 1}$ denoting the time-varying extended manifold vector of the i-th user given as follows

$$\underline{h}_i\,[n] = \underline{S}_i\,[n] \otimes \underline{w}_i \tag{4.15}$$

with $\mathcal{N}_{\text{ext}} = \mathcal{N}_c$. Furthermore, at the transmitter, if the user being tracked does not include the weight $\underline{w}_i$, then $\underline{w}_i = \underline{1}_{\mathcal{N}_{\text{ext}}}$ may be used. In this case, the extended manifold vector of Equ 4.15 is simplified to

$$\underline{h}_i\,[n] = \underline{S}_i\,[n] \otimes \underline{1}_{\mathcal{N}_{\text{ext}}} \tag{4.16}$$

Therefore, the extended manifold vector here has two forms/cases as described in Equ 4.15 and Equ 4.16 although other forms from [2], [19] may be included. In addition, if the manifold extender is not employed in this model, then $\mathcal{N}_{\text{ext}} = 1$ and

$$\underline{h}_i[n] = \underline{S}_i[n] \tag{4.17}$$

Thus, the vector $\underline{h}_i\,[n] \in \mathcal{C}^{N\mathcal{N}_{\text{ext}}\times 1}$ can be expressed as follows

$$\underline{h}_i\,[n] = \left\{ \begin{array}{ll} \underline{S}_i\,[n] \otimes \underline{w}_i, & \mathcal{N}_{\text{ext}} = \mathcal{N}_c \\ \underline{S}_i\,[n] \otimes \underline{1}_{\mathcal{N}_{\text{ext}}}, & \mathcal{N}_{\text{ext}} = \mathcal{N}_c \\ \underline{S}_i\,[n]\,, & \mathcal{N}_{\text{ext}} = 1 \end{array} \right| \tag{4.18}$$

Note that the array locations that constitute the extended manifold vector $\underline{h}_i[n]$ may be a function of time (changing from symbol to symbol), depending on whether the array is rigid or flexible.

4.3 Mobility model

4.3.1 Source/User Mobility Model

Since the array operates in the presence of M co-channel users, Figure 4.3 illustrates the mobility model of the i-th user, for $i = 1, 2, ..., M$ relative to the array reference point. As shown in Figure 4.3, the i-th user moves in an arbitrary direction with velocity-vector $\underline{v}_i \in \mathcal{R}^{3\times 1}$ given as follows

$$\underline{v}_i = v_{\rho_i}\underline{u}_{v_{\rho_i}} + v_{\theta_i}\underline{u}_{v_{\theta_i}} \tag{4.19}$$

where the velocity vector $\underline{v}_i$ is decomposed into two other vectors:

- the radial component $v_{\rho_i}\underline{u}_{v_{\rho_i}}$, and
- the orthoradial (angular) component $v_{\theta_i}\underline{u}_{v_{\theta_i}}$,

with v_{ρ_i} denoting the radial velocity of the i-th source and v_{θ_i} representing its angular velocity. The vectors $\underline{u}_{v_{\rho_i}}$ and $\underline{u}_{v_{\theta_i}}$ are unity vectors that are mutually orthogonal. The radial velocity v_{ρ_i} causes the Doppler effects which is modelled as $\exp(j2\pi F_i t)$ in Equs 4.5 and 4.11. Note that F_i is given by

$$\mathcal{F}_i = -\frac{F_c v_{\rho_i}}{c} \tag{4.20}$$

As shown in Equ 4.13, the Doppler coefficient has been incorporated into the combined vector-signal $\underline{m}[n]$ which will then be estimated and utilised by the proposed tracking algorithms. Thus, the radial velocity does not affect the DOA/azimuth θ_i. If the i-th user moves with an angular velocity v_{θ_i}, which can be constant or variable, its azimuth angle may be described as

$$\theta_i(t) = \theta_i(t_0) + v_{\theta_i}(t_0)\,T \tag{4.21}$$

where

$$T = t - t_0 \tag{4.22}$$

is the time elapsed between t and t_0. If T is assumed to be equal to the sampling period, i.e.

$$t_0 = (n-1)T \tag{4.23}$$

$$t = nT \tag{4.24}$$

then Equ 4.21 is discretised and becomes

$$\theta_i[n] = \theta_i[n-1] + v_{\theta_i}[n]T \tag{4.25}$$

Thus, let us define the discrete-time state vector for the i-th user as $\underline{b}_i[n]$, i.e.

$$\underline{b}_i[n] \triangleq \begin{bmatrix} \theta_i[n] \\ v_{\theta_i}[n] \end{bmatrix} \tag{4.26}$$

Then, the discrete time *kinematic model* for the i-th user for $t = nT$ is given as

$$\underline{b}_i[n] = \mathbb{G}_i\underline{b}_i[n-1] + \widetilde{\underline{b}}_i[n] \tag{4.27}$$

where $\mathbb{G}_i \in \mathcal{R}^{2\times 2}$ is the transition matrix given by

$$\mathbb{G}_i = \begin{bmatrix} 1, & T \\ 0, & 1 \end{bmatrix} \tag{4.28}$$

In Equ 4.27, $\widetilde{\underline{b}}_i[n] \in \mathcal{R}^{2\times 1}$ represents perturbations about the azimuth angle and the angular velocity, and can be modelled as "noise" with zero mean and covariance matrix $\mathbb{R}_{\widetilde{b}_i\widetilde{b}_i} \in \mathcal{R}^{2\times 2}$ given by

$$\mathbb{R}_{\widetilde{b}_i\widetilde{b}_i} = \sigma^2_{\theta_i} \begin{bmatrix} \frac{T^3}{3}, & \frac{T^2}{2} \\ \frac{T^2}{2}, & T \end{bmatrix} \tag{4.29}$$

where $\sigma^2_{\theta_i}$ denotes the continuous time model intensity for the azimuth-velocity.

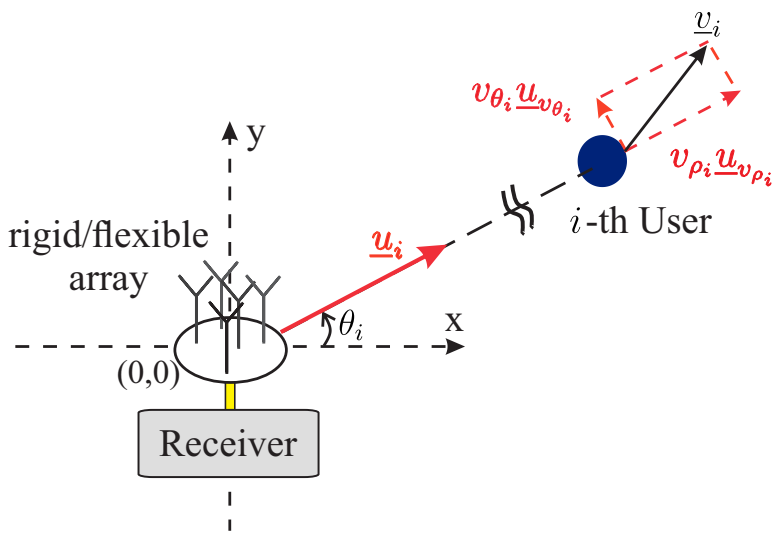

Figure 4.3: Illustration of the mobility model of the i-th source/user. The velocity vector $\underline{v}_i$ of the source is decomposed into its radial term $v_{\rho_i}\underline{u}_{v_{\rho_i}}$ and the orthoradial term $v_{\theta_i}\underline{u}_{v_{\theta_i}}$, respectively. The direction (DOA) θ_i of the source is measured with respect to the array reference point. The array geometry at the receiver may be rigid or flexible.

4.3.2 Flexible Array Mobility Model

With reference to Figure 4.3, it is shown that the array at the receiver can be either rigid or flexible. The movement of the flexible array may include

- a known motion of the whole array which is represented by the motion of the array's reference point and does not affect the array geometry,
- a known motion of its individual elements relative to the reference point, and
- small unknown motion or perturbations caused by any unknown forces[3]

with the last two motions changing the array geometry. Thus, in a flexible array the tracking of the array geometry (i.e. the tracking of the locations of the array elements) is essential.

[3]Note that, even in fixed array geometries, constant uncertainties in the array locations may decrease the performance of the direction-finding system [93].

With a sampling period T, the discrete time mobility model of the array locations[4] is expressed as follows

$$\underline{b}_{xy}[n] = \mathbb{G}_{xy}\underline{b}_{xy}[n-1] + \widetilde{\underline{b}}_{xy}[n] \tag{4.30}$$

where the vector $\underline{b}_{xy}[n]$ is given as follows

$$\underline{b}_{xy}[n] = \begin{bmatrix} \underline{r}_x[n] \\ \underline{r}_y[n] \end{bmatrix} \in \mathcal{R}^{2N\times 1} \tag{4.31}$$

which includes the instantaneous array locations on the x-axis and y-axis, respectively. The vector $\widetilde{\underline{b}}_{xy}[n] \in \mathcal{R}^{2N\times 1}$ in Equ 4.30 denotes the perturbations associated with their respective locations, with its intensity σ^2_{xy}, and its covariance matrix is given as follows

$$\mathbb{R}_{\widetilde{\underline{b}}_{xy}\widetilde{\underline{b}}_{xy}} = \sigma^2_{xy}\mathbb{I}_{2N} \tag{4.32}$$

The matrix $\mathbb{G}_{xy} \in \mathcal{R}^{2N\times 2N}$ is a block diagonal matrix containing known transition matrices of all the array elements shown as

$$\mathbb{G}_{xy} = \begin{bmatrix} \mathbb{F}_1, & \mathbb{O}_2, & \cdots, & \mathbb{O}_2 \\ \mathbb{O}_2, & \mathbb{F}_2, & \cdots, & \mathbb{O}_2 \\ \vdots & \vdots & \ddots & \vdots \\ \mathbb{O}_2, & \mathbb{O}_2, & \cdots, & \mathbb{F}_N \end{bmatrix} \tag{4.33}$$

where $\mathbb{F}_j \in \mathcal{R}^{2\times 2}$ represents a known transition matrix of j-th array element. For instance, if ω_j denotes the angular velocity of the j-th array element about the reference point, then

$$\mathbb{F}_j = \begin{bmatrix} \cos\omega_j T, & -\sin\omega_j T \\ \sin\omega_j T, & \cos\omega_j T \end{bmatrix} \tag{4.34}$$

[4] With no loss of generality, the antenna array elements are assumed to be located on the (x, y) plane, i.e. $\underline{r}_z[n] = \underline{0}_N$.

4.3.3 Overall Mobility Model

The overall mobility model, which is the discrete time M-user *kinematic* model, is constructed based on Equs. 4.27 and 4.30, as follows

$$\underline{b}[n] = \mathbb{G}\underline{b}[n-1] + \widetilde{\underline{b}}[n] \tag{4.35}$$

where $\underline{b}[n]$ is the overall discrete-time state vector which is constructed as

$$\underline{b}[n] = \begin{cases} \left[\underline{b}_1^T[n], \underline{b}_2^T[n], \ldots, \underline{b}_M^T[n]\right]^T \in \mathcal{R}^{2M\times 1} & \text{rigid array} \\ \left[\underline{b}_{xy}^T[n], \underline{b}_1^T[n], \ldots, \underline{b}_M^T[n]\right]^T \in \mathcal{R}^{(2N+2M)\times 1} & \text{flexible array} \end{cases} \tag{4.36}$$

and its perturbation vector $\widetilde{\underline{b}}[n]$ is given as follows

$$\widetilde{\underline{b}}[n] = \begin{cases} \left[\widetilde{\underline{b}}_1^T[n], \widetilde{\underline{b}}_2^T[n], \ldots, \widetilde{\underline{b}}_M^T[n]\right]^T \in \mathcal{R}^{2M\times 1} & \text{rigid array} \\ \left[\widetilde{\underline{b}}_{xy}^T[n], \widetilde{\underline{b}}_1^T[n], \ldots, \widetilde{\underline{b}}_M^T[n]\right]^T \in \mathcal{R}^{(2N+2M)\times 1} & \text{flexible array} \end{cases} \tag{4.37}$$

The matrix $\mathbb{G}$ represents the overall transition matrix given by

$$\mathbb{G} = \begin{cases} \mathbb{I}_M \otimes \mathbb{G}_i & \text{rigid array} \\ \begin{bmatrix} \mathbb{G}_{xy}, & \mathbb{O}_{2N\times 2M} \\ \mathbb{O}_{2M\times 2N}, & \mathbb{I}_M \otimes \mathbb{G}_i \end{bmatrix} & \text{flexible array} \end{cases} \tag{4.38}$$

Based on the above equations, the covariance matrix $\mathbb{P}[n]$ of the discrete time state vector $\underline{b}[n]$ is constructed as follows

$$\mathbb{P}[n] = \mathbb{G}\mathbb{P}[n-1]\mathbb{G}^T + \mathbb{R}_{\widetilde{b}\widetilde{b}} \in \mathcal{R}^{N_{\text{dim}}\times N_{\text{dim}}} \tag{4.39}$$

where

$$N_{\text{dim}} = \begin{cases} 2M & \text{rigid array} \\ 2N + 2M & \text{flexible array} \end{cases} \tag{4.40}$$

and the perturbation matrix $\mathbb{R}_{\widetilde{bb}}$ is given as

$$\mathbb{R}_{\widetilde{bb}} = \begin{cases} \mathbb{I}_M \otimes \mathbb{R}_{\widetilde{b}_i \widetilde{b}_i} & \text{rigid array} \\ \begin{bmatrix} \mathbb{R}_{\widetilde{\underline{b}}_{xy} \widetilde{\underline{b}}_{xy}}, & \mathbb{O}_{2N \times 2M} \\ \mathbb{O}_{2M \times 2N}, & \mathbb{I}_M \otimes \mathbb{R}_{\widetilde{b}_i \widetilde{b}_i} \end{bmatrix} & \text{flexible array} \end{cases} \tag{4.41}$$

Table 4.1 provides the dimensionality of the various vector/matrix parameters used in the mobility models. The mobility models employed in this section can be seen as some representative examples but other mobility models may be used in this proposed framework.

Table 4.1: The dimensionality of the vector/matrix parameters used in the mobility models

Variables	Dimensionality	Array type
$\underline{b}_i[n]$, $\widetilde{\underline{b}}_i[n]$	$2M \times 1$	rigid
$\mathbb{R}_{\widetilde{b}_i \widetilde{b}_i}$	$2M \times 2M$	rigid
$\mathbb{G}_i$	2×2	rigid
$\underline{b}_{xy}[n], \widetilde{\underline{b}}_{xy}[n]$	$2N \times 1$	flexible
$\mathbb{R}_{\widetilde{\underline{b}}_{xy} \widetilde{\underline{b}}_{xy}}$	$2N \times 2N$	flexible
$\mathbb{G}_{xy}$	$2N \times 2N$	flexible
$\underline{b}[n], \widetilde{\underline{b}}[n]$	$2M \times 1$ $(2N + 2M) \times 1$	rigid flexible
$\mathbb{G}$	$2M \times 2M$ $(2N + 2M) \times (2N + 2M)$	rigid flexible
$\mathbb{R}_{\widetilde{bb}}$	$2M \times 2M$ $(2N + 2M) \times (2N + 2M)$	rigid flexible
$\mathbb{P}[n]$	$2M \times 2M$ $(2N + 2M) \times (2N + 2M)$	rigid flexible

4.4 Tracking Algorithms based on Spatiotemporal State-space Model

In this section, based on the antenna array models presented in Sections 4.2 and 4.3, two tracking algorithms are proposed which belong to the Kalman family of techniques for non-linear "measurement" models. We will call them "arrayed-EKF" and "arrayed-UKF" as they are based on the integration of

- the array signal model of Section 4.2 for both "rigid" and "flexible" antenna arrays,
- the mobility models of Section 4.3, and
- the EKF/UKF iterative theoretical tools.

Based on the snapshot at Point-F in Figure 4.1, modelled by Equ 4.13, and the overall mobility model given by Equ 4.36, the spatiotemporal state-space model is constructed as follows

$$\underline{b}[n] = \mathbb{G}\underline{b}[n-1] + \widetilde{\underline{b}}[n] \tag{4.42}$$

$$\underline{x}[n] = \mathbb{H}(\underline{b}[n])\,\underline{m}[n] + \underline{\mathrm{n}}[n] \tag{4.43}$$

describing the dynamics of all users' motion (Equ 4.42) and the vector signal received by the rigid or flexible arrays (Equ 4.43).

The two proposed algorithms are summarised in Tables 4.2 and 4.3.Note that the notation has been simplified, by replacing the symbol index $[n]$ with a subscript n and, thus, the following notation is employed in Tables 4.2 and 4.3

$$\underline{b}_n \triangleq \underline{b}[n] \in \mathcal{R}^{N_{\mathrm{dim}}\times 1} \tag{4.44a}$$

$$\mathbb{P}_n \triangleq \mathbb{P}[n] \in \mathcal{R}^{N_{\mathrm{dim}}\times N_{\mathrm{dim}}} \tag{4.44b}$$

$$\underline{x}_n \triangleq \underline{x}[n] \in \mathcal{C}^{N\mathcal{N}_{\mathrm{ext}}\times 1} \tag{4.44c}$$

$$\underline{m}_n \triangleq \underline{m}[n] \in \mathcal{C}^{M\times 1} \tag{4.44d}$$

Table 4.2: First proposed approach (arrayed-EKF algorithm)

Tracking Algorithm
Given:
$\underline{b}_0 \in \mathcal{R}^{N_{\text{dim}}\times 1}; \gamma \in \mathcal{R}^1$
Initialisation:
$\mathbb{P}_0 = \gamma \mathbb{I}_{N_{\text{dim}}} \in \mathcal{R}^{N_{\text{dim}}\times N_{\text{dim}}}$
for n = 1, 2, 3... (for all available data symbols)
A Priori Estimation of States
$\underline{b}_n = \mathbb{G}\underline{b}_{n-1}$
$\mathbb{P}_n = \mathbb{G}\mathbb{P}_{n-1}\mathbb{G}^T + \mathbb{R}_{\widetilde{bb}}$
Estimation of the Transmitter Baseband Signals
$\underline{m}_n = \mathbb{R}_{mm}\mathbb{H}^H(\underline{b}_n)\left(\sigma_{\text{n}}^2\mathbb{I}_{N\mathcal{N}_{\text{ext}}} + \mathbb{H}(\underline{b}_n)\mathbb{R}_{mm}\mathbb{H}^H(\underline{b}_n)\right)^{-1}\underline{x}_n$
A Posteriori Estimation of States
$\mathbb{D}_n = \nabla_{\underline{b}_n}\left(\mathbb{H}\left(\underline{b}_n\right)\underline{m}_n\right)\vert_{\underline{b}_n}$
$\mathbb{K}_n = \mathbb{P}_n\mathbb{D}_n^H\left(\mathbb{D}_n\mathbb{P}_n\mathbb{D}_n^H + \sigma_{\text{n}}^2\mathbb{I}_{N\mathcal{N}_{\text{ext}}}\right)^{-1}$
$\underline{b}_n = \underline{b}_n + \text{Re}\left\{\mathbb{K}_n\left(\underline{x}_n - \mathbb{H}(\underline{b}_n)\underline{m}_n\right)\right\}$
$\mathbb{P}_n = \left(\mathbb{I}_{N_{\text{dim}}} - \mathbb{K}_n\mathbb{D}_n\right)\mathbb{P}_n$
end

It is important to point out that, in the presentation of the two algorithms in these two tables, the selection of a common Kalman structure is deliberately maintained for better clarification of each step. However, in the arrayed-UKF, which is based on the square-root UKF, the state-vector $\underline{b}\,[n]$ of Equ 4.36 and the non-linear "measurement" vector $\underline{x}\,[n]$ of Equ 4.43 should be further processed to form two matrices $\mathbb{B}_n$ and $\mathbb{X}$. In particular, the matrix $\mathbb{B}_n \in \mathcal{R}^{N_{\text{dim}}\times(2N_{\text{dim}}+1)}$ can be formed as follows

$$\mathbb{B}_n = \left[\underline{B}_1, \underline{B}_2, ..., \underline{B}_j, ..., \underline{B}_{2N_{\text{dim}}+1}\right] \tag{4.45}$$

$$= \underline{b}_n \otimes \underline{1}_{2N_{\text{dim}}+1}^T + \left[\underline{0}_{N_{\text{dim}}}, \eta\mathbb{T}_n, -\eta\mathbb{T}_n\right] \tag{4.46}$$

where

- $\underline{B}_j$ is the j-th column of the matrix $\mathbb{B}_n$ which is known as the j-th "sigma point-vector".
- η is a scaling factor
- $\mathbb{T}_n$ is an $N_{\text{dim}} \times 2N_{\text{dim}}$ matrix which is the Cholesky factorisation[5] of the covariance matrix $\mathbb{P}_n$ of the state vector of Equ 4.36. That is

$$\mathbb{P}_n = \mathbb{T}_n \mathbb{T}_n^H \tag{4.47}$$

Then, by applying the nonlinear function to these "sigma point vectors" the measurement matrix $\mathbb{X} \in \mathcal{C}^{N\mathcal{N}_{\text{ext}} \times (2N_{\text{dim}}+1)}$ is formed, i.e.

$$\mathbb{X} = \left[\mathbb{H}\left(\underline{B}_1\right)\underline{m}_n, \mathbb{H}\left(\underline{B}_2\right)\underline{m}_n, \ldots, \mathbb{H}\left(\underline{B}_{2N_{\text{dim}}+1}\right)\underline{m}_n\right] \tag{4.48}$$

Thus, using the unscented transformation instead of the Jacobian matrix of the nonlinear measurement, and propagating the Cholesky factor $\mathbb{T}_n$ instead of the covariance of the estimate error $\mathbb{P}_n$, the proposed arrayed-UKF algorithm is summarised in Table 4.3.

Note that in Table 4.3, the matrices $\mathbb{W}^{(m)}$ and $\mathbb{W}^{(c)}$ are diagonal matrices whose diagonal values are the weights to compute the mean and the covariance of the measurement, respectively. These matrices have the following definitions:

$$\mathbb{W}^{(m)} = \frac{1}{N_{\text{dim}} + \mu} \text{diag}\left\{\begin{bmatrix} \mu \\ \frac{1}{2}\underline{1}_{2N_{\text{dim}}} \end{bmatrix}\right\} \tag{4.49}$$

$$\mathbb{W}^{(c)} = \frac{1}{N_{\text{dim}} + \mu} \text{diag}\left\{\begin{bmatrix} \beta \\ \frac{1}{2}\underline{1}_{2N_{\text{dim}}} \end{bmatrix}\right\} \tag{4.50}$$

where the scaling parameters μ and β are as follows

$$\mu = N_{\text{dim}}(\alpha^2 - 1) \tag{4.51}$$

$$\beta = \mu + (1 - \alpha^2 + \rho)(N_{\text{dim}} + \mu) \tag{4.52}$$

[5] The Cholesky factorisation of $\mathbb{P}_n$ is unique as $\mathbb{P}_n$ is a positive definite matrix.

with the constant α controlling the spread of the "sigma point-vectors" around $\underline{b}_n$, and ρ compensating for the distribution of $\underline{b}_n$. Furthermore, the parameter η in Equ 4.46 is related to μ as follows

$$\eta = \sqrt{(N_{\text{dim}} + \mu)} \tag{4.53}$$

With reference to Table 4.2 and Table 4.3, the initial state $\underline{b}_0$ can be provided by a

Table 4.3: Second proposed approach (arrayed-UKF algorithm)

Given: $\underline{b}_0 \in \mathcal{R}^{N_{\text{dim}} \times 1}; \gamma, \mu, \beta, \eta \in \mathcal{R}^1$

Define: $w_0^{(c)} = \frac{\beta}{N_{\text{dim}}+\mu}, \mathbb{W}_1^{(c)} = \frac{1}{2(N_{\text{dim}}+\mu)} \mathbb{I}_{2N_{\text{dim}}}$

Initialisation:

$\mathbb{P}_0 = \gamma \mathbb{I}_{N_{\text{dim}}} \in \mathcal{R}^{N_{\text{dim}} \times N_{\text{dim}}}, \mathbb{T}_0 = \text{chol}\left(\mathbb{P}_0\right) \in \mathcal{R}^{N_{\text{dim}} \times N_{\text{dim}}}$

for n = 1, 2, 3... (for all available data symbols)

A Priori Estimation of States

$$\underline{b}_n = \mathbb{G}\underline{b}_{n-1}$$

$$\begin{bmatrix} \mathbb{T}_n^H \\ \mathbb{O}_{N_{\text{dim}} \times N_{\text{dim}}} \end{bmatrix} = \text{QR}\left(\begin{bmatrix} \mathbb{T}_{n-1}^H \mathbb{G}^H \\ \mathbb{R}_{\underset{\sim}{bb}}^{1/2} \end{bmatrix}^H \right)$$

Estimation of the Transmitter Baseband Signals

$$\underline{m}_n = \mathbb{R}_{mm} \mathbb{H}^H(\underline{b}_n) \left(\sigma_{\text{n}}^2 \mathbb{I}_{N\mathcal{N}_{\text{ext}}} + \mathbb{H}(\underline{b}_n) \mathbb{R}_{mm} \mathbb{H}^H(\underline{b}_n)\right)^{-1} \underline{x}_n$$

A Posteriori Estimation of States

$$\begin{aligned} \mathbb{B}_n &= \underline{b}_n \otimes \underline{1}_{2N_{\text{dim}}+1}^T + \left[\underline{0}_{N_{\text{dim}}}, \eta \mathbb{T}_n, -\eta \mathbb{T}_n\right] \\ &= \left[\underline{B}_1, \underline{B}_2, ..., \underline{B}_j, ..., \underline{B}_{2N_{\text{dim}}+1}\right] \end{aligned}$$

$$\mathbb{X} = \left[\underbrace{\mathbb{H}\left(\underline{B}_1\right) \underline{m}_n}_{\triangleq \underline{x}_0}, \underbrace{\mathbb{H}\left(\underline{B}_2\right) \underline{m}_n, \ldots, \mathbb{H}\left(\underline{B}_{2N_{\text{dim}}+1}\right) \underline{m}_n}_{\triangleq \mathbb{X}_1} \right]$$

$$\overline{\underline{x}} = \mathbb{X}\mathbb{W}^{(m)} \underline{1}_{(2N_{\text{dim}}+1)}$$

$$\begin{bmatrix} \mathbb{T}_{xx}^H \\ \mathbb{O}_{2N_{\text{dim}} \times 2N_{\text{dim}}} \end{bmatrix} = \text{QR}\left(\begin{bmatrix} \left(\mathbb{X}_1 - \overline{\underline{x}} \otimes \underline{1}_{2N_{\text{dim}}}^T\right) \left(\mathbb{W}_1^{(c)}\right)^{\frac{1}{2}} \\ \left(\sigma_{\text{n}}^2 \mathbb{I}_{N\mathcal{N}_{\text{ext}}}\right)^{\frac{1}{2}} \end{bmatrix} \right)$$

$$\mathbb{T}_{xx}^H = \text{triu}\left(\mathbb{T}_{xx}^H\right), \mathbb{T}_{xx}^H = \text{chol}\left(\mathbb{T}_{xx}\mathbb{T}_{xx}^H + w_0^{(c)}(\underline{x}_0 - \overline{\underline{x}})(\underline{x}_0 - \overline{\underline{x}})^H\right)$$

$$\mathbb{R}_{xb} = (\mathbb{B}_n - \underline{b}_n \otimes \underline{1}_{2N_{\text{dim}}+1}^T)\mathbb{W}^{(c)} \left(\mathbb{X} - \overline{\underline{x}} \otimes \underline{1}_{2N_{\text{dim}}+1}^T\right)^H$$

$$\mathbb{K}_n = \mathbb{R}_{xb} \left(\mathbb{T}_{xx}^H\right)^{-1} \mathbb{T}_{xx}^{-1}$$

$$\underline{b}_n = \underline{b}_n + \text{Re}\left\{\mathbb{K}_n \left(\underline{x}_n - \overline{\underline{x}}\right)\right\}$$

$$\mathbb{U} = \mathbb{R}_{xb} \left(\mathbb{T}_{xx}^H\right)^{-1} = [\underline{u}_1, \underline{u}_2, ..., \underline{u}_j, ..., \underline{u}_{N\mathcal{N}_{\text{ext}}}]$$

for $j = 1, 2, ..., N\mathcal{N}_{\text{ext}}$

$$\mathbb{T}_n^H = \text{triu}\left(\mathbb{T}_n^H\right), \ \mathbb{T}_n^H = \text{chol}\left(\mathbb{T}_n\mathbb{T}_n^H - \underline{u}_j\underline{u}_j^H\right)$$

end

priori guess or pre-estimated by any kind of the DOA estimation approaches, such as the ML, LS, or subspace approaches. The initial covariance $\mathbb{P}_0$ can be set to $\gamma\mathbb{I}_{2M}$ where γ indicates the confidence level in the accuracy of the initial estimates.

4.5 Computer Simulation Studies

The performance of the proposed algorithms are evaluated in this section using computer simulation studies. The data symbol sequence transmitted by each user is assumed to be a random complex sequence of zero mean and unity variance. The weight-codes are gold-codes of ± 1s of length $\mathcal{N}_{\text{ext}} = \mathcal{N}_c$ generated by modulo-two addition of two m-sequences described by the polynomial D^3+D^2+1 and D^3+D+1. This implies that $\mathcal{N}_{\text{ext}} = \mathcal{N}_c = 7$. The user tracking is assumed to be carried out over a time interval of 5000 spatiotemporal snapshots $\underline{x}[n] \in \mathcal{C}^{N\mathcal{N}_{\text{ext}}\times 1}$ collected at Point-F in Figure 4.1. The continuous time model intensity for the azimuth-velocity (see Equ 4.29) is set to $\sigma^2_{\theta_i} = 1.1 \times 10^{-8}(\deg/T)^2, \forall i$ and the intensity of the perturbations for the array locations is set to $\sigma^2_{xy} = 6.4 \times 10^{-7}(\lambda/T)^2$. The parameter γ of the initialisation stage of the proposed algorithms is set to 10^{-6}. The parameters used in Equs 4.51 and 4.52 are set to $\alpha = 10^{-4}$, and $\rho = 2$.

4.5.1 Rigid Array Geometry

For the rigid antenna array, the geometry is assumed (without any loss of generality) to be a grid planar array of 9 elements and its locations are shown in Figure 4.4. Furthermore, it is assumed that the array operates in the presence of 4 far-field moving sources/users and their initial angular velocities are assumed to be 0 $\deg/T$ which then change according to the velocity trajectory shown in Figure 4.5.

Figure 4.6 shows an example of DOA trajectory tracking of four far field moving sources using the proposed arrayed-EKF and arrayed-UKF approaches for

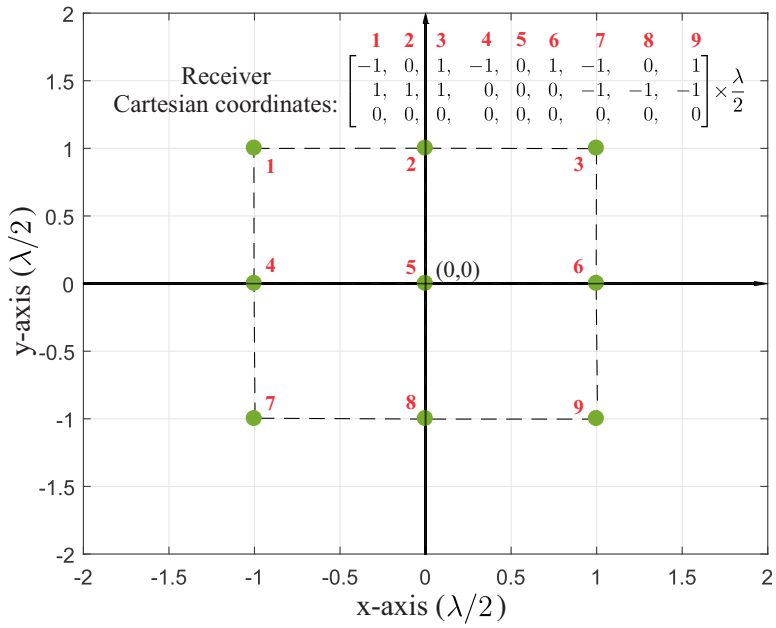

Figure 4.4: Rigid array case: Grid planar array geometry of $N = 9$ antennas, and the Cartesian coordinates of the array elements. Note: for the flexible array, this is the initial array geometry.

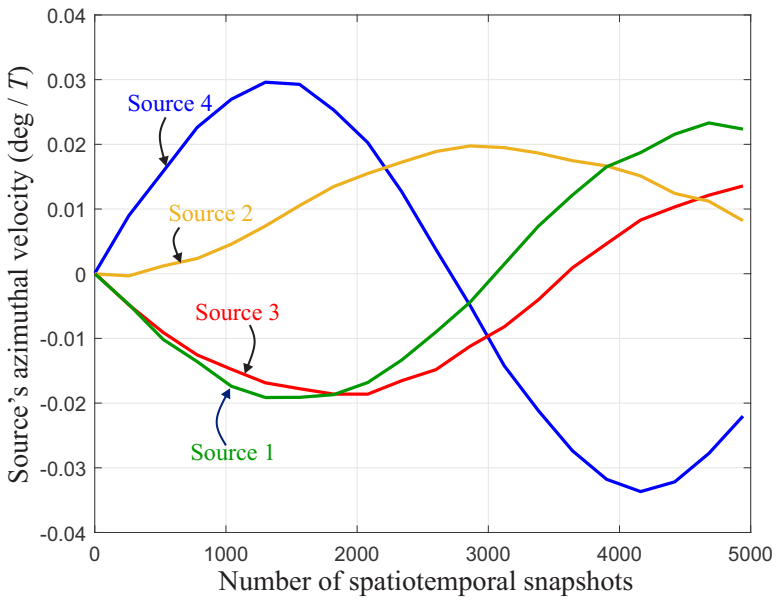

Figure 4.5: Rigid array case: the azimuthal velocity trajectories of four moving sources.

SNR = 10 dB. In Figure 4.6, the tracking results of the "Source 2" between the 3700-th snapshot and the 3800-th snapshot (framed area) are zoomed in to show the tracking performance using both approaches. It is clear that both approaches track the DOAs with high accuracy, especially the arrayed-UKF approach. Then, the performance of the proposed arrayed-EKF and arrayed-UKF approaches for all three cases of Equ 4.18 is examined using Monte Carlo simulation studies. The results are shown in Figure 4.7 where the Root Mean Square Error (RMSE) of the estimated azimuth angles is plotted as a function of the SNR for 500 Monte Carlo simulations, where in each simulation the error is averaged over the whole trajectory corresponding to 3000 snapshots. It is evident in Figure 4.7 that the proposed approaches with the extended manifold vectors $\underline{h}_i[n] = \underline{S}_i[n] \otimes \underline{w}_i$ have better source tracking accuracy over the whole SNR range than with the vectors $\underline{h}_i[n] = \underline{S}_i[n] \otimes \underline{1}_{\mathcal{N}_{\text{ext}}}$ and $\underline{h}_i[n] = \underline{S}_i[n]$. In addition, the arrayed-UKF approach outperforms the arrayed-EKF approach.

Then, under the same simulation environment as in Figure 4.7, the proposed algorithms with the extended manifold vector $\underline{h}_i[n] = \underline{S}_i[n] \otimes \underline{w}_i$ are compared with

- the subspace tracking algorithm presented in [77] which employs an H-infinity filter for estimating the noise subspace which is then used to track snapshot-by-snapshot the DOAs of multipaths,
- the particle filter approach of [101], but integrated with the received array vector-signal model for both *rigid* and *flexible* antenna arrays and the overall mobility model with the state vector of Equ 4.36. This particle filter will be referred here as "arrayed-PF".

The comparative results are shown in Figure 4.8 and it is evident that the proposed algorithms outperform both the subspace tracking and the "arrayed-PF" algorithms.

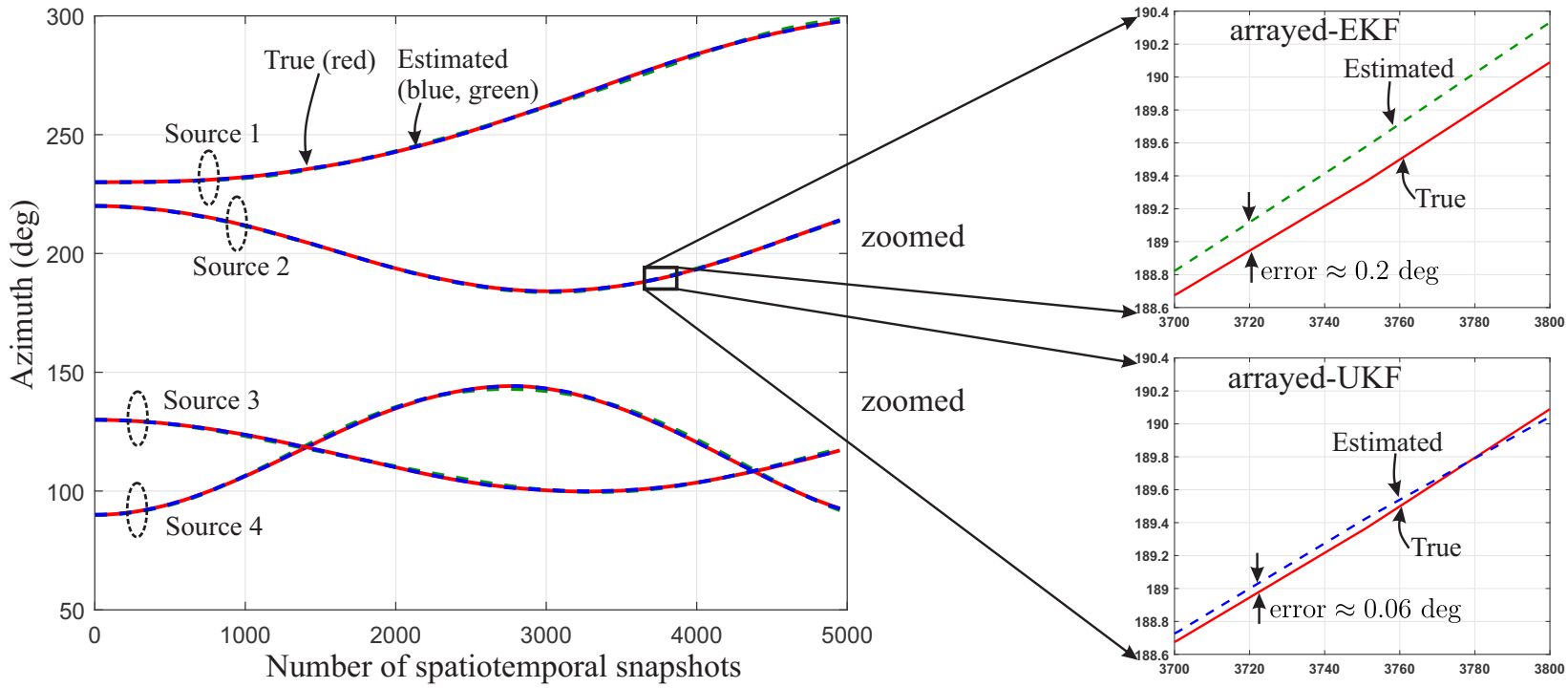

Figure 4.6: Rigid array geometry: True (solid red lines) and estimated (dashed lines) trajectories of four moving sources using the proposed arrayed-EKF (green lines) and arrayed-UKF (blue lines) approaches.

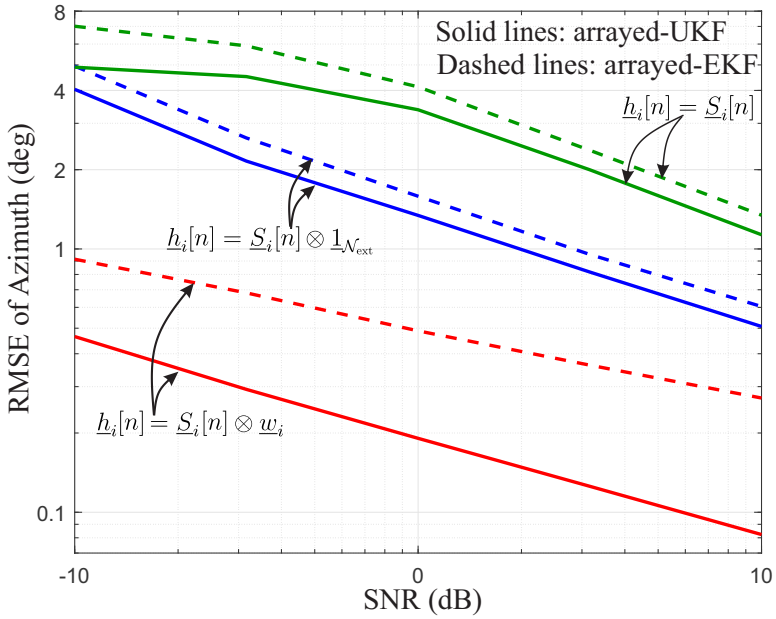

Figure 4.7: RMSE of the estimated source azimuth angles averaged over 3000 spatiotemporal snapshot evaluations using the arrayed-EKF and arrayed-UKF approaches for the three cases of Equ 4.18 (500 iterations).

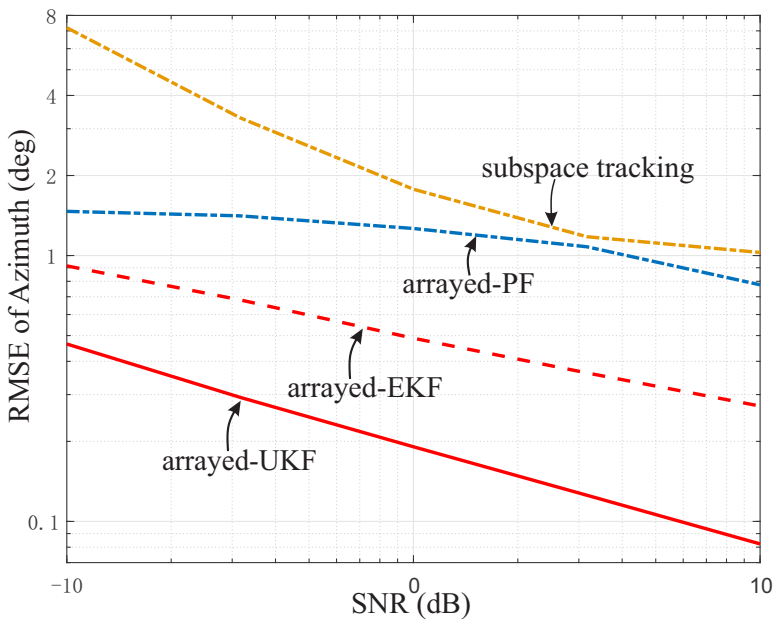

Figure 4.8: Comparison of the proposed arrayed-EKF and arrayed-UKF algorithms with other algorithms (the subspace tracking [77] and an arrayed-PF algorithm based on [101] using 100 particles).

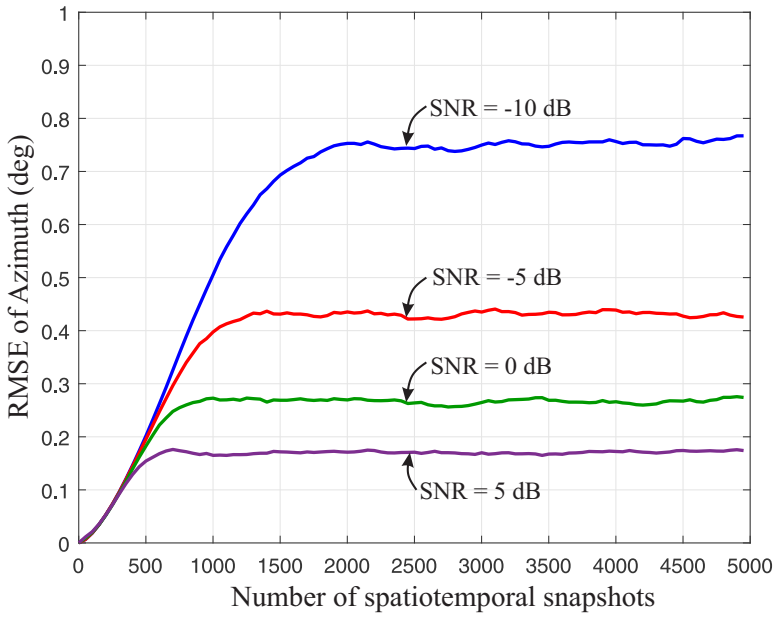

Figure 4.9: RMSE of the estimated source azimuth angles versus number of spatiotemporal snapshots using the arrayed-UKF approach with the extended manifold vector $\underline{h}_i[n] = \underline{S}_i[n] \otimes \underline{w}_i$ under different SNR levels (1000 iterations). The initial azimuth is assumed known.

Next the RMSE performance of the arrayed-UKF algorithm for the extended manifold vector $\underline{h}_i[n] = \underline{S}_i[n] \otimes \underline{w}_i$ is examined. Figures 4.9 and 4.10 show the RMSE of the estimated DOA angles as a function of the number of spatiotemporal snapshots using the proposed arrayed-UKF algorithm for different SNRs. Note that, in Figure 4.9, the initial DOAs are assumed known, and in Figure 4.10 the initial DOAs are obtained from a random Gaussian distribution with unity variance. The results show that the estimation error for different signal environments is small and remains constant over time, which illustrates the stability of the proposed arrayed-UKF approach. Overall, based on the results of both Figures 4.7 and 4.9, it can be concluded that the arrayed-UKF algorithm offers significant tracking accuracy over the SNR range, which indicates its robustness to noise.

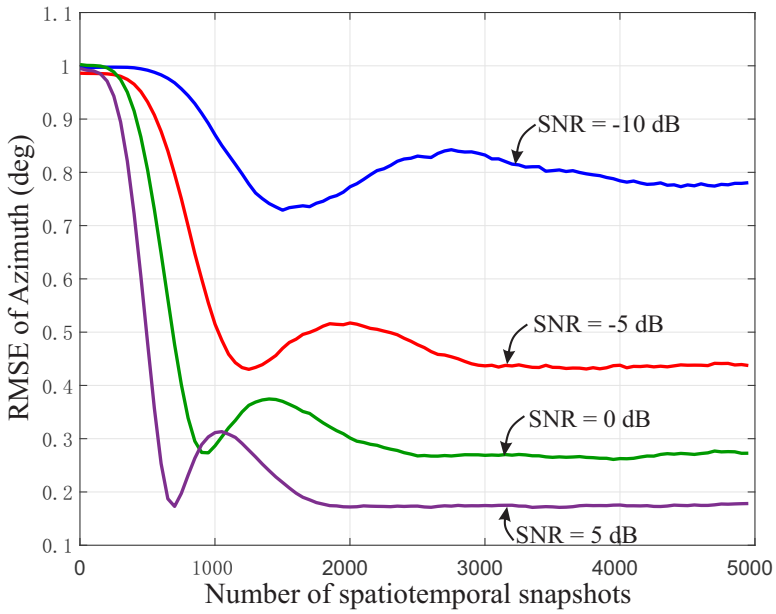

Figure 4.10: RMSE of the estimated source azimuth angles versus number of spatiotemporal snapshots using the arrayed-UKF approach with the extended manifold vector $\underline{h}_i[n] = \underline{S}_i[n] \otimes \underline{w}_i$ under different SNR levels (1000 iterations). The initial azimuth is assumed unknown.

4.5.2 Flexible Array Geometry

For the flexible antenna array, the initial geometry is assumed to be also given by Figure 4.4 but then the geometry will change randomly and a representative trajectory of the 9 antennas relative to the array reference point is shown in Figure 4.11. The fifth antenna array element is assumed to be the array reference[6] point. For this trajectory, the angular velocity for each flexible array element is assumed to be $\omega_j = 0.01(\deg/T), \forall j$. The angular velocities of the sources are shown in Figure 4.12.

Figure 4.13 shows another example of DOA trajectory tracking of four moving sources using the proposed arrayed-EKF and arrayed-UKF approaches with a flexible array geometry for SNR = 10 dB. The tracking results of "Source 1" between the 3700-th snapshot and the 3800-th snapshot are zoomed in. It can be observed

[6]The array reference point also moves but this motion is not shown (only the relative motion with respect to this reference point is shown).

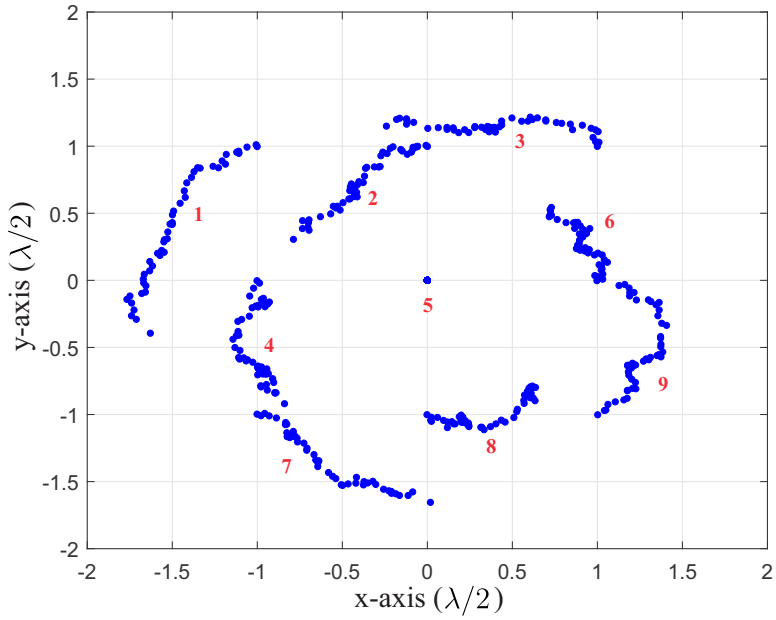

Figure 4.11: Flexible array geometry: a representative trajectory of the flexible array locations. The instantaneous array locations are plotted every 100 snapshots.

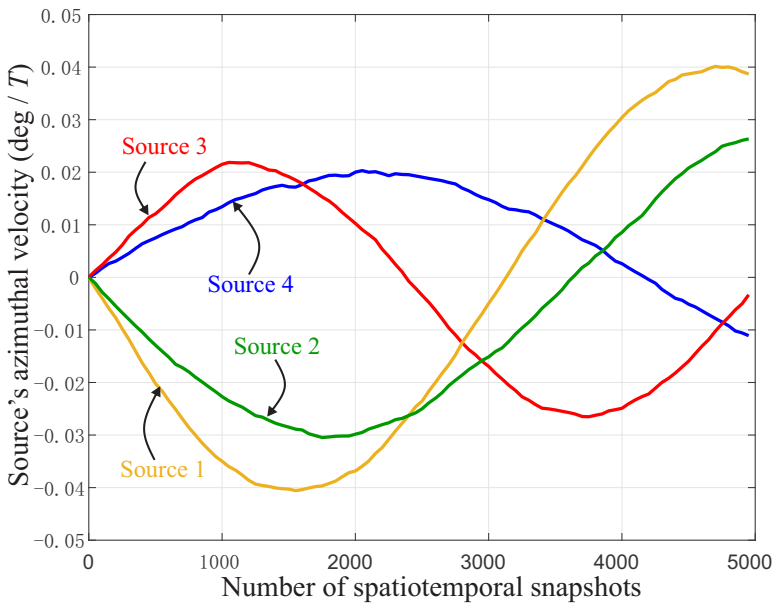

Figure 4.12: Flexible array case: the azimuthal velocity trajectories of four moving sources.

that the DOA tracking works well with a flexible array.

The estimated array locations for $n = 3000$ and 5000 by the two algorithms are illustrated in Figures 4.14 and 4.15, respectively. Furthermore, the trajectories of the flexible array locations and the trajectories of the estimated array locations using the arrayed-UKF algorithm are shown in Figure 4.16. It is clear that the array geometry changes dramatically with time and its instantaneous array locations are successfully estimated by the proposed approaches.

Then, for the flexible array case, 500 Monte-Carlo simulations have been carried out under the same simulation environment as used in Figure 4.13. The two proposed algorithms are also compared with the "arrayed-PF" approach (using 150 particles) for the flexible array case under the same simulation environment. Note that the "subspace tracking" algorithm [77] examined in Figure 4.8 is not able to work in the case of flexible arrays. The results are shown in Figures 4.17 - 4.20 where the RMSE of the estimated array locations (Figures 4.17 and 4.18) and azimuth angles (Figures 4.19 and 4.20) are plotted as a function of the SNR where in each simulation the error over the DOA trajectory of 3000 snapshots is averaged for each moving source. These figures indicate that the proposed arrayed-UKF algorithm with the extended manifold vector $\underline{h}_i[n] = \underline{S}_i[n] \otimes \underline{w}_i$ has superior tracking accuracy in both the estimated array locations and the estimated azimuth angles.

Finally, it can be seen from Figures 4.6 and 4.13 that the proposed algorithms do not suffer from the data association problem when the source trajectories cross each other. This is because of the use of the spatiotemporal state space model which provides a one-to-one mapping between the sources and their manifold vectors.

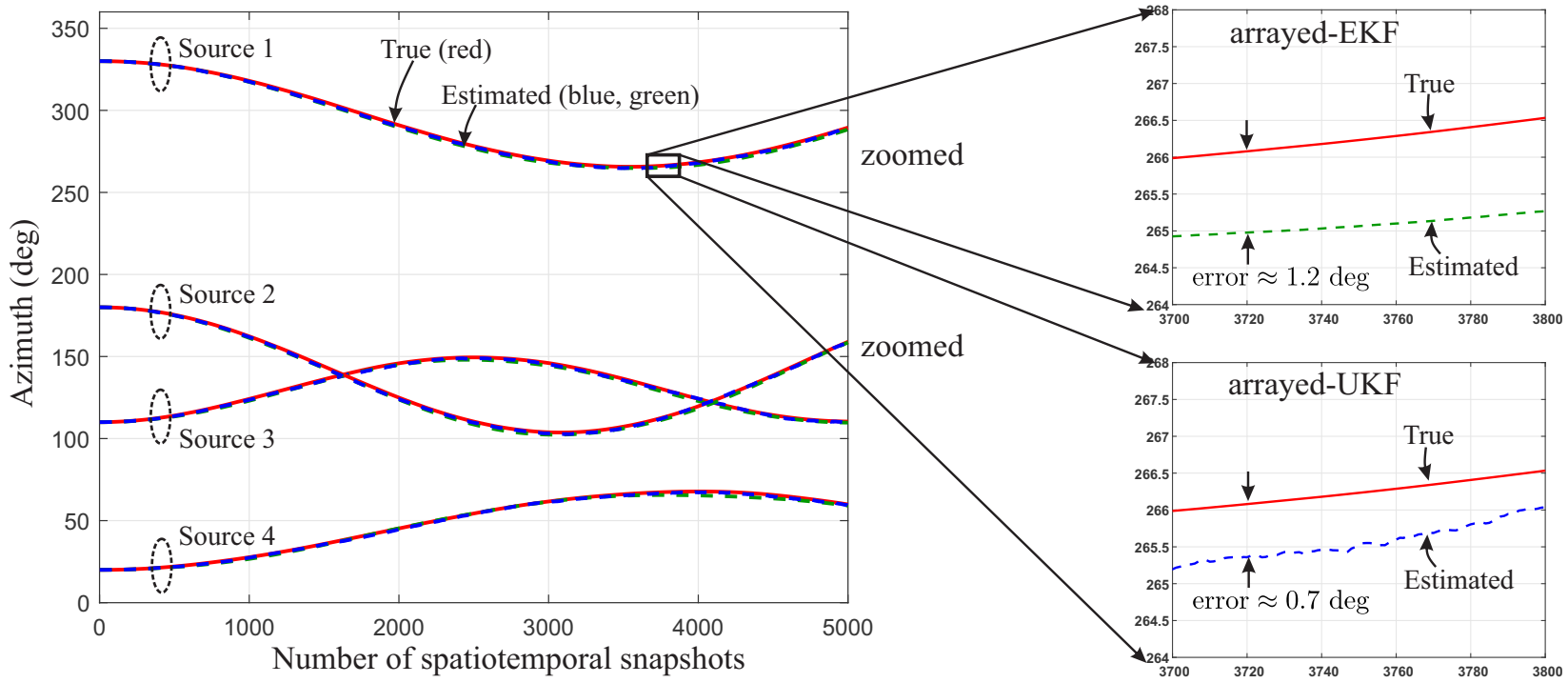

Figure 4.13: Flexible array geometry: True (solid red lines) and estimated (dashed lines) trajectories of the moving sources using the proposed arrayed-EKF (green lines) and arrayed-UKF approaches (blue lines).

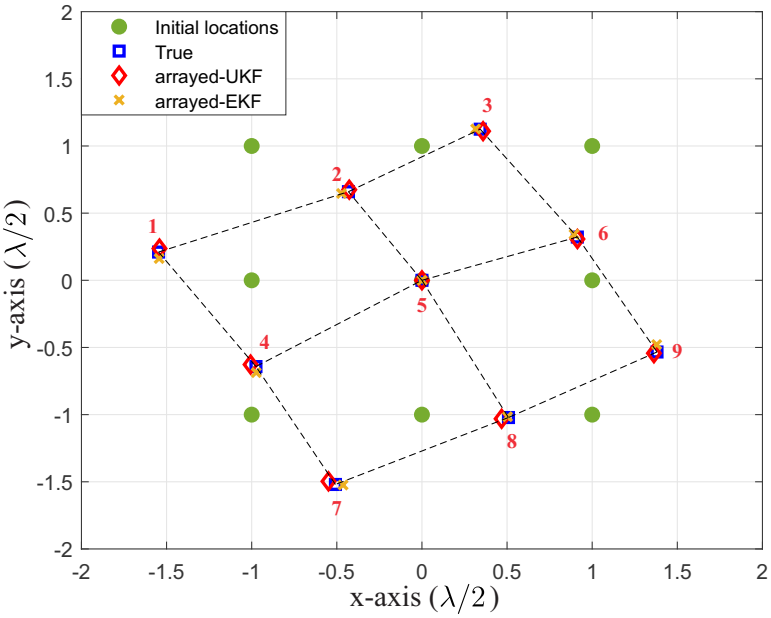

Figure 4.14: Array geometry at $n = 3000$ showing the initial array locations (circle), the true array locations (square) and the estimated array locations using the arrayed-UKF (diamond) and the arrayed-EKF (cross).

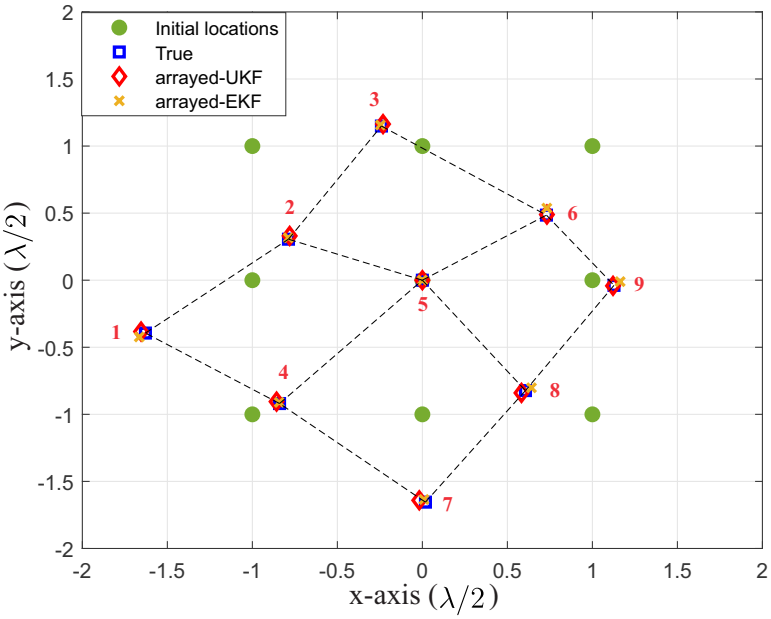

Figure 4.15: Array geometry at $n = 5000$ showing the initial array locations (circle), the true array locations (square) and the estimated array locations by the arrayed-UKF (diamond) and the arrayed-EKF (cross).

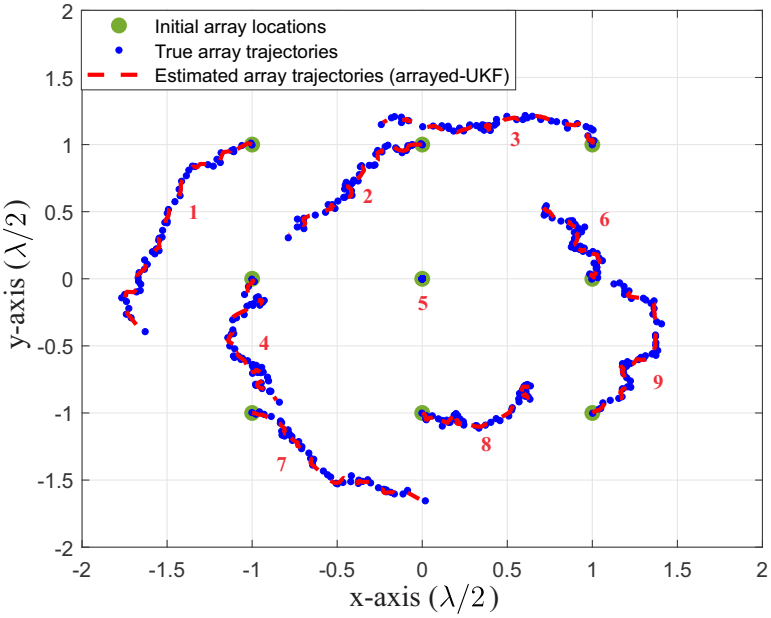

Figure 4.16: Trajectories of the flexible array locations over 5000 snapshots. The instantaneous array locations are plotted every 100 snapshots.

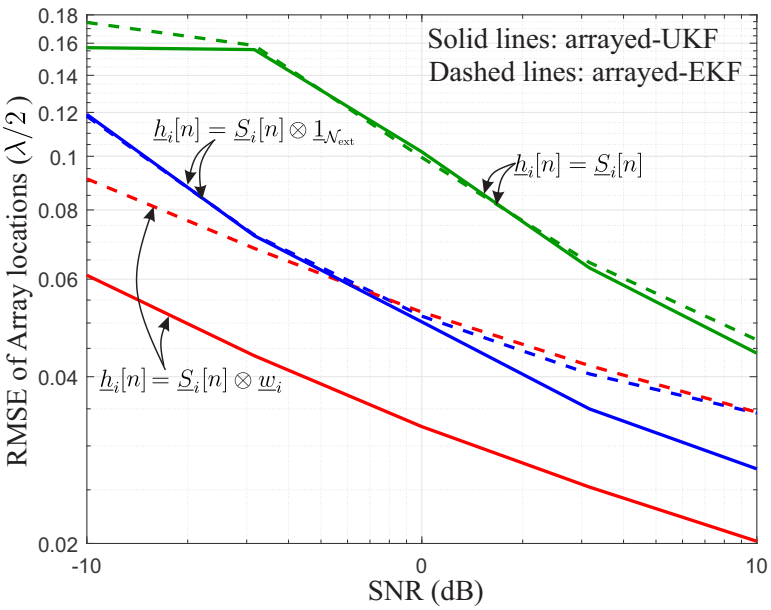

Figure 4.17: RMSE of the estimated array locations averaged over 3000 spatiotemporal snapshot evaluations using the arrayed-EKF approach and the arrayed-UKF approach for the three cases of Equ 4.18 (500 iterations).

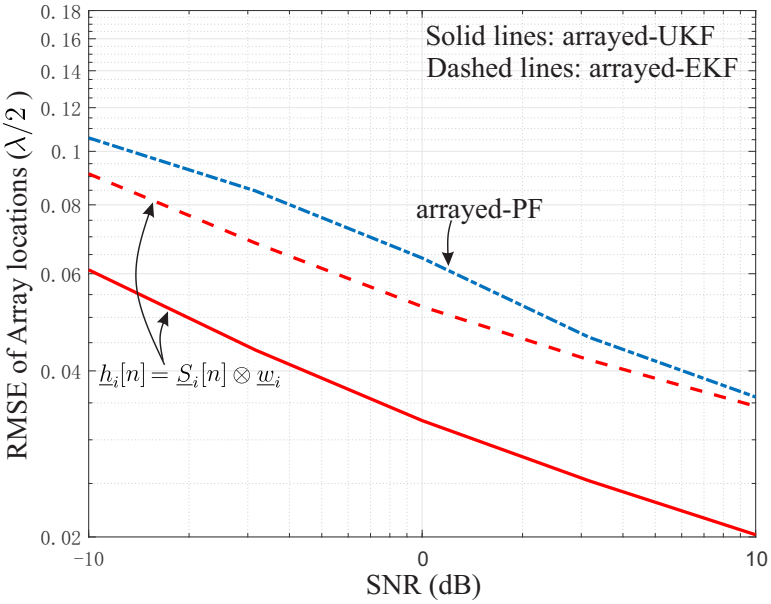

Figure 4.18: Comparison of the proposed arrayed-EKF and arrayed-UKF algorithms with an arrayed-PF algorithm based on [101] using 150 particles in terms of the RMSE of the estimated array locations.

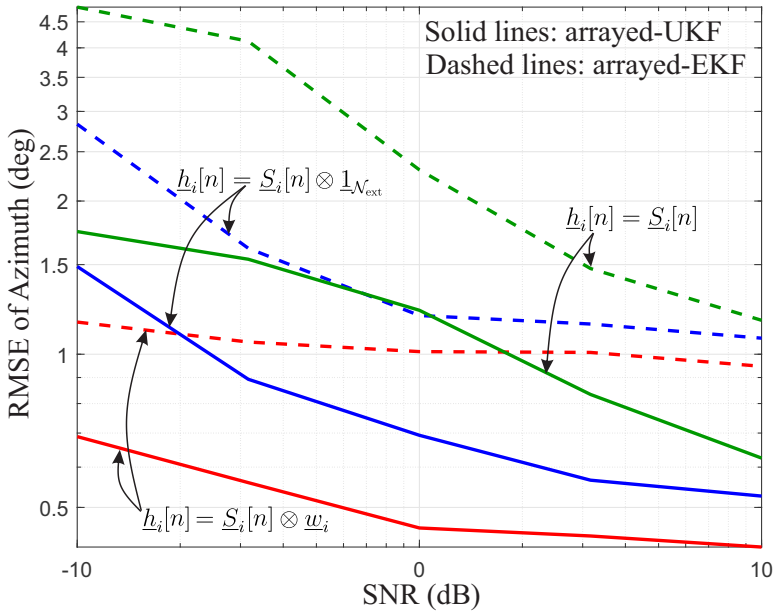

Figure 4.19: RMSE of the estimated source azimuth angles with the flexible array averaged over 3000 spatiotemporal snapshot evaluations using the arrayed-EKF approach and the arrayed-UKF approach for the three cases of Equ 4.18 (500 iterations).

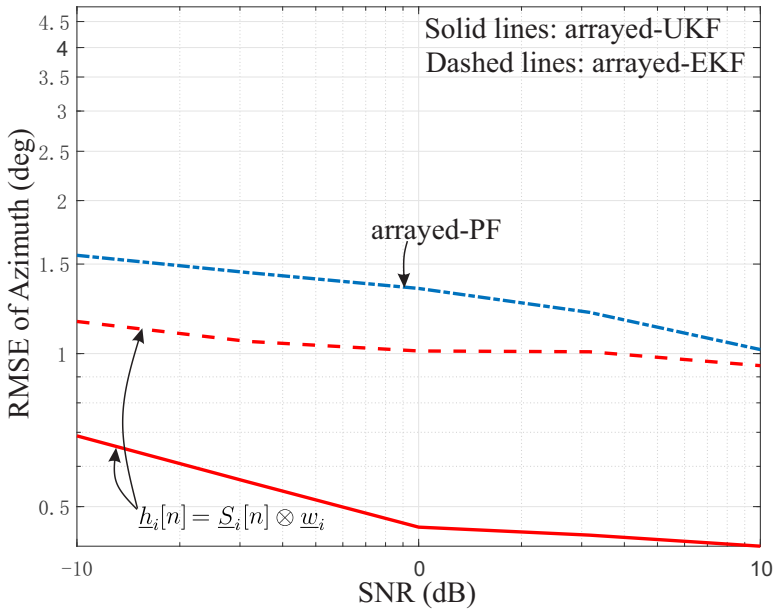

Figure 4.20: Comparison of the proposed arrayed-EKF and arrayed-UKF algorithms with an arrayed-PF algorithm based on [101] using 150 particles in terms of the RMSE of the source azimuth angles with the flexible array.

4.6 Summary

In this chapter, a theoretical framework is presented for tracking far-field sources in an non-stationary environment using both rigid and flexible antenna array geometries. The proposed multi-source tracking framework is based on the integration of a spatiotemporal state-space modelling, the extended manifold concept and EKF/UKF theoretical iterative tools, for both rigid and flexible array geometries. The performance of the proposed approaches was examined using computer simulation studies under various noise levels and compared with a subspace tracking and a particle filter algorithms. The results indicate that the arrayed-UKF algorithm has better tracking performance than the other algorithms for both rigid and flexible array geometries, while it shows robustness to noisy environments.

For further extension of the current work, antenna arrays may be deployed at each transmitter of Figure 4.1 (i.e. MIMO). In such system, the manifold vector $\underline{S}_i[n]$ in Equ 4.18 can be replaced by $\overline{\underline{S}}_i^*[n] \otimes \underline{S}_i[n]$, which is known as "virtual

array manifold", where $\overline{\underline{S}}_i[n]$ denotes the manifold vector of the transmitter. In this case, the tracking performance could be further improved.

Chapter 5

Conclusions and Further Work

This thesis is concerned with several multi source parameter estimation and tracking approaches using antenna arrays in the context of wireless communication systems. The first part of this thesis presents MIMO system structures and algorithms for multi-source parameter estimation. The second part presents algorithms and approaches for tracking of multiple non-stationary sources using rigid and flexible arrays. Different manifold extenders have been proposed to increase the dimensionality of the signal observation space, which consequently increase the degrees of freedom.

In Chapter 2, a MIMO system model is provided and the received signal vector is presented based on a parametric channel model. The parametric channel model is employed through the thesis, as such model more accurately describes the actual wave propagation environment. Then, a virtual manifold extender is proposed to form the virtual manifold vectors and to extend the dimensionality of the signal observation space from N to $N\overline{N}$. Based on the virtual manifold vectors, two superresolution algorithms are proposed to estimate the delay, DOD and DOA of all the paths of the desired user in the presence of multiple access interference. The performance of the proposed algorithms is evaluated with a range of SNR values and the number of snapshots, and it is compared with a traditional estimation

approach. The results show the superiority of the proposed approach.

In Chapter 3, a virtual-spatiotemporal MIMO system is proposed which extends the MIMO system in Chapter 2, and extends the dimensionality of the signal observation space from N to $2N\overline{N}\mathcal{N}_c$ by using a proposed virtual-spatiotemporal manifold extender. The degrees of freedom is thus enhanced and the enhancement of the degrees of freedom leads to the ability of

- accommodating more number of sources,
- more accurate source parameters estimation,
- increased interference cancellation capabilities,
- and higher array gain.

All the aforementioned objectives have been realised in this chapter. A delay-Doppler estimation algorithm, a DOD-DOA estimation algorithm and a beamformer weight design algorithm are proposed, all of which are subspace-based algorithms. In the simulation studies, the proposed system is compared with a spatial-only system, a virtual system and a spatiotemporal system. The results showed that the proposed system provides highest estimation accuracy, is able to accommodate the most number of signals, and achieves steady high array gain which is independent of the Tx array geometry, the DOD and the design of the transmit weight. In addition, the proposed algorithms are not restricted by the array geometries employed at either the transmitter or the receiver.

In Chapter 4, tracking the DOA of multiple moving sources in wireless communications using antenna arrays is considered. Two tracking approaches based on an arrayed-EKF algorithm and an arrayed-UKF algorithm, in conjunction with a spatiotemporal state-space model and a "manifold extender" are proposed. Both the rigid array and the flexible array are employed. If the array is flexible, apart from tracking multiple DOAs and their angular velocities, the array locations are

also simultaneously tracked as they change arbitrarily with time. In the proposed approaches, all the sources and the array locations are tracked in a unified way snapshot-by-snapshot which is suitable for tracking even of fast moving sources using antenna array systems. The performance of the proposed approaches are evaluated under three cases and under various SNR levels, and compared with a subspace tracking approach and a particle filter approach. The results show the proposed approaches achieve better tracking accuracy for both rigid and flexible array geometries.

5.1 List of Contributions

The novel contributions presented in this thesis are the following:

1. Designing a multi source parameter (delay, DOD and DOA) estimation approach using virtual manifold extender for MIMO systems in wireless communications.

2. Investigating and comparing the estimation performance using virtual manifold extender with a conventional MIMO approach.

3. Designing a virtual-spatiotemporal system that is capable of enhancing the degrees of freedom.

4. Proposing a virtual-spatiotemporal receiver to estimate delay, Doppler, DOD and DOA of all paths of the desired user in the presence of MAI.

5. Investigating the performance of the channel estimation of virtual-spatiotemporal receiver with varying noise levels and varying number of snapshots, and comparing its performance with a spatiotemporal receiver, virtual receiver and a spatial-only receiver.

6. Proposing a virtual-spatiotemporal subspace beamformer which has constant SNIR output and the performance independent of the DOD, Tx array geometry and transmit weight.

7. Comparing the virtual-spatiotemporal beamformer with various beamformers in terms of NFR, DOD, Tx array geometry and the number of signals.

8. Proposing several algorithms for tracking the DOA of multiple moving sources in wireless communications using rigid array and flexible array, where all the antenna array elements (in a constant or a time varying geometry) work together as one unit.

9. Proposing algorithms for tracking the array locations with the DOA of multiple moving sources simultaneously using flexible array.

10. Investigating and comparing the proposed several tracking algorithms using both rigid and flexible arrays with a subspace tracking algorithm and a particle filter algorithm.

5.2 Suggestions for Further Work

The following list outlines ideas and suggestions for the future work based on the research presented in this thesis

- Chapter 2 presents a novel MIMO system for multiple source parameter estimation using a proposed virtual manifold extender which increases the signal dimensionality. Based on this, the system can be utilised to design appropriate beamformers at the reception, such as subspace type beamformers. Such beamformers may achieve higher SNIR output than the conventional beamformers.

- The systems proposed in Chapter 2 and Chapter 3 are single carrier systems. Thus, to increase the degrees of freedom further, these systems can be extended to multi-carrier system where each user could be modulated by a set of orthogonal subcarriers.

- Chapter 3 presents a MIMO system design with powerful channel parameter estimators and beamformers for wireless communications. Since the format of the transmitted signal is similar to the radar's, the signal model, signal environment and array system can be extended to form a radar-communication system. In this aspect, the clutters can also be added in the channel model as it is a part of a typical radar system. In addition, corresponding algorithms at the receiver should be enhanced to remove these clutters. With such modification, this system design can be applied in both fields of communications and radar.

- Chapter 4 considers a SIMO multiple user wireless channel, i.e. each transmitter employs single antenna. Thus, antenna arrays may be deployed at each transmitter and the virtual manifold vector proposed in Chapter 2 can therefore be used to further increase the degrees of freedom. Therefore, the tracking performance may be further improved.

- Chapter 4 is concerned with developing algorithms for DOA tracking with a small aperture array. The proposed algorithms can be extended to be applicable with a large aperture array. In this case, apart from the source DOAs, the source ranges can also be tracked by including the ranges and the range velocities in the state space model.

- The signal model proposed in Chapter 4 may be further extended to include the multipath of the sources and the multiple access interference. The algorithms can be enhanced to deal with the multipath component and sup-

press the multiple access interference. In addition, the array system model presented in this chapter is two-dimensional which can be extended to three-dimensional. In this case, the azimuth and elevation of the sources as well as the array locations at both the x-axis and y-axis can be tracked simultaneously.

References

[1] Z. Tang and A. Manikas, "DOA and DOD Channel Estimation in MIMO Access Networks," in *IEEE International Conference on Communications (ICC)*, May 2019, pp. 1–6. p17, p71, p79

[2] Z. Tang and A. Manikas, "Direction-of-Arrival Tracking of Multiple Fast-Moving Sources in Antenna Array based Access Networks," in *IEEE International Conference on Communications (ICC)*, Jun. 2020, pp. 1–6. p17, p92, p100

[3] Z. Tang and A. Manikas, "Multi Direction-of-Arrival Tracking Using Rigid and Flexible Antenna Arrays," *IEEE Transactions on Wireless Communications*, vol. 20, no. 11, pp. 7568–7580, Nov. 2021. p17, p93

[4] Z. Tang and A. Manikas, "DOD-DOA Estimation using MIMO Antenna Arrays with Manifold Extenders," in *IEEE International Symposium on Personal, Indoor and Mobile Radio Communications (PIMRC)*, Sep. 2022, pp. 1–6. p17

[5] Z. Lin, T. Lv, W. Ni, J. A. Zhang, and R. P. Liu, "Nested Hybrid Cylindrical Array Design and DoA Estimation for Massive IoT Networks," *IEEE Journal on Selected Areas in Communications*, vol. 39, no. 4, pp. 919–933, Aug. 2021. p21

[6] X. Wang, L. Wan, M. Huang, C. Shen, Z. Han, and T. Zhu, "Low-Complexity Channel Estimation for Circular and Noncircular Signals in Virtual MIMO Vehicle Communication Systems," *IEEE Transactions on Vehicular Technology*, vol. 69, no. 4, pp. 3916–3928, Feb. 2020. p21

[7] D. Fan, F. Gao, B. Ai, G. Wang, Z. Zhong, Y. Deng, and A. Nallanathan, "Channel Estimation and Self-Positioning for UAV Swarm," *IEEE Transactions on Communications*, vol. 67, no. 11, pp. 7994–8007, Aug. 2019. p21

[8] G. Wang, J. Xin, J. Wang, N. Zheng, and A. Sano, "Subspace-based two-dimensional direction estimation and tracking of multiple targets," *IEEE Transactions on Aerospace and Electronic Systems*, vol. 51, no. 2, pp. 1386–1402, Apr. 2015. p21, p91

[9] E. G. Larsson, O. Edfors, F. Tufvesson, and T. L. Marzetta, "Massive MIMO for next generation wireless systems," *IEEE Communications Magazine*, vol. 52, no. 2, pp. 186–195, Feb. 2014. p21

[10] F. Shu, Y. Qin, T. Liu, L. Gui, Y. Zhang, J. Li, and Z. Han, "Low-Complexity and High-Resolution DOA Estimation for Hybrid Analog and Digital Massive MIMO Receive Array," *IEEE Transactions on Communications*, vol. 66, no. 6, pp. 2487–2501, Feb. 2018. p21

[11] A. Gupta and R. K. Jha, "A Survey of 5G Network: Architecture and Emerging Technologies," *IEEE Access*, vol. 3, pp. 1206–1232, Jul. 2015. p22, p33

[12] H. Akaike, "A new look at the statistical model identification," *IEEE Transactions on Automatic Control*, vol. 19, no. 6, pp. 716–723, Dec. 1974. p22

[13] R. Veras and C. Collins, "Optimizing Hierarchical Visualizations with the Minimum Description Length Principle," *IEEE Transactions on Visualization and Computer Graphics*, vol. 23, no. 1, pp. 631–640, Aug. 2017. p22

[14] R. Schmidt, "Multiple emitter location and signal parameter estimation," *IEEE Transactions on Antennas and Propagation*, vol. 34, no. 3, pp. 276–280, Mar. 1986. p22, p29, p35, p91

[15] R. Roy and T. Kailath, "ESPRIT-estimation of signal parameters via rotational invariance techniques," *IEEE Transactions on Acoustics, Speech, and Signal Processing*, vol. 37, no. 7, pp. 984–995, Jul. 1989. p22, p35

[16] J. Capon, "High-resolution frequency-wavenumber spectrum analysis," *Proceedings of the IEEE*, vol. 57, no. 8, pp. 1408–1418, Aug. 1969. p23, p35

[17] H. Cox, "Resolving power and sensitivity to mismatch of optimum array processors," *The Journal of the acoustical society of America*, vol. 54, no. 3, pp. 771–785, Sep. 1973. p23

[18] A. Manikas, *Differential Geometry In Array Processing*. Imperial College Press, 2004. p25, p26, p46, p77

[19] G. Efstathopoulos and A. Manikas, "Extended array manifolds: Functions of array manifolds," *IEEE Transactions on Signal Processing*, vol. 59, no. 7, pp. 3272–3287, Mar. 2011. p25, p26, p33, p36, p95, p100

[20] H. Ren and A. Manikas, "MIMO Radar With Array Manifold Extenders," *IEEE Transactions on Aerospace and Electronic Systems*, vol. 56, no. 3, pp. 1942–1954, Jun. 2020. p26

[21] V. Sridhar, T. Gabillard, and A. Manikas, "Spatiotemporal-MIMO Channel Estimator and Beamformer for 5G," *IEEE Transactions on Wireless Communications*, vol. 15, no. 12, pp. 8025–8038, Dec. 2016. p26, p71, p79, p81

[22] X. Gao, F. Tufvesson, and O. Edfors, "Massive MIMO channels - Measurements and models," in *2013 Asilomar Conference on Signals, Systems and Computers*, Nov. 2013, pp. 280–284. p28

[23] C. R. Sastry, E. W. Kamen, and M. Simaan, "An efficient algorithm for tracking the angles of arrival of moving targets," *IEEE Transactions on Signal Processing*, vol. 39, no. 1, pp. 242–246, Jan. 1991. p29, p91

[24] C. K. Sword, M. Simaan, and E. W. Kamen, "Multiple target angle tracking using sensor array outputs," *IEEE Transactions on Aerospace and Electronic Systems*, vol. 26, no. 2, pp. 367–373, Mar. 1990. p29, p91, p92

[25] B. Panzner, W. Zirwas, S. Dierks, M. Lauridsen, P. Mogensen, K. Pajukoski, and D. Miao, "Deployment and implementation strategies for massive MIMO in 5G," *IEEE Globecom Workshops, GC Wkshps*, pp. 346–351, Dec. 2014. p33, p58

[26] Q.-U.-A. Nadeem, A. Kammoun, M. Debbah, and M.-S. Alouini, "A Generalized Spatial Correlation Model for 3D MIMO Channels Based on the Fourier Coefficients of Power Spectrums," *IEEE Transactions on Signal Processing*, vol. 63, no. 14, pp. 3671–3686, May 2015. p33

[27] A. M. Sayeed, "Modeling and capacity of realistic spatial MIMO channels," in *2001 IEEE International Conference on Acoustics, Speech, and Signal Processing*, vol. 4, May 2001, pp. 2489–2492. p34

[28] W. Weichselberger, M. Herdin, H. Ozcelik, and E. Bonek, "A stochastic MIMO channel model with joint correlation of both link ends," *IEEE Transactions on Wireless Communications*, vol. 5, no. 1, pp. 90–100, Jan. 2006. p34

[29] R. Ertel, P. Cardieri, K. Sowerby, T. Rappaport, and J. Reed, "Overview of spatial channel models for antenna array communication systems," *IEEE Personal Communications*, vol. 5, no. 1, pp. 10–22, Feb. 1998. p34

[30] M. S. Bartlett, "Smoothing Periodograms from Time-Series with Continuous Spectra," *Nature*, vol. 161, no. 4096, pp. 686–687, May 1948. p35

[31] H. Krim and M. Viberg, "Two decades of array signal processing research: The parametric approach," *IEEE Signal Processing Magazine*, vol. 13, no. 4, pp. 67–94, Jul. 1996. p35

[32] A. G. Jaffer, "Maximum likelihood direction finding of stochastic sources: a separable solution," in *ICASSP-88., International Conference on Acoustics, Speech, and Signal Processing*, vol. 5, Jan. 1988, pp. 2893–2896. p35

[33] Y. Bresler and A. Macovski, "Exact maximum likelihood estimation of superimposed exponential signals in noise," in *ICASSP '85. IEEE International Conference on Acoustics, Speech, and Signal Processing*, vol. 10, Apr. 1985, pp. 1824–1827. p35

[34] M. Feder and E. Weinstein, "Parameter estimation of superimposed signals using the EM algorithm," *IEEE Transactions on Acoustics, Speech, and Signal Processing*, vol. 36, no. 4, pp. 477–489, Apr. 1988. p35

[35] J. A. Fessler and A. O. Hero, "Space-alternating generalized expectation-maximization algorithm," *IEEE Transactions on Signal Processing*, vol. 42, no. 10, pp. 2664–2677, Oct. 1994. p35

[36] M. Viberg and B. Ottersten, "Sensor array processing based on subspace fitting," *IEEE Transactions on Signal Processing*, vol. 39, no. 5, pp. 1110–1121, May 1991. p35

[37] A. Barabell, "Improving the resolution performance of eigenstructure-based direction-finding algorithms," in *ICASSP '83. IEEE International Conference on Acoustics, Speech, and Signal Processing*, vol. 8, Apr. 1983, pp. 336–339. p35

[38] E. Gonen and J. M. Mendel, "Subspace-based direction finding methods," *The digital signal processing handbook*, vol. 62, 1999. p35

[39] Z. Chen and A. Manikas, "Direction-of-Departure Estimation Using Cooperative Beamforming," in *7th International Symposium on Wireless Communication Systems*, Sep. 2010, pp. 120–124. p36

[40] R. Pöhlmann, S. Zhang, A. Dammann, and P. A. Hoeher, "Manifold Optimization Based Beamforming for DoA and DoD Estimation with a Single Multi-Mode Antenna," in *European Signal Processing Conference (EUSIPCO)*, Jan. 2021, pp. 1841–1845. p36

[41] L. Hao, J. Rodríguez-Piñeiro, X. Cai, X. Yin, J. Hong, G. F. Pedersen, and S. Schwarz, "Measurement-based Double-Directional Polarimetric Characterization of Outdoor Massive MIMO Propagation Channels at 3.5GHz," in *IEEE 21st International Workshop on Signal Processing Advances in Wireless Communications (SPAWC)*, May 2020, pp. 1–5. p36

[42] B. H. Fleury, M. Tschudin, R. Heddergott, D. Dahlhaus, and K. Ingeman Pedersen, "Channel parameter estimation in mobile radio environments using the SAGE algorithm," *IEEE Journal on Selected Areas in Communications*, vol. 17, no. 3, pp. 434–450, Mar. 1999. p36

[43] A. Richter, D. Hampicke, G. Sommerkorn, and R. S. Thoma, "Joint estimation of DoD, time-delay, and DoA for high-resolution channel sounding," in *IEEE 51st Vehicular Technology Conference Proceedings*, vol. 2, May 2000, pp. 1045–1049. p36, p37

[44] D. Zhu, J. Choi, and R. W. Heath, "Two-Dimensional AoD and AoA Acquisition for Wideband Millimeter-Wave Systems With Dual-Polarized MIMO," *IEEE Transactions on Wireless Communications*, vol. 16, no. 12, pp. 7890–7905, Dec. 2017. p36, p37

[45] M. Godavarti and A. O. Hero, "Diversity and Degrees of Freedom in Wireless Communications," *IEEE International Conference on Acoustics, Speech, and Signal Processing*, vol. 3, pp. 2861–2864, May 2002. p54

[46] S. A. Jafar and S. Shamai, "Degrees of freedom region of the MIMO X channel," *IEEE Transactions on Information Theory*, vol. 54, no. 1, pp. 151–170, Jan. 2008. p54

[47] P. Pal and P. P. Vaidyanathan, "Nested arrays: A novel approach to array processing with enhanced degrees of freedom," *IEEE Transactions on Signal Processing*, vol. 58, no. 8, pp. 4167–4181, Apr. 2010. p54, p55

[48] A. T. Moffet, "Minimum-redundancy linear arrays," *IEEE Transactions on Antennas and Propagation*, vol. AP-16, no. 2, pp. 172–175, Mar. 1968. p54

[49] S. U. Pillai, Y. Bar-Ness, and F. Haber, "A new approach to array geometry for improved spatial spectrum estimation," *Proceedings of the IEEE*, vol. 73, no. 10, pp. 1522–1524, Oct. 1985. p55

[50] S. Pillai and F. Haber, "Statistical analysis of a high resolution spatial spectrum estimator utilizing an augmented covariance matrix," *IEEE Transactions on Acoustics, Speech, and Signal Processing*, vol. 35, no. 11, pp. 1517–1523, Nov. 1987. p55

[51] B. Porat and B. Friedlander, "Direction finding algorithms based on high-order statistics," *IEEE Transactions on Signal Processing*, vol. 39, no. 9, pp. 2016–2024, Apr. 1991. p55

[52] P. Chevalier, L. Albera, A. Ferreol, and P. Comon, "On the virtual array concept for higher order array processing," *IEEE Transactions on Signal Processing*, vol. 53, no. 4, pp. 1254–1271, Mar. 2005. p55

[53] W.-K. Ma, T.-H. Hsieh, and C.-Y. Chi, "DOA Estimation of Quasi-Stationary Signals With Less Sensors Than Sources and Unknown Spatial Noise Covariance: A Khatri-Rao Subspace Approach," *IEEE Transactions on Signal Processing*, vol. 58, no. 4, pp. 2168–2180, Oct. 2010. p55

[54] P. Pal and P. P. Vaidyanathan, "Coprime sampling and the music algorithm," in *2011 Digital Signal Processing and Signal Processing Education Meeting (DSP/SPE)*, Jan. 2011, pp. 289–294. p55

[55] S. Qin, Y. D. Zhang, and M. G. Amin, "Generalized Coprime Array Configurations for Direction-of-Arrival Estimation," *IEEE Transactions on Signal Processing*, vol. 63, no. 6, pp. 1377–1390, Jan. 2015. p55

[56] A. Raza, W. Liu, and Q. Shen, "Thinned coprime arrays for DOA estimation," in *2017 25th European Signal Processing Conference (EUSIPCO)*, Aug. 2017, pp. 395–399. p55

[57] X. Wang and X. Wang, "Hole Identification and Filling in k-Times Extended Co-Prime Arrays for Highly Efficient DOA Estimation," *IEEE Transactions on Signal Processing*, vol. 67, no. 10, pp. 2693–2706, Feb. 2019. p55

[58] W. Zheng, X. Zhang, Y. Wang, M. Zhou, and Q. Wu, "Extended Coprime Array Configuration Generating Large-Scale Antenna Co-Array in Massive MIMO System," *IEEE Transactions on Vehicular Technology*, vol. 68, no. 8, pp. 7841–7853, Jun. 2019. p55

[59] C.-L. Liu and P. P. Vaidyanathan, "Super Nested Arrays: Linear Sparse Arrays With Reduced Mutual Coupling-Part I: Fundamentals," *IEEE Transactions on Signal Processing*, vol. 64, no. 15, pp. 3997–4012, Apr. 2016. p55

[60] J. Liu, Y. Zhang, Y. Lu, S. Ren, and S. Cao, "Augmented Nested Arrays With Enhanced DOF and Reduced Mutual Coupling," *IEEE Transactions on Signal Processing*, vol. 65, no. 21, pp. 5549–5563, Aug. 2017. p55

[61] J. Shi, G. Hu, X. Zhang, and H. Zhou, "Generalized Nested Array: Optimization for Degrees of Freedom and Mutual Coupling," *IEEE Communications Letters*, vol. 22, no. 6, pp. 1208–1211, Apr. 2018. p55

[62] Z. Zheng, W.-Q. Wang, Y. Kong, and Y. D. Zhang, "MISC Array: A New Sparse Array Design Achieving Increased Degrees of Freedom and Reduced Mutual Coupling Effect," *IEEE Transactions on Signal Processing*, vol. 67, no. 7, pp. 1728–1741, Feb. 2019. p55

[63] C.-L. Liu and P. P. Vaidyanathan, "Maximally economic sparse arrays and cantor arrays," in *2017 IEEE 7th International Workshop on Computational Advances in Multi-Sensor Adaptive Processing (CAMSAP)*, Dec. 2017, pp. 1–5. p55

[64] A. Kirschner, S. Bertl, J. Guetlein, and J. Detlefsen, "Comparison and tests of different virtual arrays for MIMO radar applications," in *12th International Radar Symposium (IRS)*, Sep. 2011, pp. 697–702. p56

[65] H. Commin and A. Manikas, "Virtual SIMO radar modelling in arrayed MIMO radar," in *Sensor Signal Processing for Defence (SSPD 2012)*, 2012, pp. 1–6. p56

[66] H. Hayashi and T. Ohtsuki, "DOA estimation in MIMO radar using temporal spatial virtual array with MUSIC algorithm," in *9th International Con-*

ference on Signal Processing and Communication Systems (ICSPCS), Dec. 2015, pp. 1–6. p56

[67] A. Manikas and M. Sethi, "A Space-Time Channel Estimator and Single-User Receiver for Code-Reuse DS-CDMA Systems," *IEEE Transactions on Signal Processing*, vol. 51, no. 1, pp. 39–51, Jan. 2003. p74

[68] Z. Liu, "Direction-of-Arrival Estimation With Time-Varying Arrays via Bayesian Multitask Learning," *IEEE Transactions on Vehicular Technology*, vol. 63, no. 8, pp. 3762–3773, Oct. 2014. p90

[69] V. Sridhar and A. Manikas, "Target Tracking with a Flexible UAV Cluster Array," in *IEEE Globecom Workshops (GC Wkshps)*, Dec. 2016, pp. 1–6. p90, p94

[70] A. Masnadi-Shirazi and B. D. Rao, "A Covariance-Based Superpositional CPHD Filter for Multisource DOA Tracking," *IEEE Transactions on Signal Processing*, vol. 66, no. 2, pp. 309–323, Jan. 2018. p90

[71] A. Panahi and M. Viberg, "Fast LASSO based DOA tracking," in *IEEE International Workshop on Computational Advances in Multi-Sensor Adaptive Processing (CAMSAP)*, Dec. 2011, pp. 397–400. p91

[72] T. Gustafsson and C. S. MacInnes, "A class of subspace tracking algorithms based on approximation of the noise-subspace," *IEEE Transactions on Signal Processing*, vol. 48, no. 11, pp. 3231–3235, Nov. 2000. p91

[73] G. W. Stewart, "An updating algorithm for subspace tracking," *IEEE Transactions on Signal Processing*, vol. 40, no. 6, pp. 1535–1541, Jun. 1992. p91

[74] E. S. Baker and R. D. DeGroat, "A correlation-based subspace tracking algorithm," *IEEE Transactions on Signal Processing*, vol. 46, no. 11, pp. 3112–3116, Nov. 1998. p91

[75] N. W. Whinnett and A. Manikas, "High-resolution array processing methods for joint direction-velocity estimation," *IEE Proceedings F - Radar and Signal Processing*, vol. 140, no. 2, pp. 114–122, Apr. 1993. p91

[76] Y. Zhou, P. C. Yip, and H. Leung, "Tracking the direction-of-arrival of multiple moving targets by passive arrays: algorithm," *IEEE Transactions on Signal Processing*, vol. 47, no. 10, pp. 2655–2666, Oct. 1999. p91

[77] A. Manikas and M. Sethi, "Joint multipath delay and direction tracking for CDMA array systems," in *Vehicular Technology Conference*, vol. 1, May 2002, pp. 175–179. p91, p113, p115, p119

[78] M. Orton and W. Fitzgerald, "A Bayesian approach to tracking multiple targets using sensor arrays and particle filters," *IEEE Transactions on Signal Processing*, vol. 50, no. 2, pp. 216–223, Feb. 2002. p91, p92

[79] V. Cevher and J. H. McClellan, "General direction-of-arrival tracking with acoustic nodes," *IEEE Transactions on Signal Processing*, vol. 53, no. 1, pp. 1–12, Jan. 2005. p91, p92

[80] P. Chavali and A. Nehorai, "Scheduling and Power Allocation in a Cognitive Radar Network for Multiple-Target Tracking," *IEEE Transactions on Signal Processing*, vol. 60, no. 2, pp. 715–729, Feb. 2012. p92

[81] R. Niu, R. S. Blum, P. K. Varshney, and A. L. Drozd, "Target Localization and Tracking in Noncoherent Multiple-Input Multiple-Output Radar Systems," *IEEE Transactions on Aerospace and Electronic Systems*, vol. 48, no. 2, pp. 1466–1489, Apr. 2012. p92

[82] H. Yan and H. H. Fan, "Signal-Selective DOA Tracking for Wideband Cyclostationary Sources," *IEEE Transactions on Signal Processing*, vol. 55, no. 5, pp. 2007–2015, May 2007. p92

[83] C. R. Rao, C. R. Sastry, and B. Zhou, "Tracking the direction of arrival of multiple moving targets," *IEEE Transactions on Signal Processing*, vol. 42, no. 5, pp. 1133–1144, May 1994. p92

[84] M. Keche, A. Ouamri, I. Harrison, and M. S. Woolfson, "Performance evaluation of an algorithm for multiple target angle tracking," *IEE Proceedings - Radar, Sonar and Navigation*, vol. 144, no. 5, pp. 252–258, Oct. 1997. p92

[85] S. B. Park, C. S. Ryu, and K. K. Lee, "Multiple target angle tracking algorithm using predicted angles," *IEEE Transactions on Aerospace and Electronic Systems*, vol. 30, no. 2, pp. 643–648, Apr. 1994. p92

[86] B. Liao, Z. Zhang, and S. Chan, "DOA Estimation and Tracking of ULAs with Mutual Coupling," *IEEE Transactions on Aerospace and Electronic Systems*, vol. 48, no. 1, pp. 891–905, Jan. 2012. p92

[87] Y. I. Kamil and A. Manikas, "Multisource Spatiotemporal Tracking Using Sparse Large Aperture Arrays," *IEEE Transactions on Aerospace and Electronic Systems*, vol. 53, no. 2, pp. 837–853, Apr. 2017. p92

[88] S. Hou, H. Hung, and Tsai-Sheng Kao, "Extended Kalman particle filter angle tracking (EKPF-AT) algorithm for tracking multiple targets," in *International Conference on System Science and Engineering*, Jul. 2010, pp. 216–220. p92

[89] M. Koivisto, M. Costa, A. Hakkarainen, K. Leppanen, and M. Valkama, "Joint 3D Positioning and Network Synchronization in 5G Ultra-Dense Networks Using UKF and EKF," in *IEEE Globecom Workshops (GC Wkshps)*, Dec. 2016, pp. 1–7. p93

[90] Y. Ge, Z. Zeng, T. Zhang, and Y. Sun, "Unscented Kalman Filter Based Beam Tracking for UAV-enabled Millimeter Wave Massive MIMO Systems,"

in *2019 16th International Symposium on Wireless Communication Systems (ISWCS)*, Aug. 2019, pp. 260–264. p93

[91] R. Van der Merwe and E. A. Wan, "The square-root unscented Kalman filter for state and parameter-estimation," in *IEEE International Conference on Acoustics, Speech, and Signal Processing. Proceedings*, vol. 6, May 2001, pp. 3461–3464. p93

[92] S. J. Julier and J. K. Uhlmann, "Unscented filtering and nonlinear estimation," *Proceedings of the IEEE*, vol. 92, no. 3, pp. 401–422, Mar. 2004. p93

[93] A. Zeira and B. Friedlander, "Direction finding with time-varying arrays," *IEEE Transactions on Signal Processing*, vol. 43, no. 4, pp. 927–937, Apr. 1995. p93, p103

[94] A. Zeira and B. Friedlander, "On the performance of direction finding with time-varying arrays," *Signal Processing*, vol. 43, no. 2, pp. 133–147, May 1995. p93

[95] D. W. Rieken and D. Fuhrmann, "Constrained Maximum-Likelihood Covariance Estimation for Time-Varying Sensor Arrays," in *Proceedings of the 9th Annual Adaptive Sensor Array Processing Workshop*, Jan. 2000, pp. 43–48. p93

[96] B. Friedlander and A. Zeira, "Eigenstructure-based algorithms for direction finding with time-varying arrays," *IEEE Transactions on Aerospace and Electronic Systems*, vol. 32, no. 2, pp. 689–701, Apr. 1996. p93

[97] D. W. Rieken and D. R. Fuhrmann, "Generalizing MUSIC and MVDR for multiple noncoherent arrays," *IEEE Transactions on Signal Processing*, vol. 52, no. 9, pp. 2396–2406, Sep. 2004. p93

[98] A. Guerra, D. Dardari, and P. M. Djurić, "Dynamic Radar Network of UAVs: A Joint Navigation and Tracking Approach," *IEEE Access*, vol. 8, pp. 116 454–116 469, Jun. 2020. p94

[99] J. M. Goldberg, "Joint Direction-of-Arrival and Array-Shape Tracking for Multiple Moving Targets," *IEEE Journal of Oceanic Engineering*, vol. 23, no. 2, pp. 118–126, Apr. 1998. p94

[100] W. D. Addison and M. D. MacLeod, "Non-stationary Bayesian direction of arrival estimation with drifting sensor locations," in *European Signal Processing Conference*, Aug. 2008, pp. 1–5. p94

[101] M. S. Arulampalam, S. Maskell, N. Gordon, and T. Clapp, "A tutorial on particle filters for online nonlinear/non-Gaussian Bayesian tracking," *IEEE Transactions on Signal Processing*, vol. 50, no. 2, pp. 174–188, Feb. 2002. p113, p115, p123, p124

Imperial College London

Department of Electrical and Electronic Engineering